Njegos
Jankovic

COMILLAS
UNIVERSIDAD PONTIFICIA

Escuela Técnica Superior de Ingeniería (ICAI)

Power Oscillation Damping using Converter Interfaced Generation

Autor: Njegos Jankovic
Director: Prof. Dr. Luis Rouco Rodriguez
Codirector: Dr. Javier Roldan Perez
Codirector: Dr. Milan Prodanovic

MADRID | Diciembre 2023

TÍTULO DE TESIS

Power Oscillation Damping using Converter Interfaced Generation

by
Njegoš Janković

supervised by
Dr. Javier Roldán Pérez
Dr. Milan Prodanović
Prof. Dr. Luis Rouco Rodríguez

a dissertation submitted to ICAI School of Engineering
in partial fulfilment of the requirements for the
degree of doctor

ICAI School of Engineering
Comillas Pontifical University

Madrid, December 2023

To my family

Festina lente

Acknowledgements

First of all, I would like to thank Dr. Javier Roldan-Perez for his guidance, willingness to share knowledge, and readiness to patiently address all possible questions that arose during this academic endeavour. He has helped by providing assistance with technical, scientific, and personal matters, making a significant and positive impact on the outcome of this work. I would also like to thank Dr. Milan Prodanovic, who has co-supervised this work. He has helped me during the cultural adaptation and taught me about different aspects of work in projects and the academic field. Furthermore, he offered constructive scientific feedback, as well as suggestions for further personal and professional development. Also, I would like to thank Prof. Dr. Luis Rouco-Rodriguez for co-supervising this thesis. His expertise in the field, eagerness to engage in discussions about the research questions from the initial stages, and clear instructions were pivotal factors that greatly contributed to this thesis.

I extend my utmost gratitude to Dr. Salvatore D'Arco and Dr. Jon Are Suul for generously hosting me during my research stay at SINTEF Energy Institute. I am deeply thankful for the invaluable discussions and feedback they provided on the scientific work, as well as for their substantial contributions to the preparation and presentation of the scientific results. Furthermore, I would like to thank Hallvar, Spyridon, Andrew, Santiago and Valentin for their help during working hours at SINTEF Energy Institute.

My thanks go to Pablo, Diana and Dionysios for the support, discussions and help in work over the years at IMDEA Energy Institute. Also, I am grateful to Alejandro and Jose Miguel for their help in the implementation of numerous setups in the SEIL laboratory. I thank Andres for the opportunity to join his research project and to collaborate on the laboratory verification of the idea. Furthermore, I thank Marco and Gabriel for the discussions and support over my last year at IMDEA Energy. My thanks go to Ebrahim and Erick, for interesting discussions over the years.

I would like to thank IMDEA Energy Institute, for allowing me to join the Electrical Systems Unit, and conduct research at SEIL facilities. Also, I am thankful to Comillas Pontifical University for accepting me for PhD studies, enabling access to excellent courses on several engineering subjects.

Throughout my work at IMDEA Energy, I have been fortunate enough to co-

supervise two master students. My appreciation goes to Laura and Marcelo, for their efforts and hard work. These projects helped me in exploring different ideas and contributed to some results of this thesis.

My thanks go to many friends all over Europe, for their support over the years. Discussions with them made this journey easier and more interesting.

With deep gratitude, I thank my mother, father, and brother for their unwavering support, without whom none of this would have been possible. Their care, patience, and encouragement have been the driving force behind my journey. The love and support they have shown inspired me to reach new heights and pursue my dreams relentlessly.

Finally, and of great importance, I extend my heartfelt gratitude to Sara for all that she has done. Her unwavering emotional support, understanding of everyday challenges, and boundless love were essential factors that empowered me to deliver the required results. I am profoundly grateful for her presence and influence throughout this journey.

Abstract

Over the last two decades, power systems have faced significant changes that affected different aspects of their operation. These changes are caused by an ever-increasing share of the converter-interfaced generation (CIG) that is used to transform energy coming from solar irradiation and wind to electric power. The initial power plants based on CIG were used to deliver electric power whenever the energy from the primary source was available. However, as the share of CIG increases, its impact on the power system operation becomes more noticeable. Some of the aspects that have been more affected are the stability and real-time management of power plants. This happens because the operation of CIG differs to a great extend to that of synchronous generators. System operators have recognised this change and have already started to request additional requirements to CIGs (i.e., grid codes) .

CIG-based power plants (e.g., wind farms and photovoltaic plants) connected to transmission networks should contribute to damp low-frequency electro-mechanical oscillations. To meet this requirement, the CIG control algorithm includes a power oscillation damping (POD) controller. This controller is designed to adjust CIG active and/or reactive power output, addressing the oscillation in the network frequency. However, the transmission system to which the CIG is connected might have multiple low-frequency oscillations. Also, the operating point and configuration of the transmission system are changing during the system operation. These factors impose a major challenge in the POD controller design. Furthermore, in the case of CIGs operating in grid-forming mode, the impact of required power for POD service has to be addressed. Also, CIG-based power plants in the majority of the cases include local CIG units and a centralised controller. The centralised controller is responsible for the coordination of the local CIG units and meeting the requirements imposed by the system operators.

This thesis deals with different aspects of power oscillation damping with CIGs. Multiple methods for POD controller design are proposed, addressing changes in the network topology and the impact of stochastic communication network on POD controller performance. Furthermore, the proposed methods are used to design the POD controller in the frequency domain, making them suitable for cases in which the detailed power system model is not available. Also, the ability of CIG operating in grid-forming

mode to provide POD service was examined, and a proposal to design a POD controller for such an application is presented. Several proposals for POD controller design were verified in the laboratory environment with real hardware and communication network deployed. Finally, conclusions and guidelines for further research are presented.

Resumen

En las últimas décadas, los sistemas eléctricos han sufrido grandes cambios, los cuales han afectado a varios aspectos de su operación. Entre ellos, el cambio principal está relacionado con una participación cada vez mayor de la generación basada en convertidores electrónicos, como puede ser la generación solar y eólica. Inicialmente, las fuentes de generación basadas en convertidores electrónicos inyectaban a la red toda la potencia eléctrica disponible en la fuente primaria de energía (turbina eólica o paneles solares, por ejemplo). Sin embargo, a medida que ha aumentado la participación de los convertidores electrónicos en el mix de generación, su impacto en la operación del sistema eléctrico ha aumentado. En este sentido, uno de los aspectos más afectados ha sido la estabilidad. Esto se debe a que los convertidores electrónicos operan de manera diferente a como lo harían los generadores eléctricos de las plantas convencionales. Los operadores del sistema eléctrico han reconocido este cambio y han comenzado a imponer requisitos adicionales de operación a los convertidores electrónicos, principalmente basándose en el desarrollo de códigos de red.

Las plantas de generación basadas en convertidores electrónicos deben contribuir al amortiguamiento de oscilaciones electromecánicas de baja frecuencia. Para cumplir este requisito, una solución común es añadir un algoritmo de amortigumiento de oscilaciones de potencia (POD) sobre los lazos de control originales del convertidor electrónico. Este controlador modula la cantidad de potencia activa y/o reactiva inyectada a la red, con el fin de recudir las oscilaciones en la frecuencia. Sin embargo, los electricos pueden tener múltiples oscilaciones (modos) de baja frecuencia. Además, el punto de operación y la topología de la red eléctrica afectan al amortiguamiento de las oscilaciones electromecánicas, y estos pueden cambiar en función en función del estado de la red. Estos aspectos suponen un gran desafío para el diseño de controladores POD para convertidores electrónicos. In addition, cuando los convertidores electrónicos operan con algoritmos de formación de red (*grid-forming*), un aspecto esencial es la cantidad de potencia requerida para prestar servicos de POD. La mayoría de las plantas de generación basadas en convertidores electrónicos incluyen un controlador local por cada convertidor, y un convertidor centralizado de planta. Este control centralizado es el responsable de coordinar la acción de los convertidores y, además, de cumplir con los

requisitos del cógido de red impuesto por el operador del sistema.

En esta tesis se abordan diferentes aspectos relacionados con el amortiguamiento de oscilaciones de potencia utilizando convertidores electrónicos. Se proponen diferentes métodos para diseñar controladores POD. En particular, se aborda el diseño de estos controladores cuando cambia la topología de la red eléctrica, y cuando se tiene en cuenta la naturaliza estocástica del retraso de las comunicaciones en las plantas de generación. Los métodos propuestos se utilizan para diseñar el controlador POD en el dominio de la frecuencia, lo que hace que estos métodos sean adecuados cuando no está disponible un modelo detallado del sistema eléctrico. Además, se explora la capacidad que tienen los convertidores electrónicos con estrategias de control para formación de redes de proporcionar serivicios de POD, y se presenta una propuesta para diseñar un controlador POD para este caso. Algunas de las propuestas de control se verificaron en un entorno de laboratorio, con convertidores reales y una infraestructura de comunicaciones realista. Finalmente, se presentan las conclusiones y directrices para abordar futuros trabajos de investigación.

Contents

List of Figures

List of Tables

List of Symbols

Greek Symbols

$\hat{\omega}_g$	Estimated network frequency
λ	Eigenvalue, see (6.1)
$\mathbf{\Omega}$	Set of oscillation frequencies in all network configurations, see page 52
$\mathbf{\Phi_{Pp}}$, $\mathbf{\Phi_{Pp}}$	Set of phases of plant in active and reactive power loops in all network configurations, see page 52
Ω_n	Set of oscillation frequencies of interests, see page 51
ω_o	Frequency of oscillation, see (3.2)
ϕ	Phase of frequency response of transfer function
$\Phi_{Pp,n}$, $\Phi_{Pq,n}$	Set of phases of plant in active and power loops at oscillation frequencies, see page 51
σ	Network traffic, see (B.1)
τ_{min}, τ_{max}	Minimum and maximum delay duration, see (5.4)
θ_{PLL}	Angle estimated by phase-locked loop
$\vartheta(t)$	Delay of variable length, see (5.3)

Lowercase Latin Symbols

$\mathbf{x}$	Set of unknown variables in controller design procedure, see pages 54, 70
c	Number of time constants in compensator, see (4.9)

e	Error cost in optimisation problem, see page 54
$f(\vartheta)$	Delay probability density function, see (5.4)
f_{max}	Nyquist frequency, see page 72
f_s	Sampling frequency, see page 72
i_{out}	CIG output current
k	Active power margin for POD service, see (3.16)
m	Slope of linear function, see (3.26)
n_p, n_q	Number of lead-lag compensators in series in active and reactive power loops, see (3.19)
p_d, q_d	Decoupled active and reactive power references, see (7.2)
p_l, q_l	Limits in active and reactive power references
p_r, q_r	External active and reactive power references
p_s, q_s	Output of compensators in active and reactive power loops
p_t, q_t	Total active and reactive power references
r	Constant value of linear function, see (3.26)
t	Time variable
v_{out}	Voltage at CIG output terminal
w	Padé approximation coefficients, see (5.17)

Functions and Operators

$\dot{\cdot}$	Derivative
$\hat{\cdot}$	Estimated quantity
$\mathcal{L}\{\cdot\}$	Laplace transformation
$E[\cdot]$	Expected value of PDF, see (5.6)
$f(\omega_o)$	Fitted linear function, see (3.26)
s	Laplace operator

Subscripts and Superscripts

$*$	Specified points for vector fitting algorithm, see (6.11)
B	Band-pass filter
C	Compensator in POD controller
G	Open loop
H	High-pass filter
P	Plant
p, q	Variables in active and reactive power loops

Uppercase Latin Symbols

$\hat{\mathbf{A}}$	State matrix, see page 68
$\hat{\mathbf{B}}$	Input matrix, see page 68
$\hat{\mathbf{X}}(t)$	State vector, see page 68
$\mathbf{D}$	Feed-through matrix, see (6.1)
$\mathbf{E}$	Descriptor matrix, see (6.1)
$\mathbf{I}$	Number of oscillation frequencies $\omega_{o,i}$
$\mathbf{M}$	Matrix for decoupling power references, see (7.2)
$\mathbf{R}$	Residue of transfer function at certain pole, see (6.1)
$\mathbf{U}(t)$	Input vector, see page 68
$\mathcal{C}$	Set of network configurations considered , see page 51
A	Magnitude of frequency response of transfer function
$B(s)$	Band-pass filter transfer function
C	Number of considered network configurations, see page 51
$C(s)$	POD controller compensator transfer function
$D(s)$	Delay transfer function, see (5.6)
$D'(s)$	Delay Padé approximation, see (5.17)

D_v	Virtual droop constant, see Fig. 7.1 (c)
$E(s)$	Closed-loop error transfer function, see (6.2)
E_p, E_q	Design error for compensators in active and reactive power loops, see page 57
$F(s)$	Closed-loop transfer function, see (3.1)
G	Synchronous generator unit
$G(s)$	Open-loop transfer function, see (3.1)
$H(s)$	High-pass filter transfer function
$I_{n,lab}, I_{n,mod}$	Current levels in the PHIL environment and emulated network model (see (A.2))
J_v	Virtual moment of inertia constant, see Fig. 7.1 (c)
K_i	Current scaling factor (see (A.3))
K_p, K_q	POD controller proportional gain in active and reactive power loops
K_s	Power scaling factor (see (A.2))
K_V	Reactive power droop, see Fig. 7.1 (c)
K_v	Voltage scaling factor (see (A.1))
L	Communication network loading level, see (B.1)
N_s	Transfer function order in vector fitting algorithm, see (6.12)
N_t	Number of specified points for vector fitting algorithm, see (6.12)
$P(s)$	Plant transfer function
P_C, Q_C	Active and reactive power references sent from the central controller, see Fig. 5.8
P_L, Q_L	Active and reactive power references received by the local controller, see Fig. 5.8
$S_{n,lab}, S_{n,mod}$	Power levels in the PHIL environment and emulated network model (see (A.2))
T	Time constant of compensator in POD controller

T_h	High-pass filter time constant
T_l	Low-pass filter time constant
$V_{n,lab}, V_{n,mod}$	Nominal voltage levels in the PHIL environment and emulated network model at the connection point (see (A.1))

List of Acronyms

AC	Alternating current
AVR	Automatic voltage regulator
CIG	Converter-interfaced generation
CPU	Central processing unit
DC	Direct current
EMT	Electro-magnetic transient
ESA	Eigenvalue sensitivity analysis
FFT	Fast Fourier transform
FOPID	Fractional-order proportional-integral-derivative
LQG	Linear quadratic Gaussian
MMAC	Multiple model adaptive control
PC	Personal computer
PDF	Probability density function
PHIL	Power Hardware-in-Loop
PI	Proportional-integral
PID	Proportional-integral-derivative
PLL	Phase-locked loop
POC	Point of connection
POD	Power oscillation damping
PRBS	Pseudo-random binary signal
PSS	Power system stabiliser

PV	Photovoltaic
RAM	Random access memory
RES	Renewable energy source
RTPC	Real-time personal computer
SG	Synchronous generator
SRF	Synchronous reference frame
STATCOM	Static synchronous compensator
SVM	Space-vector modulation
TCP/IP	Transmission control protocol/internet protocol
TSO	Transmission system operator
VF	Vector fitting
VSC	Voltage-source converter
VSM	Virtual synchronous machine
WAMS	Wide-area measurement system

Chapter 1

Introduction

1.1 Topic of this Thesis

The work presented in this thesis is focused on the contribution of converter interfaced generation (CIG) in the damping of low-frequency oscillations in power systems. Such oscillations occur when groups of synchronous generators (SGs) start oscillating in opposition to each other. In systems dominated by SGs, a power system stabiliser (PSS) control loop is commonly introduced in the control system of SGs to improve the damping of low-frequency modes. However, the increasing proportion of energy produced by CIG units has led to the dismantling of many SGs throughout the system. As a consequence, transmission system operators (TSOs) are introducing new requirements for CIG units and currently they should help in damping oscillations by using a power oscillation damping (POD) controller. Nonetheless, there are many factors in the system operation that can have an important impact on the damping action of CIG units.

The work presented in this thesis addresses the design of POD controllers with special attention to the following factors:

- *Network reconfiguration:* During normal operation, power systems suffer modifications due to the planned or unplanned disconnection of elements (e.g., lines, generators, etc.). In terms of power system stability, network reconfiguration is an important factor since it changes the plant on which the POD controller is acting. If not addressed properly, these changes could lead to system instabilities as damping controllers become ineffective when are not tuned adequately. One way to address this problem is to update the parameters of POD controllers based on information sent by the TSO with respect to the system topology. However, such an approach requires an additional communication layer between TSOs and CIG units, and this increases the system complexity and could have a negative impact on the system reliability. Therefore, it is of interest to address the changes caused by network reconfiguration by using only local measurements and some

predefined rules in control algorithms.

- *Stochastic communication network delay:* Large power plants based on renewable energy sources (RES) (e.g., photovoltaic (PV) plants) often include a centralised controller that coordinates the actions of local CIG units taking into consideration the requirements of TSOs. In this case, a communication network is deployed within the power plant to coordinate the local CIG units from a centralised PV plant controller. Also, the local CIG units might be inaccessible for any further modification due to the intellectual property of the manufacturer. This means that, if the TSO asks a PV plant to contribute in damping low-frequency modes, a centralised POD controller has to be used. However, the presence of a communication network introduces a stochastic delay that appears due to the protocols used to exchange information between devices. Therefore, the analysis of the stochastic delay and the design of a centralised POD controller taking such delay into account is of interest.

- *Multi-mode POD controller design:* Commonly, power systems have multiple low-frequency modes that cause oscillations between different groups of SGs. Designing a POD controller for several modes is challenging since the problem is highly nonlinear. This issue can be addressed by adjusting the controller parameters in closed loop and verifying the POD controller impact on all the modes, in an iterative procedure. However, such a method requires a linearised parametric model of the power system, which might not be always available. Therefore, it is of interest to define methods for designing multi-mode POD controllers in open loop using the system frequency response, exclusively. In that case, the POD controller design criteria are defined in the frequency domain and this can be translated into a transfer function with some desired frequency response. In this thesis, two ideas in this regard are presented. In the first one, the parameters lead-lag filters connected in series are calculated for a given set of points, which represent the desired frequency response of the POD controller. To do so, an optimisation problem is defined, where the unknowns are the parameters of the lead-lag filters. In the second method, the vector fitting (VF) algorithm is used for synthesising the POD controller. In this case, the set of desired points in the frequency domain is used as a starting point for the VF algorithm. This algorithm is used to calculate the parameters of a transfer function, which is then used as a POD controller. Therefore, these two methods try to match the response of a transfer function (that represents the POD controller) at multiple points. Depending on the specific case, one or the other might result in a better POD controller design.

- *POD controller for CIG units operating in grid-forming mode:* The control algorithm of CIG units operating in grid-forming mode replicates the dynamic char-

acteristics of SGs. This means that the CIG unit detects changes in the output active and reactive powers and adjusts the output voltage angle and magnitude accordingly. Therefore, the active and reactive powers delivered to the grid are not regulated in the same way as in grid-following operating mode. This difference plays an important role in the operation of CIG units, especially if the energy of the primary source is taken into consideration (e.g., PV panel). Namely, if not addressed properly, the power requested from the PV panel could surpass the maximum power available and this would inevitably lead to a system collapse. Therefore, it is of interest to develop a method that independently controls the active and reactive power reference generated by a POD controller, in grid-forming mode.

1.2 Objectives of this Thesis

The objective of this thesis has been to investigate and improve the control algorithms of CIG units that contribute in damping low-frequency oscillations in power systems. This is achieved by introducing a POD controller and it covers CIG units operating in both grid-following and grid-forming control modes. The research work has been focused on several factors with important impact on the power system stability, such as changes in the network topology, presence of stochastic delays and limited power available from the primary source of energy. The objectives along these lines can be summarised as follows:

1. Study the impact of changes in the network topology and total inertia on the system frequency response, in the range of low-frequency oscillations.

2. Develop a POD controller with an adaptive mechanism that updates the parameters of POD controllers based on the system changes. These changes are detected by using local measurements, exclusively.

3. Design a POD controller with a fixed structure and fixed parameters that is robust against changes in the network topology.

4. Develop a centralised multi-mode POD controller that compensates for the effect of stochastic communication delay.

5. Define a method to synthesise a multi-mode POD controller by using the VF algorithm.

6. Propose a method to design POD controllers by using active and reactive power, independently.

7. Develop a control strategy for CIG units operating in grid-forming mode that allows providing POD action by using active and reactive powers, independently.

8. Propose a method for designing POD controllers for CIG units operating in grid-forming mode without modifications of any existing control loop.

The starting assumptions for all the objectives are:

- Undamped low-frequency oscillations were present in the system prior to the connection of the CIG.
- CIG control algorithms shall rely only on local measurements of currents and voltages.
- There is no information exchange with the TSO regarding the system configuration (e.g., network topology, total system inertia, etc.)
- The system frequency response shall be used for to design of POD controllers.
- The real-time implementation and reliability of POD controllers shall be addressed in the development phase.

1.3 Thesis Outline

This thesis is divided into eight chapters and two appendices − chapters include the main work of this thesis and appendices describe the laboratory set-ups used to verify the proposed control algorithms and factors affecting the communication network delay. The information from the appendices can be omitted in the first reading, although it should be helpful for a complete understanding of the work presented in the chapters.

Chapter 1 provides an overview of the topics addressed in this thesis, as well as the objectives of the work described in the document.

Chapter 2 presents the state of the art of power oscillation damping with CIG units. Different aspects of POD controllers are analysed, both for local and centralised implementations. Furthermore, the impact of network reconfiguration and the options to address such changes at the design stage of POD controllers are discussed.

Chapter 3 presents the proposed POD controller, which includes an adaptive mechanism that tackles the changes caused by network reconfiguration. The impact of changes in the network topology on the system frequency response is studied. The results of this analysis were used to define the adaptive mechanism, which is then used to update the parameters of the POD controller.

Chapter 4 provides a different option aimed at effectively tackling the challenges arising from changes in the network configuration. An optimisation problem is defined to find a fixed set of parameters for a POD controller based on lead-lag filters. The

result meets the specified design constraints and achieves a frequency response based on a given set of points. However, depending on the specific set of points, the solution might achieve less error for certain points than for others. This problem was noted during development and is also addressed in Chapter 6, where another method for designing POD controllers is presented. This POD controller is supposed to increase the damping of low-frequency modes for any of the network topologies considered during the design procedure.

Chapter 5 describes a centralised multi-mode POD controller designed to compensate for the impact of stochastic communication channels. A method to model both the communication channel delay length and the sampling rate based on measurements is introduced. Furthermore, a method for designing a POD controller for a system with multiple low-frequency modes in the frequency domain is presented.

Chapter 6 presents a method to synthesise a multi-mode POD controller by using the VF algorithm. The proposed design method addresses the impact of the POD controller within and outside the frequency range of low-frequency oscillations. The VF algorithm is used to find the parameters of a transfer function that meets the POD controller design criteria. The benefit of this approach compared with the method presented in Chapter 4 is that the solution achieves a similar error for all the given points. However, the main disadvantage are undesired peaks in the magnitude of the POD controller frequency response.

Chapter 7 presents a POD controller for virtual synchronous machines (VSMs) that provides decoupled control of active and reactive power. Design procedures for both the POD controller and the decoupling mechanism are presented. These procedures are based on frequency response techniques.

Chapter 8 highlights the conclusions and gives guidelines for further research.

This thesis ends with two appendices. Appendix A describes the power hardware-in-the-loop (PHIL) setup used in Chapters 3 and 5. Also, it depicts the communication network setup used to exchange data in Chapter 5. The factors affecting the communication network performance and their impact on signal quality are given in Appendix B.

Chapter 2

Power Oscillation Damping Controller: State of the Art

2.1 Motivation

Over the last two decades, the global energy portfolio has changed significantly [IEA, 2021]. This change is driven by a series of political decisions aimed at diminishing the reliance on fossil fuels and promoting electrification of various sectors [EU, 2010]. From the power system perspective, this change is seen as an ever-increasing share of renewable energy sources (RES) in the energy production. The transition from a power system dominated by SGs to one with increased presence of RES is sketched in Fig. 2.1. Namely, power plants based on SGs are being replaced by converter-interfaced generation (CIG), such as wind farms and PV plants. Furthermore, battery systems are being introduced in the system to maintain the power balance and increase the system reliability. This change is taking place at both the transmission and distribution network levels as the technology used to inject the power generated from RES is rapidly evolving.

Besides the change in the energy portfolio, this transition has important effects on many aspects of the power system operation. For example, the balance between supply and demand has to be modified considering weather conditions, as these affect the production of RES [Impram et al., 2020]. Power system reliability is another aspect affected by the high share of RES [Kumar et al., 2020]. This is a consequence of the uncertainty in the available power, which is caused by the intermittent nature of wind and irrandiance [Aien et al., 2016]. Furthermore, these variations in the production of RES usually lead to unplanned connection and disconnection of conventional generation units. As a consequence, the system inertia varies over time and this results in unpredictable responses of the system frequency [IEA, 2021]. These challenges have already been identified in the power systems of several coun-

tries [AEMO, 2016], [EirGrid, 2009], [ENTSOE, 2015]. Currently, many TSOs request network support services from CIG units to overcome these challenges. The provision of these services and their impact on the power system are of significant scientific interest.

2.2 Small-Signal Rotor Angle Stability

2.2.1 Description

Small-signal rotor angle stability represents the ability of a power system to retain synchronism under small disturbances [Hatziargyriou et al., 2021]. Small disturbances are defined as changes in the system for which the deviation of the equilibrium point is negligible. In this case, linearisation of the dynamic equations that represent the system around the equilibrium point does not introduce significant errors [Kundur et al., 1994]. There are mainly two types of small disturbance instabilities. The first one is caused by the lack of synchronising torque, which results in non-oscillatory instabilities. The solution to non-oscillatory instabilities is the application of automatic voltage regulators (AVRs) that act upon changes in SGs output voltage (this is done by adjusting the field currents). The second type of instabilities is produced by insufficient damping torque, and this induces oscillatory instabilities. These are linked with rotor angle oscillations in SGs. Such oscillations generate an additional power component in the system that is exchanged between groups of SGs. Depending on the position and number of generators involved, these oscillations are divided into two categories. The first category includes one or several SGs forming a local-area oscillation. The second category includes large groups of SGs across the system oscillating against each other. This category receives the name of inter-area oscillations. The frequency of these electromechanical oscillations is in the range from 0.1 to 1 Hz for inter-area, and from 1 to 2 Hz in the case of local-area oscillations [Rogers, 2012]. The initial recordings of such oscillations in power systems date back to the 1960s [Schleif and White, 1966]. Nowa-

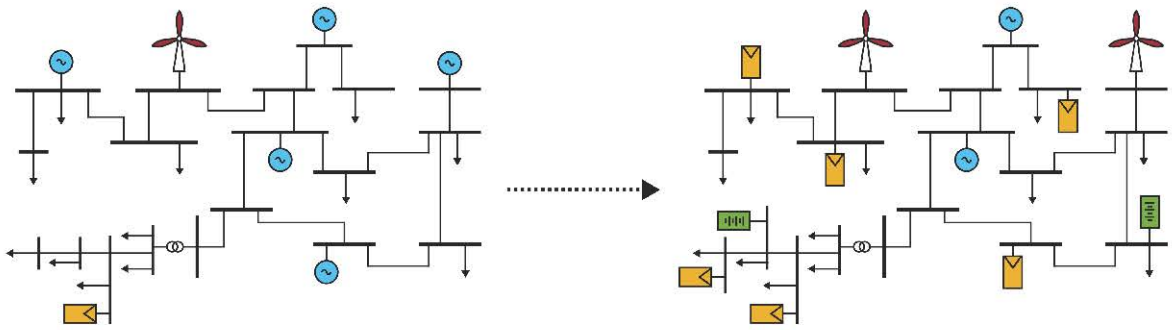

Figure 2.1: Evolution of power systems. (left) Dominated by SGs to (left) with a high-share of RES.

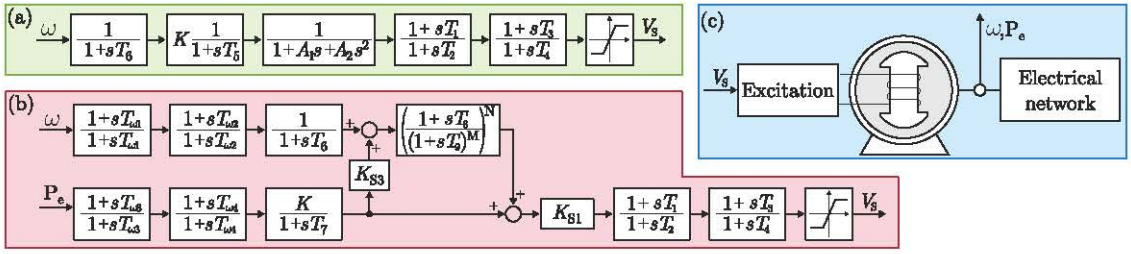

Figure 2.2: Block diagram of PSS with (a) single-input and (b) double-input implementation. (c) SG with excitation connected to an electrical network.

days, in the United States of America (USA) such events occur on average every five years, either as cause or effect of previous events in the system [NAERC, 2019]. In Continental Europe, the first event of this type happened in the 1970s when an oscillation appeared between Yugoslavia and Greece. The main reason was the interconnection of areas by a weak line. More recent events include an oscillation between Spain and France in 2016 [ENTSOE, 2017] and an interaction between Southern and Northern Europe in 2017 [ENTSOE, 2018]. The post-fault analysis revealed that is required to readjust the control systems of the SGs connected across the network, as well as to perform detailed dynamic simulations.

The presence of low-frequency oscillations in power systems has fostered academia and TSOs to develop reliable solutions to damp oscillations. Over the years, an additional control loop called power system stabiliser (PSS) has been introduced into the control system of SGs. Two types of PSS structures have been established as standard solutions for this application [Kundur et al., 1994]. The first type is a control loop that acts upon oscillations in the SG rotor speed deviation by adjusting the reference voltage of the AVR. The second type regulates the excitation voltage by acting upon changes in both the rotor speed deviation and the electrical output power of the SG. These types are named single-input and double-input PSS, respectively, based on the number of input signals [IEEE, 2005]. Fig. 2.2 shows the block diagram of the aforementioned PSS structures together with an SG connected to an electrical network.

2.2.2 Evolution of PSS Design Approach

Phase Compensation Method

The methods to select the structure of PSSs and design their parameters have evolved over the years. The initial works in this field considered a test case with a single machine connected to an infinite bus [Demello and Concordia, 1969], [Larsen and Swann, 1981a]. This representation allows an understanding of the instability phenomena of SGs with a relatively simple test case. In these works, the performance of PSSs with different input signals [Larsen and Swann, 1981b] and the impact of variations in

the system parameters [Demello and Concordia, 1969] were examined. These studies established general criteria for the selection of the PSS input signal and to understand the performance limitations.

Robust PSS

After the first initial steps, the studies were extended to include cases with more complex scenarios. In [Kundur et al., 1989], the PSS was designed using the phase-compensation technique for a system with one local and one inter-area mode. Martins *et al.* [Martins and Lima, 1990] present a method for determining the location of a generation unit with a PSS that improves the stability margins of the whole power system. Namely, by calculating closed-loop transfer functions and their associated residues, a suitable location for such a device was determined. The deployment of generation units with PSS at the selected nodes greatly improved the system stability margins. These works focus on the design of one PSS in the context of a power system. However, there might be multiple PSSs in a power system acting on different SGs. The design of the PSSs in such cases is studied in [Boukarim et al., 2000], and three approaches are evaluated. The first approach is to design each PSS, separately, trying to maximise the damping factor of multiple modes. In the second approach, the speed measurements of two SGs are fed to a centralised PSS that defines the control action of two SGs, simultaneously. This approach assumes the availability of a fast communication network for exchanging information. The third case covers the use of a linear matrix inequality approach for the coordinated design of PSSs. It was concluded that a centralised PSS requires less gain to achieve the same control action, although it requires the implementation of a fast communication network. Furthermore, it was concluded that a decentralised implementation of PSSs provides better performance in terms of disturbance rejection.

Eigenvalue Sensitivity Analysis Approach

The availability of a detailed power system model allows analysing modes and participation factors (these represent the significance of each state in each mode of the system). By using this information, it is possible to identify the subsystems involved in certain low-frequency modes, as well as to determine the best locations to place a PSS in the system [Pagola et al., 1989]. This approach was further developed and applied to design the PSS of superconducting magnetic energy storage systems [Rouco et al., 1996]. The location of the devices that carry a PSS controller, as well as the selection of the PSS inputs and outputs, was determined based on the eigenvalue sensitivities analysis (ESA). The results obtained from ESA allow the coordinated design of multiple PSSs aimed at damping low-frequency oscillations [Rouco, 2001]. The procedure is divided into two parts. First, the phase compensation filters of each PSS are designed

individually. Then, a coordinated approach determines the value of the PSS gains in all the units under consideration. This approach and its effectiveness in improving the damping of multiple modes show that ESA can be used for the design of both the phase compensation networks and the gain values of PSSs.

The generality of the results obtained with ESA allows to design the PSS control loops of devices that are not SGs. For example, in [Rouco and Pagola, 1997] the results from ESA are used for determining the location where the modulation of series reactances would improve the damping factor of certain modes. Furthermore, in [Renedo et al., 2021] the PSS implemented in the terminals of a high-voltage dc network of a meshed ac-dc network were designed using the ESA approach. The terminal units adjusted their active and reactive power injections based on the difference between the local frequency and the average frequency measured at the ac terminals. These pieces of work demonstrate the applicability of ESA for designing the PSS of multiple devices throughout the system. Nevertheless, these studies depend on detailed power system models to acquire pertinent information for the design and placement of PSS controllers.

In [Renedo et al., 2019], the PSS design problem is tackled, and it is demonstrated that ESA can be used to design PSSs even with limited information about the power system. In this case, the PSS is engineered for robustness against changes in the power system, specifically addressing the variation of the impedance between areas involved in low-frequency oscillations. This work shows that the results obtained with ESA can be used in both cases (with and without a linearised parametric power system model), thus extending the applicability of this approach. Such a conclusion is ever more important since the discrepancy between power system models and the actual plant in which the PSS is acting on can change significantly when changes in the power system operation and increased penetration of CIG units are considered.

2.2.3 Impact of CIG Units

The impact of the massive integration of CIG units in the small-signal rotor angle stability has several implications [Boukhenfouf et al., 2023]. The aforementioned replacement of SGs and thus the unavoidable reduction of inertia is resulting in an increased value of the frequency of the oscillations. This is a consequence of reduction of the kinetic energy stored in the rotating masses of SGs. However, such a negative impact is not present in every situation. From the study of the power system of the western USA, it has been noted that the negative effect is relevant once the penetration of CIG units surpasses the 15 % of the total energy generation [Elliott et al., 2014]. The significantly higher CIG penetration level of 65 % was studied in the power system model of the eastern USA. In this case, an increase in the oscillation frequency was reported, together with a reduction in the system damping [You et al., 2017]. These results show

that the impact of CIG penetration on the small-signal rotor angle stability is not uniform. In [Musca et al., 2022], it was noted that the impact of CIG units depends on whether the CIG operates in grid-forming or grid-following mode.

Another aspect is the placement of CIG units in the network since low-frequency oscillations are present all along the power system. In [Shah et al., 2013a], the degree of CIG dispersity on the small-signal stability was studied. It has been noted that the increase in CIG penetration level degrades system stability. However, for the same level of CIG penetration, the system stability margins improved in case of more CIG units of lower power rating connected across the system compared with one large group of CIG units.

Most of the CIG units operate in grid-following mode [Blaabjerg, 2021]. This means that during operation CIG units are synchronised with the voltage space vector at the point of connection (POC). For this purpose, a phase-locked loop (PLL) is commonly used. In [Jia et al., 2017a], it was noted that the proportional gain of the PLL has a negative impact on both the system damping and the oscillation frequency in weak grids. Then, the same group of authors proposed an additional virtual inductance loop to reduce these negative effects [Jia et al., 2017b]. Adib *et al.* [Adib et al., 2018] conclude that the X/R ratio of the grid impedance plays a significant role in the system stability. They propose several alternatives that result in a less sensitive CIG control, such as increasing the values of the CIG output filter or introducing damping resistors.

TSOs have identified the negative implications of CIG penetration on small-signal stability of power systems and have defined two main lines to address this issue. The first one is the revision and tuning of PSS controllers already deployed in power systems [NAERC, 2019], [ENTSOE, 2018]. The second one is the active participation of CIG units in the provision of POD services. For that reason, newly published regulations (i.e., grid codes) request POD services to CIG units [Red Eléctrica, 2019].

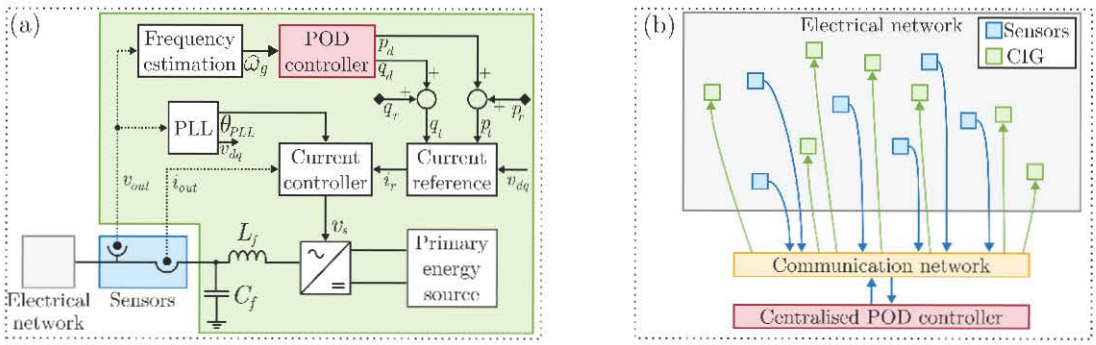

Figure 2.3: (a) CIG with a local POD controller, (b) system-level centralised POD controller regulating multiple (green) CIG units across the system and receiving (red) measurements from various locations in the system. The exchange of information is achieved through (yellow) a communication network.

2.3 POD Controller Design

2.3.1 Overview

Fig. 2.3 shows the structure of a power system where CIG units are providing POD services. CIG units are adjusting their output powers to act upon low-frequency oscillations in the power system. The power used for this purpose can be either active, reactive or a combination of both power components, depending on the POD controller design specifications. The sensors are used to measure voltages and currents. Then, the measurements are sent to the POD controller, which can be placed at the device level or in a central controller. Fig. 2.3 shows the diagram of both (a) decentralised and (b) centralised implementations of POD controllers. The link is direct if the POD controllers are implemented locally. This means that the sensor measurements are processed in the device in which the POD controller is implemented. A communication network is necessary if the sensors and the control board are physically separated. This happens for POD controllers acting on several CIG units within the same power plant. In this case, the command signal must be sent to the local CIG units forming the power plant and for that a communication link is required. Another case where a communication link is necessary is when the POD controller is coordinating CIG units across the power system. Commonly, in this application, the sensors are placed across the electrical network in a configuration known as a wide-area measurement system (WAMS). Both local and central POD controllers can be implemented in various ways. Fig. 2.4 shows control systems for several implementations of POD controllers. These implementations are discussed in the following sections. Tables 2.1 and 2.2 summarise the POD controllers for CIG units operating in grid-following mode reviewed in this chapter.

By comparing Fig. 2.2 and Fig. 2.3, it can be seen that POD action of SGs and CIG units is different. For SGs, the controller is acting over the voltage reference of the excitation system, whereas in the case of CIG units the controller is acting over the active and reactive powers references. This gives more versatility and control gain to damp oscillations in the case of CIG units since the speed of the internal loops is faster than in the case of the SGs.

2.3.2 Local POD Controller

Implementation of POD controllers for CIGs on the local level has been in focus since the 1980s. The first papers on this topic were based on standard PSS controllers replicated in the control system of wind turbines [Larsen and Swann, 1981a] and PV generators [Ghali et al., 1994], [Kalaitzakis and Vachtsevanos, 1987]. This was followed by a proposal to use superconducting magnetic energy storage systems for improving the damping of low-frequency oscillations [Rouco et al., 1996]. In these proposals, the

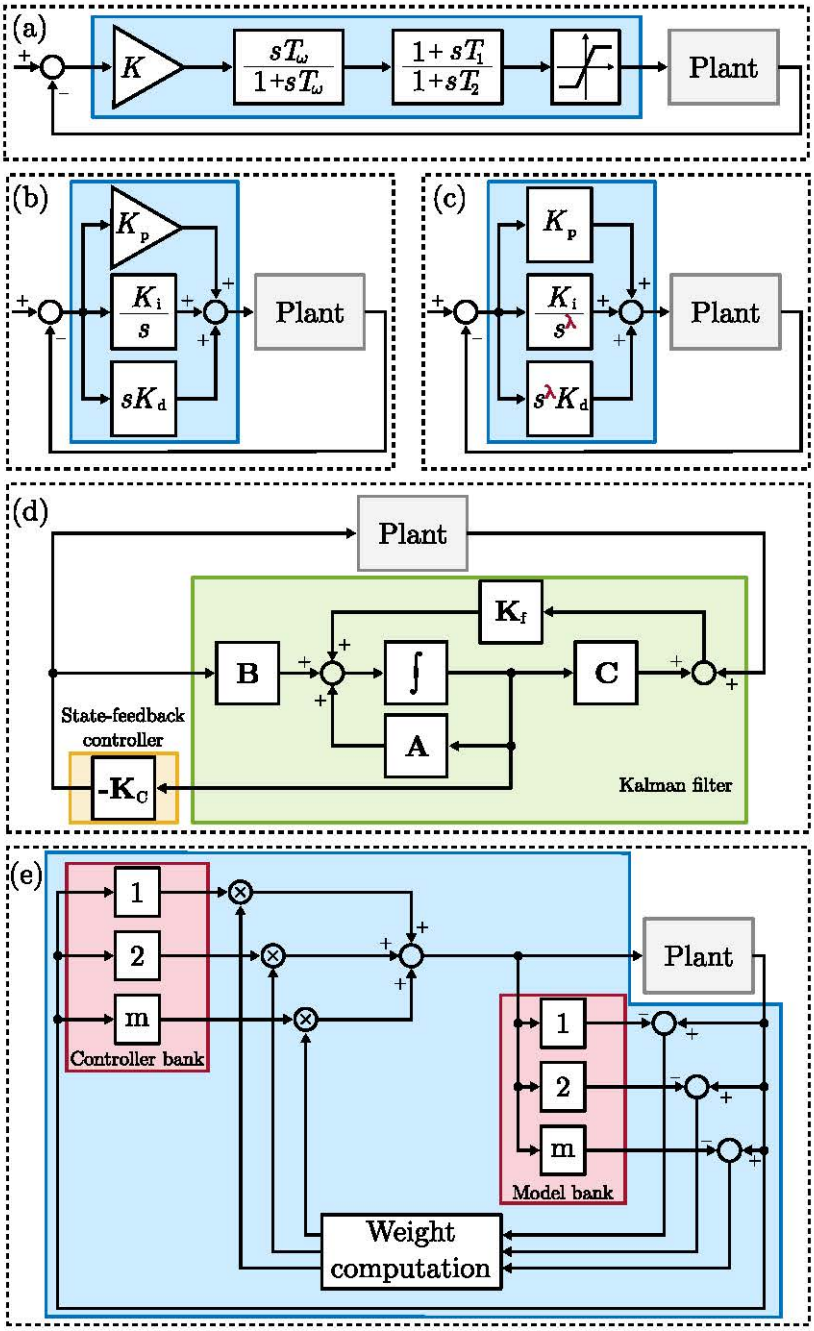

Figure 2.4: Control system block diagram of POD controller designed as (a) lead-lag, (b) proportional-integral-derivative (PID), (c) fractional order PID, (d) state-feedback, or (e) multiple-model adaptive controller.

oscillations in the network frequency were damp by controlling the CIG output voltage magnitude. More recent studies on this topic show the effectiveness of controlling active power for damping the oscillations in both wind farms [Zeni et al., 2016] and PV plants [Liu et al., 2016]. Although effective, these solutions are difficult to implement

in power plants based on RES. Namely, the active power reserved for POD services results in less power delivered to the network, in steady-state operation. This has a negative economic impact on the operation of the power plant since the revenue depends on the amount of energy delivered to the network. To overcome this issue, Silva *et al.* [Silva-Saravia et al., 2021] propose a method to reduce the active power reference during oscillatory events and the available active power is modulated to damp the oscillations. A similar approach is presented in [Varma and Maleki, 2019], where the active power reference of the PV plant is set to zero during oscillations. However, here the CIG capacity is used to deliver reactive power. In both cases, once the oscillation is mitigated, the active power reference is restored. Nonetheless, modifying the active power reference during oscillations can cause other network issues (e.g., reduction of the system frequency), in addition to those that triggered the low-frequency oscillation. Thus, new regulations for CIG units impose a margin reserved for the provision of POD action [Red Eléctrica, 2019]. In [Knuppel et al., 2012], the combined action of wind turbines in a wind park is proposed to damp oscillations by using reactive power, exclusively. Another approach is to use the combined action of active and reactive powers to damp oscillations [Basu et al., 2021]. This idea was recently tested in a wind farm [Edrah et al., 2016] and in a PV plant [Li et al., 2020]. Although the combined action of the two power components increases the damping performance, there can be a negative interaction between active and reactive power. This depends on the power system characteristics, as well as on the method used to design the POD controller. For example, Rimorov *et al.* [Rimorov et al., 2015] use a PSS-based controller in both the active and reactive power control loops. Although the control structure is simple, depending on the values given to the controller parameters, an undesired coupling between the two control loops was detected.

POD controllers can be implemented in other configurations, besides the PSS-based one. For example, in [Shabani et al., 2013] the POD controller is implemented as a proportional-integral-derivative (PID) controller. This structure is well-known and widely used in controllers for various applications. Some researchers focused on fractional-order PID (FOPID) controllers, which provide an additional degree of freedom in the design procedure. In [Abumeteir and Vural, 2022], a FOPID controller was applied to a CIG unit. It was designed by using a particle swarm optimisation algorithm. A similar approach was used in [Saadatmand et al., 2021a] to optimally design the POD controllers across a power system. In this case, an optimisation function was used to obtain the control parameters for the POD controllers of CIG units and the PSS controllers of SGs. The FOPID configuration offers more degrees of freedom compared to the PSS-based one. This results in improved stability margins for power systems with several oscillation modes. In the literature, power systems with two or more oscillation modes in the low-frequency range have been reported [Jin et al., 2017]. In this case, POD controllers should be able to increase the damping of more than

one oscillation mode. However, the implementation of more complex control structures requires additional computational power that might not be available in the case of local POD controllers.

During the operation of CIG units, the power system can change significantly. This change can come from modifications in the operating points or from changes in the system topology. These changes have an important impact on the power system stability [Chung et al., 2003]. This means that the POD controller should guarantee the system stability under various scenarios and network conditions. In many proposals, this is not considered and the POD controller presented is adjusted only for a certain operating point. Proposals addressing the variation in the system can be grouped into two groups. The first group includes POD controllers that adapt to changes in the system while the second group includes POD controllers robust against those changes. The proposals for designing POD controllers from both groups are described in the following two sections.

2.3.3 Adaptive POD Controller

The changes in the network configuration or system operating conditions are followed by changes in the damping of low-frequency modes [Ramakrishna and Malik, 2010]. To address this change, the *adaptive* POD controller paradigm can be applied. Such a controller includes a mechanism to adapt to system changes, which are detected by monitoring a system variable. One method that is used in this respect is the multiple model adaptive control (MMAC) strategy. In this strategy, a bank of linearised plant models is used, representing the power system at different operation states [Chaudhuri et al., 2004]. Recently, this method was modified and used in the control of a PV plant [Zhou et al., 2017]. After a fault, a Bayesian approach is used to calculate the probability of each plant model. Then, the weighted average of the individual dampers is applied reactive power reference of the CIG unit.

To address variations in the controller plant, Shah *et al.* [Shah et al., 2012] propose a minimax Linear Quadratic Gaussian (LQG) controller. The POD controller improves the stability for a wide range of operating conditions. In [Chau et al., 2018], the parameters of a POD controller are updated based on the demand prediction by using an additional neural network. A similar approach was implemented in [Li et al., 2021], where a real-time decision-making agent adjusts the POD controller to the near-optimum settings. To do so, the agent is trained by using a reinforcement learning procedure, for different operating conditions. On the other hand, Beza *et al.* [Beza and Bongiorno, 2015] use recursive least squares to adjust the parameters of POD controllers if changes in the network are detected. Other methods such are fuzzy logic [Chaiyatham and Ngamroo, 2017] and Kalman filter [Liao et al., 2019] have also been explored. In this case, the update of the

controller parameters improved the damping action under different operating conditions.

In summary, these alternative options provide adequate damping of oscillations. However, they are quite complex and require knowledge of advanced engineering tools (e.g., artificial intelligence techniques). Moreover, their implementation at the device level would require important engineering efforts. For that reason, the development of adaptive POD strategies suitable for implementation at the device level is of interest.

2.3.4 Robust POD Controller

One drawback of the *adaptive* POD controller structure is the fact that its parameters are modified after certain changes. This imposes an additional challenge for the TSO since the POD controller adjustment mechanism has to be included in the power system stability analysis. For this reason, TSOs prefer POD controllers with a fixed structure. In this regard, the *robust* POD controller paradigm could be used. It has a fixed structure and parameter values, and it is able to provide sufficient damping in case of network changes. In that case, the controller parameters have to be designed to guarantee system stability under different operating conditions. To do so, Konara *et al.* [Konara and Annakkage, 2016] propose a design methodology based on eigenstructure assignment. In this paper, the POD controller helps to damp critical modes for different operating conditions. In [Werner et al., 2003], the impact of changes in the system operating conditions was analysed. A POD controller was designed to ensure a certain damping ratio for all the critical modes, under different operating conditions. The results show that the POD controller with a group of first and second-order filters can meet this objective. However, the design procedure relies on the power system model, which is also needed to verify closed-loop stability. In [Shah et al., 2014], a POD controller with a fixed second-order structure that is robust against changes in the system is presented. To improve the system robustness, the POD controller can be designed by solving an optimisation problem. In [Yuan and Yan, 2020], the objective function takes into consideration transient stability aspects as well. The same problem was also addressed considering both regional pole placement and $\mathcal{H}_2$ performance metrics [Deng et al., 2019].

These proposals show that POD controllers can contribute to the damping of critical modes when the power system changes, for example when the system operating point is modified. Although these variations have an impact on the dynamic properties, they do not include aspects such as a disconnection of system elements, despite them having an important impact on both the operating point and the dynamic properties. Therefore, the development of POD controllers robust against network reconfiguration is of interest.

Table 2.1: Summary of local POD controller types.

Reference	Modulated power Active/Reactive	Network reconfiguration	Controller structure
[Larsen and Swann, 1981a], [Ghali et al., 1994], [Kalaitzakis and Vachtsevanos, 1987], [Zeni et al., 2016], [Liu et al., 2016], [Silva-Saravia et al., 2021]	Active	No	Lead-lag
[Varma and Maleki, 2019], [Knuppel et al., 2012], [Rouco et al., 1996]	Reactive	No	Lead-lag
[Knuppel et al., 2012], [Basu et al., 2021], [Edrah et al., 2016], [Li et al., 2020], [Rimorov et al., 2015]	Both	No	Lead-lag
[Shabani et al., 2013], [Chaiyatham and Ngamroo, 2017]	Active	No	PID
[Abumeteir and Vural, 2022], [Jin et al., 2017]	Active	No	FOPID
[Chaudhuri et al., 2004], [Zhou et al., 2017]	Active	Yes	MMAC
[Shah et al., 2012], [Liao et al., 2019], [Shah et al., 2014], [Yuan and Yan, 2020]	Active	Yes	State-feedback
[Konara and Annakkage, 2016], [Werner et al., 2003]	Active	Yes	Lead-lag
[Chau et al., 2018], [Li et al., 2021], [Deng et al., 2019]	Active	Yes	Neural-network

2.3.5 Centralised POD Controller

Centralised POD controllers are another type of controller that can be used to improve the system damping by using CIG units. In general, this approach relies on WAMS for obtaining the system measurements. Thus, the constraints imposed by communication networks (e.g., data packet dropouts and delays) need to be addressed. However, the studies on the impact of the communication infrastructure differ among recent proposals. For example, a centralised controller for a PV power plant has been studied in [Ge et al., 2016]. The optimal feedback signal is selected based on the dominant mode ratio. Thanks to this, the system stability is improved. However, the proposed procedure does not address the impact of the communication channel. This issue is studied in [Shah et al., 2013b] for a centralised PV plant controller, with special emphasis on the delay. It is shown that the compensation of the delay effects improves the system performance. Nonetheless, in this case, a constant delay model is used. This means that the varying nature of the communication channel delay is not considered.

In [Liu and Milano, 2018], a numerical approach is used for determining the impact of the communication channel delay on the system small-signal stability. The shape of the communication channel delay is modelled in three ways, by using a sinusoidal, a sawtooth and a square wave. This work was further extended in [Liu et al., 2019], where a realistic communication channel delay was used. It is shown that the combination of an approximated system matrix and the Newton correction technique allows for a good representation of the system in small-signal stability analyses. The work presented in [Gurung et al., 2019] proposes a probabilistic approach to design a POD controller that addresses the stochastic nature of communication channel delay. To do so, a probabilistic model of the delay is used, together with probabilistic models of generation and demand. Various swarm-based algorithms are used to determine the POD controller parameters. Then, the final solution is selected based on a comparison of the POD controller effectiveness. On the other hand, Nan *et al.* [Nan et al., 2021] present a centralised controller for a wind farm that is able to compensate for both the delays in the communication channel and the losses of data package. For this purpose, a networked predictive control method is proposed. In this case, the communication channel delay and message dropout are determined during the system operation. Thus, the communication channel model is not explicitly defined.

Recently, a comparison among different POD controllers has been published, focusing on the differences in the effectiveness of various design methods [Saadatmand et al., 2021b]. Among others, the POD controllers were compared in terms of robustness against time delays. For this purpose, the comparison was made among five common methods to design POD controllers, which are depicted in Fig. 2.4. It is shown that lead-lags and PID controllers are the worst in terms of performance. Furthermore, both LQG and MMAC methods show different outcomes, depending on

the disturbance and the delay length. Overall, the FOPID control method achieved the best results in terms of robustness across various test scenarios. However, the test scenarios used for comparison include only constant delays of different lengths. Thus, it remains unclear how the stochastic nature of the communication channel delay affects the performance of different POD controllers. Also, in the comparison, the delay is introduced once the POD controller is designed, and no further modifications to the controller parameters are applied. It remains unclear if the performance of various POD controllers would improve if the delay model is included in the design procedure. Thus, studying the design of lead-lag-based POD controllers with stochastic delay compensation is of interest.

Table 2.2: Summary of centralised POD controller types.

Reference	Delay compensation	Controller structure
[Ge et al., 2016]	No	Lead-lag
[Shah et al., 2013b], [Nan et al., 2021]	Yes	LQR
[Liu and Milano, 2018], [Gurung et al., 2019]	Yes	Lead-lag

2.3.6 POD Controller for Virtual Synchronous Machine

The VSM controller directly affects the small-signal rotor angle stability of power networks [Zhou et al., 2022]. When a VSM is connected to an existing power network, the VSM parameters can be set to avoid undesired small-signal interactions with the rest of the network [Roldán-Pérez et al., 2019]. On the other hand, if the VSM is connected to a network that already has a poorly-damped low-frequency mode, additional control loops can be added to the VSM in order to help damp that mode [Roldán-Pérez et al., 2018]. Another approach in this regard is to modify the VSM active power reference once an oscillation is detected [Silva-Saravia et al., 2021]. The PSS-based POD controller acts on the active power reference while the oscillation is present. However, for the rest of the time, a constant value of active power is delivered to the system. This control algorithm allows to damp low-frequency oscillations with a large control action (since the PSS gain can be made very large). However, switching between different operating modes is challenging and can be a limiting factor in practical implementations. Namely, if the amplitude of the oscillation seen in the terminals of the CIG is small, the CIG would not act upon it. From the TSO point of view, this behaviour is undesirable since the POD control action depends on the type of event that took place in the system.

An alternative option to such implementation is using a control structure similar to that used in SGs (see Fig. 2.2). The implementation of control loops acting on either

change in the estimated frequency at the point of connection or frequency defined by VSM is discussed in [Rodríguez-Amenedo and Gómez, 2021]. In both cases, the POD controller is connected to the virtual swing equation by modifying the output voltage angle. Furthermore, an alternative option in which the POD controller defines the output voltage magnitude is also presented. However, the combined action on both voltage angle and magnitude was not examined. On the other hand, in [Li et al., 2023] the impact of the reference voltage angle and magnitude are measured. Then, a virtual inductance loop is introduced, which defines additional active and reactive power references. These works show that VSMs can help in damping low-frequency oscillations by using either active or reactive power. However, the two power components are coupled and it is difficult to know beforehand the amount of active and reactive power required to damp oscillations. The case of active power is particularly important in CIG units since it is directly linked to the primary source of energy [Pawar et al., 2021].

The coupling between active and reactive powers is a natural phenomenon in power networks and depends on the system parameters and the network topology [Kundur et al., 1994]. When a VSM is connected to a power network, this coupling is also affected by the parameters of the VSM. A decoupling mechanism can be added to the control system to avoid this coupling. One approach is to add decoupling terms in the inner current control loop [Li et al., 2016]. Another one is to add additional terms in the virtual swing equation and the reactive power controller so that the voltage and angle generated by the VSM are modified [Shintai et al., 2014]. These works show that it is possible to control active and reactive powers in a decoupled manner. However, the implementation of such mechanisms requires a modification of the internal control loops of the CIG, which may not be approved by the CIG manufacturer (and its intellectual property policy). Therefore, the implementation of a POD controller using decoupled active and reactive powers in VSM is of interest.

2.4 Study Approach

2.4.1 Types of Models

The work presented in this thesis has been done using both simulation models and models emulated in a PHIL environment. The simulation models used were developed using Matlab-Simulink, and its SimPowerSystems toolbox [MATLAB, 2019]. Electromagnetic transient (EMT) models were used for the majority of the simulations (see Table 2.3. The EMT models describe the electrical elements over a wide range of frequencies, representing fast element dynamics as well as dynamics in the range of low-frequency oscillations. This modelling option was selected since it provides an accurate representation of fast current and voltage dynamics [Lacerda et al., 2023]. These dynamics are important in systems with CIG units since they play an important role

in the performance of inner control loops. On the other hand, the electro-mechanical models are sufficiently precise and more common for addressing low-frequency oscillation phenomena in power systems [Kundur et al., 1994]. With this type of model, the simulation speed is greatly increased. Therefore, it is used to study large power systems, where many electrical lines and complex network elements are interconnected. For this reason, an electro-mechanical power system model is used in Chapter 4.

The models used for emulation in the PHIL environment were based on EMT models, adjusted for real-time execution. This adjustment included two steps. First, the models of both control systems and electrical elements were discretised. The purpose of this step was to synchronise the calculations with the execution rate of the control platform used for the execution of the real-time control algorithms. Second, a connection was established between the emulated electrical elements and the PHIL setup [Roldán-Pérez et al., 2021]. Following this procedure, the power system models were emulated by one actual converter while the control system with the proposed POD controllers was implemented in the control platform of another actual converter.

2.4.2 System Identification

In this thesis, one of the starting assumptions (see Chapter 1.2) was that a detailed linearised model of the network is not available. However, information about the system is still required to design POD controllers. This raises a need for a method to accurately identify the system within the frequency range of interest (in this case, the range of low-frequency oscillations). Furthermore, the selected method should be adequate for the real-time control platform used in the PHIL environment. Therefore, the additional computational burden cannot be excessive and the time needed to identify the system should be reasonable (as many tests should be performed).

Taking these premises into consideration, the measurements can be processed and analysed, for example, by using Prony-based techniques [Seppanen, 2017], black-box modelling [Zhou and Beerten, 2023] or estimated frequency responses [Ljung, 1999]. These methods are widely used in power systems and provide an approximation of the system based on measurements. In this thesis, estimated frequency responses were used as the identified model directly provides the inputs for the design of the POD controllers (i.e., phase and magnitude of the frequency response). In this technique, a pseudo-random binary signal (PRBS) with adjustable amplitude was introduced in the selected input signal of the CIG unit, and the selected output signal was measured. By doing so, the additional computational requirement was minimal since the signal was loaded from an external file and used in the experiment. The selected output signal values were saved over a certain period (5−10 minutes). Then, the system frequency response was obtained from the selected input and output signals, using *System Identification Toolbox*, from Matlab [MATLAB, 2019]. Finally, the frequency response

obtained was used as a starting point for the POD controller design. The same technique was used for cases where only simulation results are shown.

2.4.3 PHIL Validation

The performance of the POD controllers designed in this thesis were validated in a PHIL environment (see Chapter 3 and Chapter 5). This validation was done to address several important aspects of real-time implementation of POD controllers. First, the POD controller needs to be discretised to be implemented in a real-time control platform [Ogata, 2010]. In this step, the discretisation method, the structure and the parameter values of the discretised POD controller are determined. Each of these points is important in designing a reliable POD controller with the desired performance [Lyons, 2004].

Furthermore, in Chapter 3, an additional mechanism to update the POD controller parameters was introduced. The reliability and accuracy of such a mechanism were a concern for applications with real hardware. Several concerns in this regard arose, including the selection of the update rate, the impact of noise on the accuracy and its performance in real-time. Furthermore, the performance of the POD controller when the control parameters were updated was a question that required verification in a PHIL environment.

The setup used in Chapter 5 was based on a real communication network deployed in the PHIL environment. The communication network allowed to study the impact of real stochastic delays on the POD controller performance. In this case, the PHIL setup enabled the verification of the proposed method to design POD controllers over a long period. Namely, the disturbances in the system were applied over a period of 30 minutes. During this period, the POD controller was acting upon changes while the communication delay was constantly changing. Without the PHIL setup, such validation would be almost impossible due to the complex nature of the delay, which includes many real-time processing tasks.

2.5 Study Overview

2.5.1 Benchmark Networks

In this thesis, three benchmark transmission networks were used, depending on the scenario considered in certain test cases. The selected networks have one or several poorly damped low-frequency modes. Such systems are stable but have poorly damped low-frequency modes. These networks are:

- *Kundur's two-area system:* This network consists of four generators G_{1-4} and two loads [Kundur et al., 1994]. In this system, there are two intra-area oscillations:

G_1 against G_2, and G_3 against G_4. Furthermore, there is an inter-area oscillation where G_1 and G_2 oscillate against G_3 and G_4. This system is widely used for studying the impact of additional elements with POD capabilities (e.g., CIG units or SGs). In this thesis, the emulated Kundur's two-area system is used in Chapter 3 while the EMT simulation model is used in Chapter 7. The relevant information from the system is obtained by using the system identification method described in Section 2.4.2.

- *Three-machine infinite bus (3MIB) system:* The transmission system includes three generators G_{1-3}, two loads and an infinite bus [IEEE, 2015a]. In this system, there are three low-frequency modes. Namely, there are oscillations between G_1 and G_2, G_3 and $G_{1,2}$, and also an oscillation between the three generators and the infinite grid. This model gives the possibility to study the performance of multi-mode POD controllers with only several network elements, making it suitable for real-time emulation. For this reason, it is used in the experiments in the PHIL environment presented in Chapter 5. A system identification method (see Section 2.4.2) was used to estimate relevant information of the emulated power network.

- *IEEE 39-Bus system:* This system includes ten generators G_{1-10} connected across the system, with several poorly damped oscillation modes [IEEE, 2015a]. Furthermore, the network has 39 Buses connected with a meshed topology. This system architecture is useful to study the effects of changes in the network topology. Therefore, this system was used in Chapter 4 and implemented as an electromechanical model (i.e., electrical interconnections are modelled as algebraic equations). Specifically, the generator units include a model of an SG, a speed regulator, an excitation voltage controller and multi-band PSS implemented in Matlab/SimPowerSystems [MATLAB, 2019]. The system information required to design the POD controller was obtained by using the *Simulink Control Design Linearization Tools*, from Matlab [MATLAB, 2019]. The linearised model obtained with the toolbox has 295 states. The model is available in [Patrice, 2016].

Table 2.3: Overview of the test cases used in this thesis.

	Chapter				
	3	4	5	6	7
Single-mode	✓				✓
Multi-mode		✓	✓	✓	
Grid-following	✓	✓	✓	✓	
Grid-forming					✓
Network model	Two-area	39-Bus	3MIB	3MIB	Two-area
Model type	EMT	Electro-mechanical	EMT	EMT	EMT
Method to obtain system frequency response	Identification	Linearised model	Identification	Identification	Identification
Simulation	✓	✓		✓	✓
PHIL	✓		✓		

2.5.2 Test Cases

Table 2.3 shows a summary of test cases used in this thesis. These cases cover single- and multi-mode POD controller designs, for CIG units operating in both grid-forming and grid-following control modes. Furthermore, changes in the network topology and presence of stochastic communication delays are addressed. Depending on the problem addressed and the need for PHIL verification, either EMT or electro-mechanical models were used.

In Chapter 3, Kundur's two-area network was used to test a single-mode *adaptive* POD controller was designed. The CIG used in this study operates in grid-following mode. This controller includes an adaptation mechanism that updates the PSS parameters according to some predefined rules. The network was represented by using an EMT model and emulated in the PHIL environment. The performance of the POD controller is evaluated with simulation results obtained in Matlab/SimPowerSystems [MATLAB, 2019] and experimental results obtained in the experimental platform. The system identification method was used to estimate the system information required to design the POD controller.

The design of a multi-mode *robust* POD controller is presented in Chapter 3 for a CIG operating in grid-following mode. The POD controller has a fixed structure. The control parameters were selected to ensure robustness against changes in the network topology. The network was modelled by using an electro-mechanical model. The POD controller performance was evaluated by using simulation results obtained with the linearised model. To this end, *Simulink Control Design Linearization Tools* from Matlab were used [MATLAB, 2019].

The three-machine infinite bus (3MIB) network was used in Chapter 5 to verify the performance of the proposed centralised multi-mode POD controller. The POD controller was designed for CIGs operating in grid-following mode and the effect of the stochastic communication channel delay is taken into consideration. This delay is introduced in the system by deploying a communication network between the centralised controller and local CIG units. The performance of the proposed centralised multi-mode POD controller was experimentally verified using a PHIL setup with a real communication network. The system information required to design the POD controller was obtained by using the system identification method.

In Chapter 6, the multi-mode POD controller synthesis using a vector fitting algorithm is presented. The CIG operating in grid-following mode is connected to the (3MIB) power system. The system identification method was used to obtain relevant system information. The power system is represented using EMT models and the POD controller performance was verified using simulation results from Matlab [MATLAB, 2019].

The single-mode POD controller for CIG operating in grid-forming mode is pre-

sented in Chapter 6. The CIG is connected to Kundur's two-area network, which is represented using EMT models. The information about the system was obtained using the system identification method (see Section 2.4.2). The POD controller performance was verified using simulation results, obtained in Matlab/SimPowerSystems.

2.6 Chapter Summary

In this chapter, the state of the art of POD controllers for CIG units has been presented. Also, the technical aspects that require further research efforts have been identified. These problems are summarised in the following list:

- The design of *adaptive* POD controllers is often addressed in the literature by using advanced design methods and complex control structures. In Chapter 3, the design of an *adaptive* POD controller with a simple adaptive mechanism is presented. This controller relies only on local measurements.

- The design of POD controllers with a fixed structure that ensures stability in the case of network topology modifications is a challenge. This problem is addressed in Chapter 4.

- The impact of stochastic communication channels on the performance of POD controllers has not been studied in detail in the literature. Also, it has been noticed that this issue has not been verified in a laboratory environment. A method to design centralised POD controllers taking into consideration the communication channel is studied in Chapter 5. Furthermore, a method to model the stochastic nature of the communication channels based on measurements is presented.

- The design of POD controllers in the frequency domain presents a major challenge, and some advanced methods are presented in the literature. Chapter 6 presents a multi-mode POD controller synthesis method based on a vector fitting algorithm. In this proposal, only a few design requirements should be specified.

- The provision of POD services with CIG units operating in grid-forming mode has been seldom addressed in the literature. In Chapter 7, a POD controller for grid-forming converters that features decoupled control of active and reactive powers is presented.

Also, in this chapter, the study approach used in this work has been presented. The types of models used to represent the transmission network have been described, together with the approach used for to identify power system dynamics based on measurements. Also, the reasons for using a PHIL validation for some proposals were

presented. Besides that, in this Chapter, a summary of the benchmark models and an overview of test cases have been presented.

Chapter 3

Single-Mode *Adaptive* POD Controllers for CIG in Grid-Following Mode

This chapter describes a POD controller with an adaptive mechanism suitable for network reconfiguration. Section 3.1 gives an overview of the system and POD controller design methodology, as well as an explanation of the adaptive mechanism. Section 3.2 describes the POD controller design procedure. The power system analysis and definition of adaptive characteristics are described in Section 3.3. In Section 3.4 the experimental results are presented. Then, a comparison with other methods for POD controller design is presented in Section 3.5. Finally, the conclusions of this chapter are summarised in Section 3.6.

3.1 System Overview and Methodology

3.1.1 System Description

Fig. 3.1 shows the electrical and control system diagrams of the network studied in this work. It can be divided into two main parts. The first part is depicted in Fig. 3.1 (a) and represents a model of a transmission network formed by four generation units (G_1 to G_4). This model is widely used as a benchmark for inter-area oscillation studies [Kundur et al., 1994]. Each generation unit includes an SG with a governor and an exciter. The unit $G2$ includes a PSS. With this configuration the system is stable, but it has a poorly damped inter-area oscillation. In the left part of Fig. 3.1, an additional power plant has been connected to the area formed by G_1 and G_2 via the POC. It consists of n CIG units in parallel connection that have identical electrical elements and control systems.

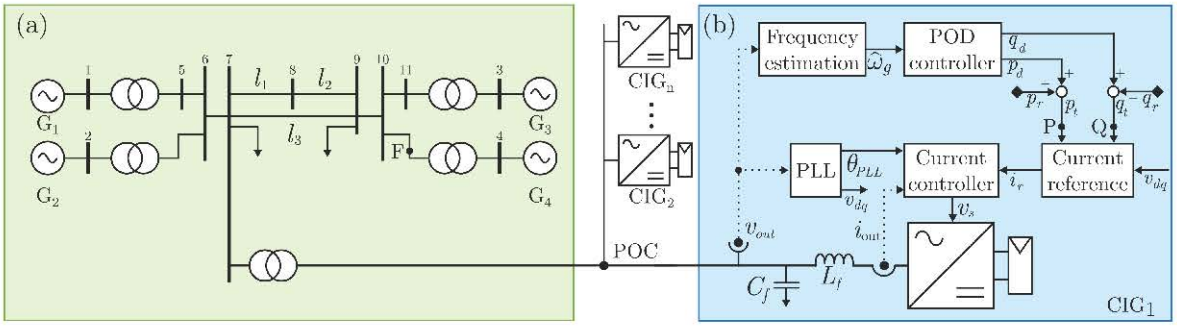

Figure 3.1: Single-line diagram of the network studied in this article and the CIG control system. It consists of a power plant with n CIG units.

Fig. 3.1 (b) shows the power stage and control system of one CIG. The power stage consists of a primary energy source on the dc side, a three-phase voltage source converter (VSC) and an LC filter. The CIG control system includes inner and outer control loops. The inner control loop regulates the VSC output current (i_{out}). This controller is implemented in a synchronous reference frame (SRF) and includes two proportional-integral (PI) controllers and a phase-locked loop (PLL) synchronised with the POC voltage (v_{out}). The outer control loop calculates the current reference for the inner control loops by using the established technique shown in [Yazdani and Iravani, 2010]. The active and reactive power references (p_t and q_t) consist of two terms. The first one is sent by the grid operator or generated internally (subscript "r"), while the second adds an oscillatory component that is used to damp oscillations (subscript "d"). A frequency estimator is used to estimate the POC frequency ($\hat{\omega}_g$). The frequency estimator is introduced, although the POC frequency can be obtained from the PLL. This is done to avoid any type of coupling between the dynamics of the PLLs [Zhao et al., 2021]. Finally, the POD controller calculates p_d and q_d according to $\hat{\omega}_g$.

3.1.2 POD Controller Overview

Fig. 3.2 shows the block diagram of the POD controller proposed in this work and the transfer functions that link active and reactive power with the estimated network frequency ($P_p(s)$ and $P_q(s)$, respectively). The POD controller can be divided into two parts. The first part is depicted in Fig. 3.2 (a) and includes the controllers for both active and reactive power. The input to the POD controller is the deviation of the estimated frequency from zero. This definition is different from the one used in PSS controllers, and results in the opposite sign of proportional gains, compared with the ones used in PSS [Rouco and Pagola, 2001]. The high-pass filter eliminates the steady-state value from the estimated frequency so that the POD controller acts only at the oscillatory frequency. Then, the lead-lag compensators (to be called $C_p(s)$ and $C_q(s)$) generate the power references (p_s and q_s) to compensate the open-loop phase

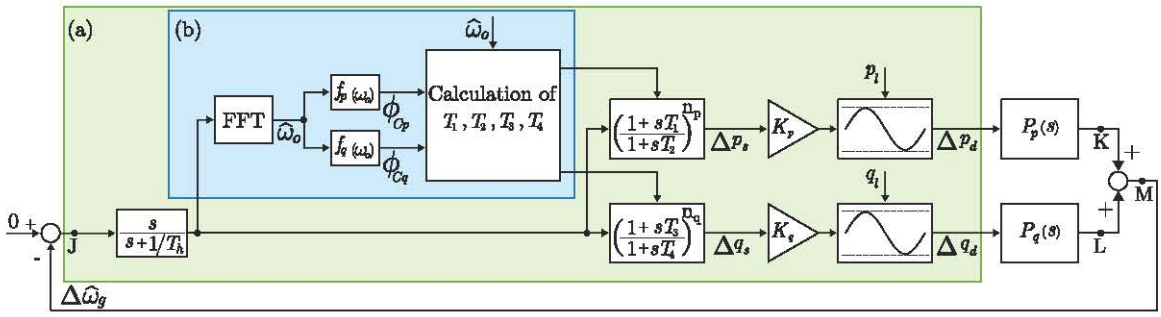

Figure 3.2: POD controller block diagram, including the dynamics of the plants.

of the plant and then maximise the damping effect. The POD controller also includes proportional gains (K_p and K_q) and saturators.

3.1.3 Real-Time Adaptation of POD Controllers

Fig. 3.2 (b) shows the part of the POD controller in which the phases to be compensated by the lead-lag compensators are calculated. First, an algorithm based on the fast Fourier transform (FFT) is applied to the estimated POC frequency in order to determine the frequency of the oscillation (ω_o). Then, the phases to be compensated (ϕ_{Cp} and ϕ_{Cq}) are calculated using the predefined functions $f_p(\omega_o)$ and $f_q(\omega_o)$. These functions are obtained using offline simulations, in which the network model is examined under different operating conditions in order to find the relationships between ω_o, ϕ_{Cp} and ϕ_{Cq}. It is worth noting that the relation between ω_o and the compensation phases is not unique nor perfectly defined since it depends on several variables of the electrical system. However, it will be shown that these variables are clearly linked, and basic adaptation rules (e.g., a linear relationship) will greatly improve the effectiveness of POD. The development, analysis and implementation of this technique represent the main contribution of this work.

3.1.4 POD Controller Design Methodology

Fig. 3.3 shows the main steps in the offline analysis of the power system and in the POD controller design procedure. The main goal is to determine the phases to be compensated by the POD controllers according to the network topology. First, the possible alternative network configurations are identified (faults, disconnections, etc.). A subset of variations in which the system remains stable is selected. In the case of an unstable system, time-domain simulation results would not be reliable. Then, for each configuration, the system oscillation frequency (ω_o) is calculated using simulation. Once this frequency is known, the phases to be compensated (ϕ_{Pp} and ϕ_{Pq}) are calculated. This process is repeated for all network configurations considered. With the data for

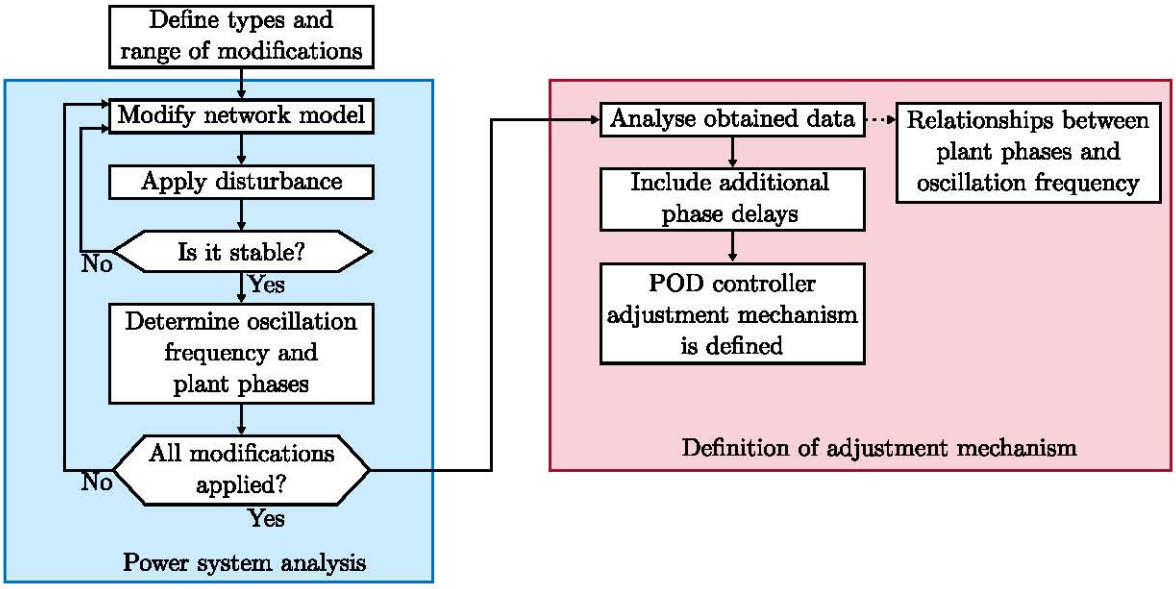

Figure 3.3: Offline model analysis used for POD controller design.

all the cases obtained, the challenge is to find the relationships between ω_o, ϕ_{Pp} and ϕ_{Pq}. Then the functions $\phi_{Pp} = f_p(\omega_o)$ and $\phi_{Pq} = f_q(\omega_o)$ are fitted.

The online operation of the POD controller is depicted in Fig. 3.4. First, the grid frequency is estimated from the POC voltage measurements. This signal is analysed and the oscillation frequency (ω_o) is extracted by using a FFT algorithm. After ω_o is estimated (called $\hat{\omega}_o$), it is inserted in the previously calculated functions $\phi_{Pp} = f_p(\omega_o)$ and $\phi_{Pq} = f_q(\omega_o)$. Finally, the lead-lag compensators are adjusted to compensate for these phases. In this paper, the analysis is carried out in a simulation model implemented in MATLAB/SimPowerSystems [MATLAB, 2019], following the acausal modelling principle. However, the same analysis can be carried out from the small-signal model. This procedure is repeated after a certain period of time. It can be seen that the tools used for the real-time implementation are readily available in microprocessors that are commonly used to control CIG units. Therefore, this strategy is suitable for the implementation on standard converter controller platforms.

3.2 POD Controller Design

In this section, the POD controller design objective is defined. It helps to understand how active and reactive powers affect the system damping. Finally, active and reactive power limits are discussed.

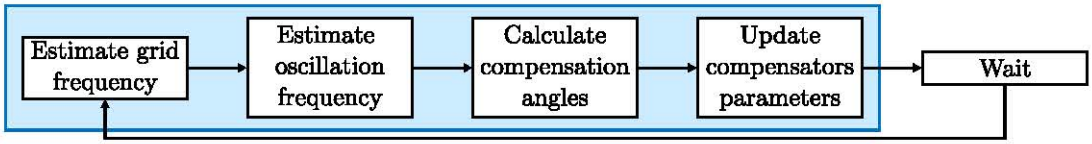

Figure 3.4: Online POD controller update procedure.

3.2.1 Design Objective

The design objective is to maximise the damping effect of the CIG at ω_o. To formulate this objective using a standard notation, the open-loop ($G(s)$) and closed-loop ($F(s)$) transfer functions are defined [Ogata, 2010]. From Fig. 3.2:

$$F(s) = \frac{G(s)}{1 + G(s)}, \tag{3.1}$$

where $G(s)$ is the transfer function from point J to point M in Fig. 3.2. As the signals involved would be of a specific frequency (ω_o), the design criteria selected is to maximise the closed-loop gain at ω_o. This can be written as:

$$\max |F(j\omega_o)| = \max \left| \frac{G(j\omega_o)}{1 + G(j\omega_o)} \right|, \tag{3.2}$$

where

$$G(j\omega_o) = A_G e^{j\phi_G}. \tag{3.3}$$

Condition (3.2) can be simplified as follows:

$$\max |F(j\omega_o)| = \max \frac{A_G}{|1 + A_G e^{j\phi_G}|}. \tag{3.4}$$

The value of A_G is the system gain so it is considered constant (in real applications, it will be limited by practical design criteria). Then, it is clear that the maximum value in (3.4) is obtained for $\phi_G = 0$. This means that the lead-lag compensator must compensate all the phase introduced by the rest of the elements at ω_o. This criteria does not actually guarantee the maximum damping for the closed-loop eigenvalues of the system. However, it greatly improves the system damping with a clear physical meaning, so it is commonly used in the literature [Kundur et al., 1994]. Furthermore, for the system with several modes with the same frequency, the criteria defined in (3.4) would contribute to the overall damping of those modes. On the other hand, if the system has several poorly damped modes in the low-frequency range, the criteria from (3.4) needs to be extended. This case will be addressed in Chapters 4 and 5.

3.2.2 Controller Definitions

The open-loop transfer function includes the active and reactive power action, and it is defined as:

$$G(s) = G_p(s) + G_q(s), \tag{3.5}$$

where

$$G_p(s) = H(s)K_pC_p(s)P_p(s), \tag{3.6}$$
$$G_q(s) = H(s)K_qC_q(s)P_q(s). \tag{3.7}$$

The transfer functions $G_p(s)$ and $G_q(s)$ represent the relation between the active and the reactive power injections, and the frequency (in Fig. 3.2, from point J to K, and from point J to L, respectively). From now on, subscript p refers to active power while subscript q refers to reactive power, $C(s)$ means phase compensator and $P(s)$ means plant. The transfer function $H(s)$ represents a high-pass filter.

The lead-lag compensators are defined as:

$$C_p(s) = \left(\frac{1+sT_1}{1+sT_2}\right)^{n_p}, \tag{3.8}$$
$$C_q(s) = \left(\frac{1+sT_3}{1+sT_4}\right)^{n_q}, \tag{3.9}$$

where T_{1-4} are time constants, and n_p and n_q represent the number of compensators. The high-pass filter is defined as:

$$H(s) = s/(s + 1/T_h)), \tag{3.10}$$

where T_h is used to control the filter bandwidth.

3.2.3 Lead-Lag Controller Design

The lead-lag compensator is designed to adjust the phase ϕ_G, which can be calculated as follows:

$$\underbrace{A_G e^{j\phi_G}}_{G(j\omega_o)} = \underbrace{A_{Gp} e^{j\phi_{Gp}}}_{G_p(j\omega_o)} + \underbrace{A_{Gq} e^{j\phi_{Gq}}}_{G_q(j\omega_o)}, \tag{3.11}$$

where A will be used from now on to represent the magnitude of a complex number, while ϕ will represent its phase. Fig. 3.5 shows a graphical representation of (3.11) in the form of a vector diagram. It can be seen that the design criteria $\phi_G = 0$ can be met by choosing any combination of $G_p(j\omega_o)$ and $G_q(j\omega_o)$ that results in $\mathrm{Im}\left\{G(j\omega_o)\right\} = 0$. However, from Fig. 3.5, it is clear that for a fixed value of A_G, $|F(j\omega_o)|$ is maximised if:

$$\phi_G = \phi_{Gp} = \phi_{Gq} = 0. \tag{3.12}$$

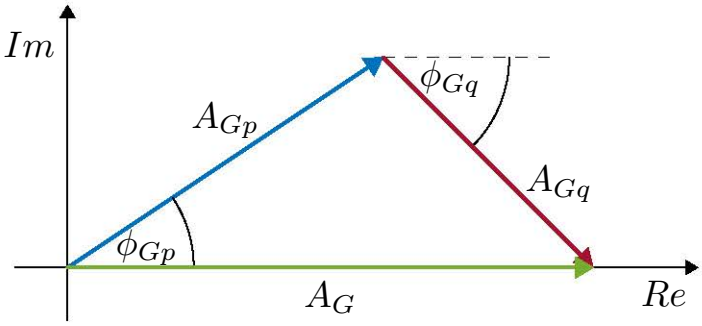

Figure 3.5: Vector diagram representation of $G(j\omega_o)$.

This mathematical condition yields an evident result: the active (reactive) power controller should compensate for the phase of the active (reactive) power plant. Furthermore, it means that the controllers in the active and reactive power loops are designed independently. Nonetheless, the positive combined control action of both controllers relies on the superposition theorem of linear control systems [Ogata, 2010].

As in (3.11), the frequency response of $G_p(s)$ and $G_q(s)$ at ω_o is obtained:

$$\underbrace{A_P e^{j\phi_P}}_{G_p(j\omega_o)} = \underbrace{A_H e^{j\phi_H}}_{H(j\omega_o)} \cdot K_p \cdot \underbrace{A_{Cp} e^{j\phi_{Cp}}}_{C_p(j\omega_o)} \cdot \underbrace{A_{Pp} e^{j\phi_{Pp}}}_{P_p(j\omega_o)}, \tag{3.13}$$

$$\underbrace{A_Q e^{j\phi_Q}}_{G_q(j\omega_o)} = \underbrace{A_H e^{j\phi_H}}_{H(j\omega_o)} \cdot K_q \cdot \underbrace{A_{Cq} e^{j\phi_{Cq}}}_{C_q(j\omega_o)} \cdot \underbrace{A_{Pq} e^{j\phi_{Pq}}}_{P_q(j\omega_o)}, \tag{3.14}$$

where subscripts Cp and Cq refer to the compensators, while Pp and Pq refer to the active and reactive power plants, respectively.

3.2.4 Controller Limits

Recalling that p_r and q_r are the active and reactive powers requested by the operator, the active and reactive power limits of the CIG can be calculated as follows:

$$p_l = k \cdot p_r, \tag{3.15}$$

$$q_l = \sqrt{S_{cn}^2 - (p_l + p_r)^2} - q_r, \tag{3.16}$$

where $k \in [0, 1)$ is a predefined active-power margin available from the primary source to provide damping services. In this section, the method to adapt the POD controller is described. First, an offline simulation is conducted and the adaptive characteristic is defined. Then, the procedure to update the POD controller parameters is introduced.

3.2.5 Controller Gain

The controller proportional gains K_p and K_q are designed following the two-step method. First, the system performance is analysed for different values of the

proportional gain. This allows for determining the gain value for which the damping of the system reaches a maximum. Then, to determine the final value of the controller gains, the system performance is verified using transient analysis. This approach is a compromise between improving the controller damping performance and ensuring robustness for different operating points.

3.3 Adaptive POD Controller

The lead-lag design criteria obtained in (3.12) can be applied to (3.13) and (3.14). Then, the following results are obtained:

$$\phi_{Cp} = -\phi_H - \phi_{Pp}, \tag{3.17}$$

$$\phi_{Cq} = -\phi_H - \phi_{Pq}. \tag{3.18}$$

This result means the compensators would compensate for the phase of the plant plus the phase of the high-pass filter (i.e., the open-loop phase). The phase that needs to be compensated can be in the range ± 180 degrees. However, the maximum phase shift introduced by one lead-lag is limited to ± 90 degrees. Therefore, the compensator is formed by two identical lead-lag compensators connected in series. This can be defined as:

$$n_p = n_q = 2. \tag{3.19}$$

The design of the gain of the compensator is simpler compared to the phase. Here, only the gain introduced by the high-pass filter is compensated. Then:

$$A_{Cp} = A_{Cq} = 1/A_H. \tag{3.20}$$

With these specifications selected, the parameters are calculated as follows [Ogata, 2010]:

$$T_1 = (\tan \phi'_{CP} + 1/\cos \phi'_{CP})/\omega_o, \tag{3.21}$$

$$T_2 = T_1 \cdot (1 - \sin \phi'_{CP})/(1 + \sin \phi'_{CP}) \tag{3.22}$$

$$T_3 = \tan \phi'_{CQ} + 1/\cos \phi'_{CQ}, \tag{3.23}$$

$$T_4 = T_3 \cdot (1 - \sin \phi'_{CQ})/(1 + \sin \phi'_{CQ}). \tag{3.24}$$

3.3.1 Off-Line Analysis

Network Reconfiguration Aspects

In [Klein et al., 1991], it was found that changes in the impedance of the tie-line between areas have a high impact on the frequency of the inter-area oscillation. This scenario happens when one line is disconnected after a fault. Another aspect that affects the

frequency of the oscillation is variations in the system's inertia. This scenario typically takes place when available renewable sources replace conventional generators in the generation mix that are then disconnected. Furthermore, the network reconfiguration causes the change in the POD controller plant, modifying the plant phase at oscillation frequency. Thus, the POD controller settings become inaccurate, deteriorating the damping performance. The impact of the network reconfiguration on the plant phase is addressed in the following sections.

Analysis of Active and Reactive Power Dynamics

The aim of this section is to find the relationships between the oscillation frequency (ω_o) and the phases that will be addressed by the lead-lag filters (ϕ_{Pp} and ϕ_{Pq}), within the frequency range of interest [Rogers, 2012]. Changes in the interconnecting lines (l_1, l_2, and l_3 in Fig. 3.1) and reductions in the inertia of generators will be applied. For each modification in the system topology, the following steps need to be taken:

1. First, the network model is modified. Then, a three-phase fault is applied and cleared in the area formed by generators G_3 and G_4, at point F in Fig. 3.1. The system response includes the inter-area oscillation, in which the frequency of the oscillation should be detected. For that purpose, the zoom-FFT algorithm is used [Lyons, 2004].

2. Then, the challenge is to find the angle to be compensated, and for that purpose, the phase of the plant at ω_o (ϕ_{Pp} and ϕ_{Pq}) should be calculated. The system is perturbed by using the CIG power references, depicted as points P and Q in Fig. 3.1. The disturbance signal is a sinusoidal of frequency ω_o that is applied in the active and reactive power references, consequently. When the simulation reaches steady-state, the angle between the sinusoidal disturbance input and the output is measured, thus obtaining ϕ_{Pp} and ϕ_{Pq} (in two separate simulations). This process is programmed in a script so it does not require manual actions.

Fig. 3.6 (a) and Fig. 3.6 (b) show the estimated phases for the aforementioned network changes. Both phases mainly decrease when the impedance of the tie-line increases (circles) and when the system inertia decreases (squares). In Fig. 3.6 (b), the linear relationship between ϕ_{Pq} and ω_o is clear. There is also a relation between ϕ_{Pp} and ω_o, although it is not as clear as for ϕ_{Pq}. It can be seen that the modification in tie-line resulted in a linearly descending angle ϕ_{Pp}, while modification in the generators inertia resulted in a non-linear relation between ϕ_{Pp} and ω_o.

Fitting the Phase-Frequency Functions

The results obtained in the previous section are used here to fit $f_p(\omega_o)$ and $f_q(\omega_o)$. For simplicity, a linear function has been considered here, although different curves may be

used here:

$$f_p(\omega_o) = m_p \cdot \omega_o + r_p, \tag{3.25}$$

$$f_q(\omega_o) = m_q \cdot \omega_o + r_q, \tag{3.26}$$

where m and r refer to the slope and constant values of the straight line. For fitting the values, any method can be used (e.g., minimum squares). The resulting functions are depicted in Fig. 3.6 (a) and Fig. 3.6 (b), in green.

3.3.2 Real-Time Operation

The calculation of functions $f_p(\omega_o)$ and $f_q(\omega_o)$ require only basic mathematical operations. Therefore, these functions can be simply implemented in local controllers. The practical implementation is shown in Fig. 3.2 (b). Firstly, the frequency of the oscillation is estimated by using the zoom-FFT algorithm. This algorithm was selected for its precision and low computational requirements, which makes it suitable

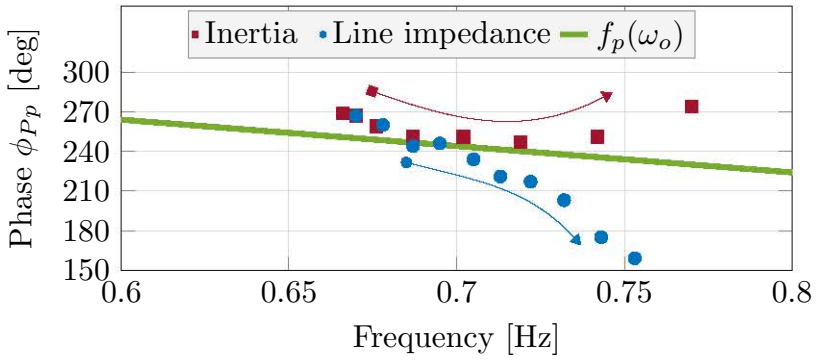

(a)

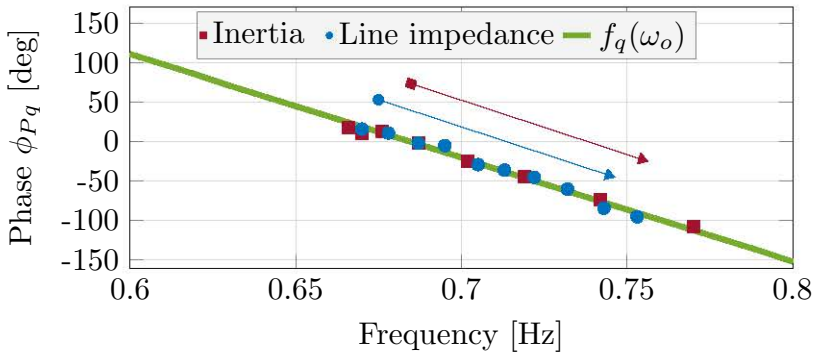

(b)

Figure 3.6: Simulation results: Phase angle that needs to be compensated by the (a) active-power POD (ϕ_{Pp}) (b) reactive-power POD (ϕ_{Pq}) when the oscillation frequency (ω_o) changes. Variation of (squares) inertia and (circles) line impedance values. (green) Line representing $f_q(\omega_o)$.

for real-time implementations. Nonetheless, the oscillation frequency can be estimated using other estimation techniques. Also, such information could be extracted from ambient data, by analysing the frequency content of measured currents and voltages. Furthermore, the proposed implementation is suitable for systems with oscillations in the low-frequency range. If the system faces oscillations at higher frequencies, the proposed method could be connected with methods used for detecting subsynchronous oscillations [Shair et al., 2022].

Once ω_o is estimated, it is used to calculate compensation angles, ϕ_{Cp} and ϕ_{Cq}. Finally, the parameters of the lead-lag compensators are adjusted to achieve new compensation angles following the procedure described in Section 3.2.3. It should be noted that the phase introduced by additional elements in the loop should also be compensated by the lead-lag compensators (e.g., if additional low-pass filters are applied). Also, the modification of the control parameters leads to a sudden increase or decrease in the power references. However, the limiters p_l and q_l would ensure that the final command signals do not exceed the allowed limits.

3.4 Experimental Results

The performance of the POD controller was verified in a laboratory setup, described in Appendix A.2. The CIG-based power-plant is modeled with installed power of 100 MVA in the emulated power system model, with a nominal voltage of 20 kV. The power-plant consists of four actual hardware CIG units, with nominal power $S_n = 15$ kVA and nominal voltage of $V_n = 400$ V. Therefore, the scaling factors between the PHIL environment and emulated power system model are $K_s = 1.66 \cdot 10^3$, $K_v = 0.02$ and $K_i = 33.3$ (see Appendix A.3 for more details).

The laboratory verification was conducted to address several points. First, the robustness of the adaptive mechanism against high-frequency noise is of interest. Namely, in the laboratory system, such noise is always present due to high switching frequency. If the adaptive mechanism is affected by the noise, POD controller parameters would be updated constantly, increasing the probability of real-time computer calculation failures. Also, the precision of real-time calculations with sudden and large changes in POD controller parameters might result in arithmetic overflows, leading to disconnection of the CIG unit. Therefore, it is of interest to verify the performance of the POD controller in which the parameter values are being updated with changes in the network configuration. The results from several experiments are presented in the following sections.

Active Power, Reactive Power and Combined POD Controller

In this section, the proposed POD controller was tested without the adaptive mechanism applied and was designed following the procedure described in Section 3.2. For this scenario, the oscillation frequency of the system was 0.64 Hz. The frequency responses of $P_p(j\omega_o)$ and $P_q(j\omega_o)$ were measured by perturbing the system at f_o. Then, from (3.17) and (3.18) the compensation angles were calculated. The POD controller parameters and CIG operating point are summarized in Table 3.1. Then, the controller proportional gains were calculated so that they do not saturate when a transient takes place. More advanced criteria can be used for the design of the gains, but this is not explored here.

Fig. 3.7 (a) shows the transient response of the grid frequency for three test cases. In (blue) only active power is used, in (red) only reactive power, and in (green) both powers are used simultaneously. In addition, the injected active and reactive power during the transient from one CIG are shown in Fig. 3.7 (b) and Fig. 3.7 (c), respectively. In all three cases, the system damping improved compared to the case without the POD controller (in gray). It can be seen that the best damping was achieved for the case in which both powers active and reactive were used. This can be verified in Fig. 3.8, where the most critical eigenvalues (those related to the inter-area oscillation) obtained in the experimental verification are shown. These eigenvalues were identified by applying a pseudo-random binary signal (PRBS) to the command of the power references and then by estimating the system model and its eigenvalues. In (gray), the critical eigenvalue without any POD controller is shown, in (blue) with the POD controller only acting with active power, in (green) only with reactive power, and in (red) with both power components. Without the POD controller, the critical eigenvalues had a natural frequency of 4.05 rad/s and a damping factor of 0.016. For the POD controllers based only on active and reactive power, the eigenvalues clearly move away from instability. However, the combined action of both power components gave the best results, and a damping factor of 0.067 was obtained.

Network Reconfiguration

In order to validate the benefits of the proposed adaptive mechanism, a representative scenario in which an inter-area oscillation appears was selected. In this scenario, the inertia constant of generators G_1 and G_3 was reduced by 10 %, while the reduction was 15 % for generators G_2 and G_4 (see Fig. 3.1). Furthermore, the proportional gain of

Table 3.1: POD Controller Parameters on CIG unit base.

Parameter	T_h [s]	p_r [pu]	q_r [pu]	p_l [pu]	q_l [pu]	K_p [pu]	K_q [pu]
Value	2	0.32	0.47	0.16	0.4	60	60

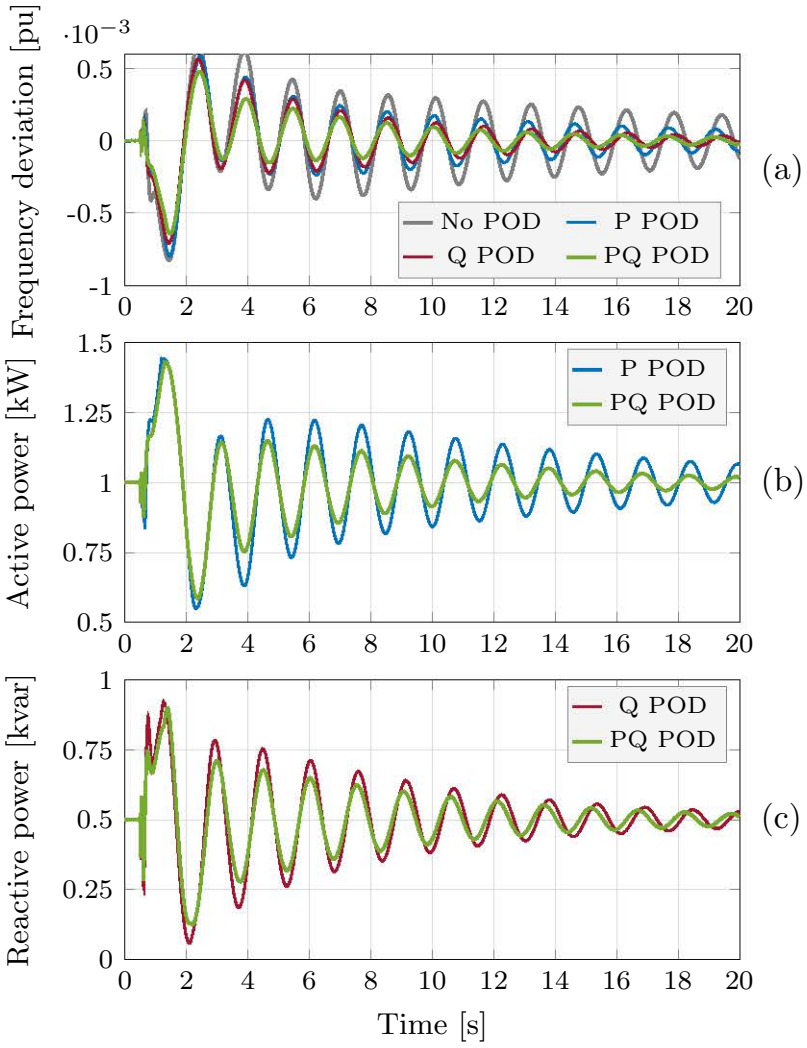

Figure 3.7: Experimental results. (a) Frequency deviation, (b) active and (c) reactive power injected by the CIG units. The meaning of colours is marked in the legends.

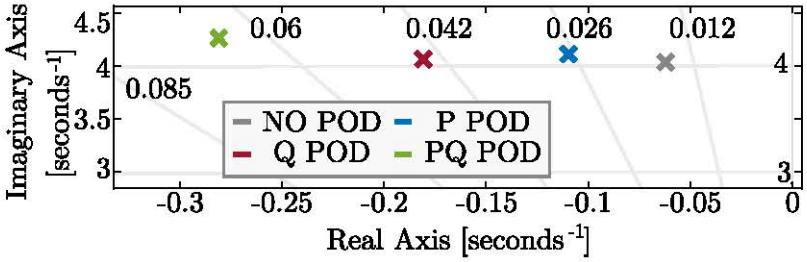

Figure 3.8: Experimental results. Critical eigenvalue identified for the POD controller options. (gray) No POD controller, (blue) only active power, (green) only reactive power and (red) active and reactive power.

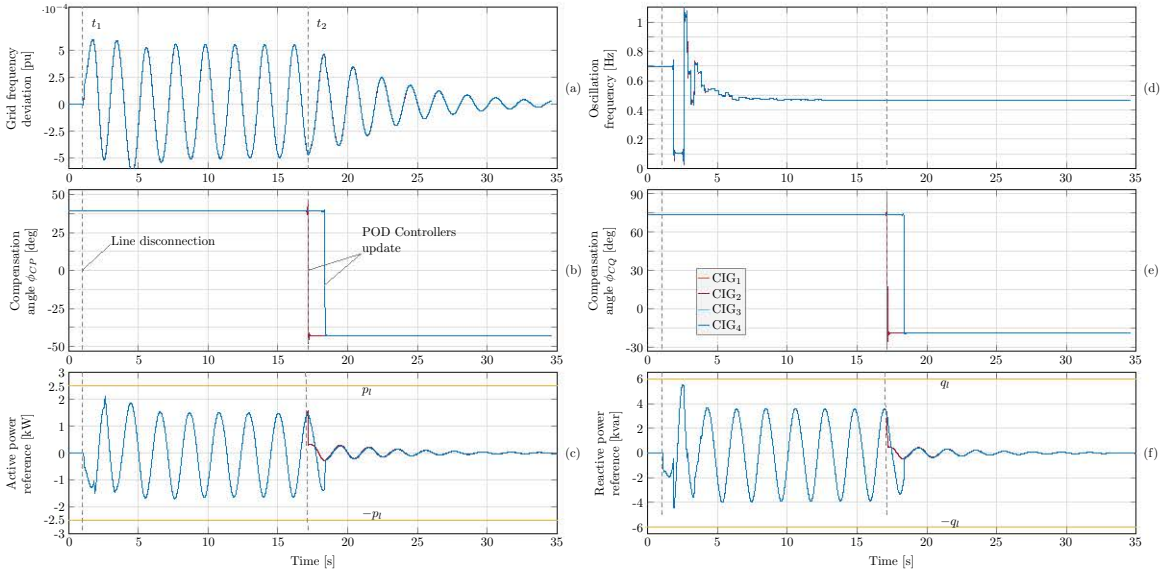

Figure 3.9: Experimental results. Transient response of (a) the grid frequency, (b) active and (c) reactive power when one line is disconnected and the adaptive mechanism is applied. (d) Compensation angles calculated in real-time. (e) Active and (f) reactive power references.

PSS in G_2 was reduced by 33 % in order to make the system marginally stable after the disconnection of a line (the remaining three generators did not include PSS, see Section 3.1.1 for details). The main objective of this change was to demonstrate the benefits of the proposed control technique. To do so, the adaptive characteristics were defined from the system prior to and after the disconnection of a line. Table 3.2 gives a summary of calculated adaptive characteristics parameters for both $f_p(\omega_o)$ and $f_q(\omega_o)$. The unit of both n, and m is [degree/Hz].

This scenario can be explained using Fig. 3.9 (a). In this scenario, the system was initially stable and the CIG-based power plant was designed to provide the maximum damping by using both active and reactive power injection. Eventually, tie-line l_3 (see Fig. 3.1) was disconnected at $t_1 = 1$ s and then the system was very close to instability. This happens because the system dynamics changed significantly and the original POD controller cannot guarantee adequate system damping. This change in the system topology also caused a shift in the oscillation frequency.

Table 3.2: Experimental results. Adaptive characteristics parameters.

	$f_p(\omega_o)$	$f_q(\omega_o)$
n	352.17	400
m	-42.46	-19.46

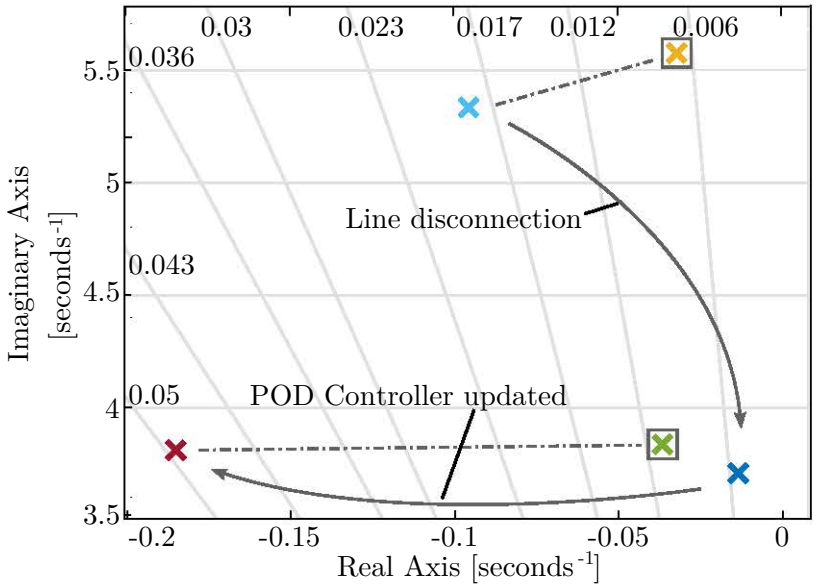

Figure 3.10: Experimental results. System eigenvalues for the system reconfiguration. (light blue) Initial state, (dark blue) after the line disconnection and (red) once the controller is adapted. (yellow, green) Initial and final states without POD controller.

During the first three oscillation periods, the FFT algorithm was estimating the oscillation frequency, and the new value was determined after approximately 6 seconds (Fig. 3.9 (b)). Then, the compensation angles updated according to $f_p(\omega_o)$ and $f_q(\omega_o)$ (instant t_2). These curves were calculated according to the realistic elements included in the laboratory (additional delays and filters, etc.) so they have differences compared to those shown in Fig. 3.6 (a) and 3.6 (a). It can be observed that the angles of all the CIG units were not updated at the same time. This happens because they are operated independently and, therefore, their controllers are not synchronised (Fig. 3.9 (c, d)). After instant t_2, the transient response shows that the sustained oscillation was clearly damped due to the action of the adaptation mechanism. The modification can also be seen in the active and reactive power references, in Fig. 3.9 (e) and (f), respectively. In both references, the adjusted parameters resulted

Table 3.3: Experimental results. Parameters change during network reconfiguration, on CIG base.

	$C_P(s)$		$C_Q(s)$	
Parameter	Before	After	Before	After
$T_1[s]$	0.48	0.15	1.54	0.24
$T_2[s]$	0.1	0.76	0.034	0.47

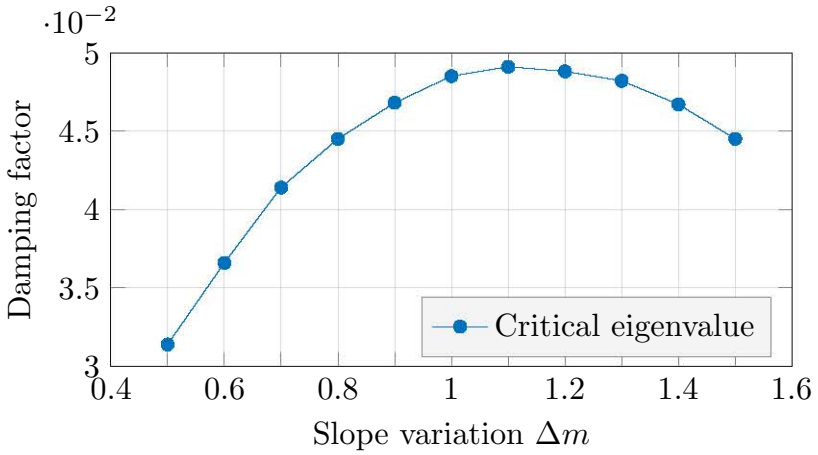

Figure 3.11: Experimental results. Damping of the most critical identified mode when the slope of the adaptive characteristic is modified.

in a sudden decrease in the signal amplitude. Fig. 3.10 shows the system eigenvalues for the aforementioned scenario. In (light blue), the system damping before the event is shown. It can be seen that the system was well-damped. Then, in (dark blue), the line was disconnected and the mode moved towards the imaginary axis, while the oscillation frequency clearly decreased. Finally, in (red), when the controller was updated, the system became well-damped again. For completeness, in (yellow, green) the system eigenvalues in the original and final states are shown, but without any POD controller. It can be seen that in these cases the system was not well damped.

Table 3.3 shows the change in the POD controllers parameters caused by the network reconfiguration. These parameters are calculated from (3.24) once the new oscillation frequency is detected and the new compensation angles are estimated.

Robustness of Adaptive Mechanism

To explore the robustness of the proposed method with respect to the selection of functions $f_p(\omega_o)$ and $f_q(\omega_o)$, the values of the slopes were intentionally modified. Fig. 3.11 shows the damping of the most critical eigenvalue for the variations of the slope, $\Delta m = m/m_s$ (the same for P and Q), where m_s was the original slope. It can be seen that for variations between 1.5 and 0.5, the damping still remained larger than 0.04. However, the damping rapidly decreased if Δm was lower than 0.5. The effect of the slope and the selection of the curve is relevant, and its selection greatly depends on the system topology. Therefore, exploring this for different power system topologies is of interest for further research.

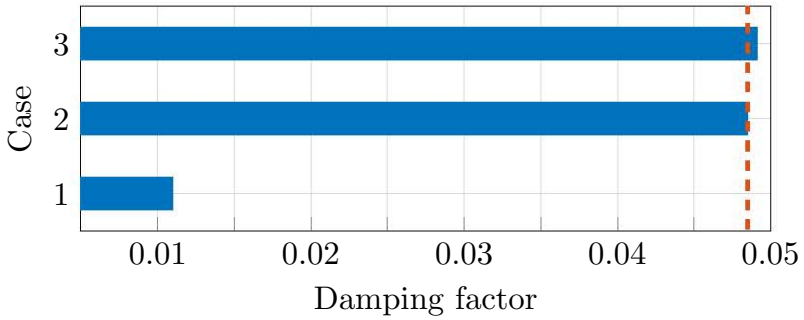

Figure 3.12: Experimental results. Damping of the most critical identified mode (1) without POD controller, POD controller design (2) with the proposed method, and (3) for the maximum damping.

3.5 Comparison with Other Methods for POD Controller Design

In the literature, the POD controllers are often designed with a focus on maximising the damping factor of the critical mode. To do so, either a single-objective [Khadanga and Satapathy, 2015] or multi-objective [Ali, 2014] optimisation functions can be defined. These objectives are defined as minimising the mode with the largest damping factor value [Eslami et al., 2014] or maximising the mode with the lowest damping ratio [Mary Linda and Kesavan Nair, 2013]. Also, these objectives can be merged to define the expected values for both the damping ratio and factors of dominant modes [Rahmatian and Seyedtabaii, 2019]. Fig. 3.12 shows the damping factor of the critical mode for three cases. *Case 1* represents the case without the POD controller, while the POD controller is included in *Case 2* and *Case 3*. In *Case 2*, the POD controller was designed with the procedure presented in this work. Then, in *Case 3*, the controller was designed for the maximum damping factor. It can be seen that if the POD controller compensates the open-loop phase shift the achieved damping factor is not at the maximum. However, it is very close to it while the analytical solution is easy to obtain.

3.6 Chapter Summary

In this chapter, a POD controller for CIG units that uses both active and reactive power has been presented. This controller maximises the capability of CIG units to damp oscillations and offers parameter adaptation when a change in the network dynamics is detected. Possible network changes are analysed offline and the value of each oscillation frequency is linked then with the angle that needs to be compensated by the active and

reactive power controllers. The information from the offline analysis is then applied in real time to adapt the POD controller. Theoretical derivations were validated in the PHIL setup. Nonetheless, the design of a POD controller with an adaptive mechanism for a system with multiple low-frequency modes and its verification on a larger system requires further research efforts.

Chapter 4

Multi-Mode *Robust* POD Controllers for CIG Units Operating in Grid-Following Mode

This chapter describes a POD controller with a fixed structure and set of parameters that is robust against network reconfiguration. Section 4.1 gives an overview of the system and POD controller structure. Section 4.2 describes the network analysis procedure in which the effect of changing the system parameters is explored. The POD controller structure and the design procedure are described in Section 4.3. Then, the results obtained in the network analysis and the validation of the POD controller are presented in Section 4.4. Section 4.5 gives the conclusion of this chapter.

4.1 System Overview and Methodology

4.1.1 System Description

Fig. 4.1 shows the diagram of the power plant and the electrical system studied in this chapter. It can be divided into three main parts. The first part is depicted in Fig. 4.1 (a) and represents a model of a transmission network formed by ten generation units (G_1 to G_{10}). Each generation unit includes an SG with a governor, an exciter and a PSS. This model represents the IEEE 39 Bus network that is widely used as a benchmark network for inter-area oscillation studies [IEEE, 2015a]. In this work, two modifications are made to the original model. First, several PSS are adjusted to reduce the damping of certain modes while keeping the system stable. The second one is an additional POC at bus 29 (see Fig. 4.1 (a)), which is used to connect a CIG-based power plant.

Fig. 4.1 (b) shows the electrical diagram of two additional CIG units that represent the power plant. It consists of two CIG units that are used to connect the primary

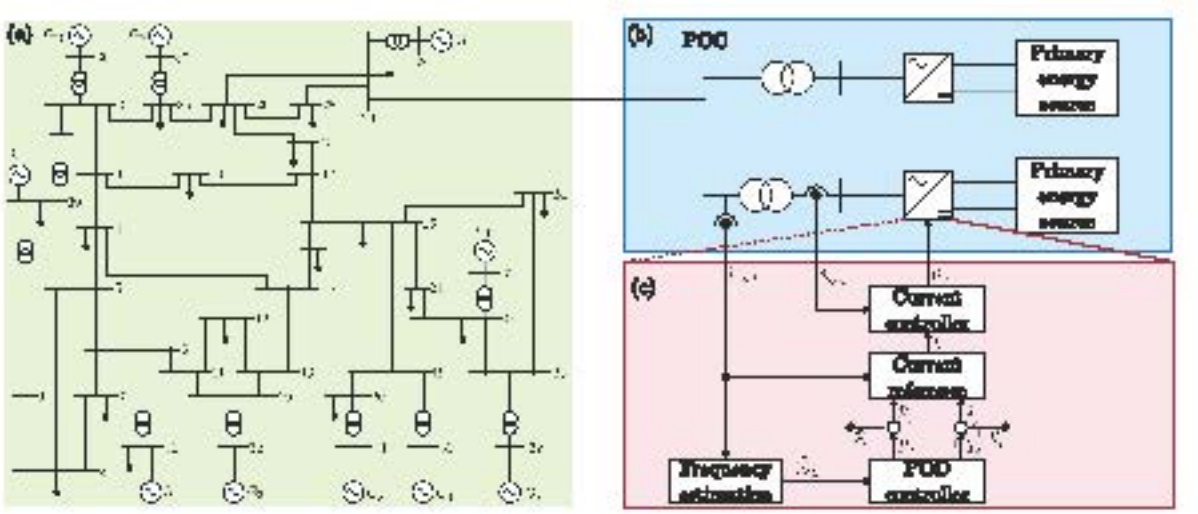

Figure 4.1: Diagram of (a) IEEE 39 bus network, (b) CIG-based power plant and (c) control diagram for one CIG.

energy sources to the network. These converters are connected to the POC via step-up transformers. The output current (i_{out}) and voltage (v_{out}) are measured and used in the control algorithm.

Fig. 4.1 (c) shows the control algorithm for one converter. First, the grid frequency ($\hat{\omega}_g$) is estimated from the voltage measurements. Then, the POD controller acts upon changes in the estimated frequency and produces references of active (p_d) and reactive (q_d) powers. The total power references (p_s and q_s) are calculated by adding the POD controller references and the references sent by the system operator (p_r and q_r). The power references are then converted to current references for the current controller by taking into account the grid voltage at the POC (v_{out}). Finally, the current controller defines the converter output voltage reference (v_s).

4.1.2 POD Controller Overview

Fig. 4.2 shows a block diagram of a small-signal representation of the system. The POD controller block diagram is depicted in Fig. 4.2 (a) and the plant models are depicted in Fig. 4.2 (b). In the plants, active and reactive powers are considered as inputs and the frequency is considered as an output. The POD controller includes several elements. The compensators $C_p(s)$ and $C_q(s)$ consist of a series of lead-lag filters. Besides those, a band-pass filter, proportional gains and saturation blocks are added. First, the band-pass filter is acting upon deviations of estimated network frequency ($\Delta\omega_g$). This means that it removes components of $\Delta\omega_g$ outside the frequency range of interest. Then, the lead-lag filters compensate the open-loop phase of the plant in order to maximise the damping action of the POD controller. The outputs of these controllers are active (p_s) and reactive (q_s) power references. The gains K_p and K_q

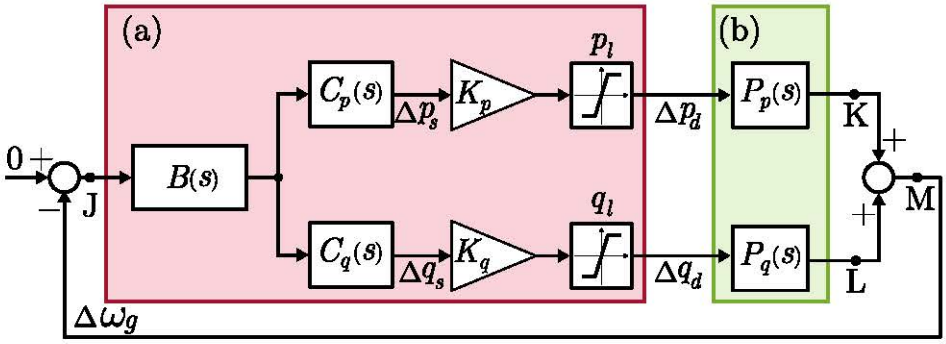

Figure 4.2: Block diagram representation of (a) POD controllers and (b) plant models.

define the proportional action. Finally, the limiting actions of saturation blocks in the active (p_l) and reactive (q_l) powers ensure the capabilities of the power plant are not exceeded. This procedure produces the active (p_d) and reactive (q_d) power references for POD.

4.1.3 POD Controller Design Methodology

Fig. 4.3 shows a flow diagram of the proposed procedure for designing network-reconfiguration-aware POD controllers. This procedure is divided into three routines, which are described in the following sections.

Network Analysis

The network analysis is used to understand how the plants $P_p(s)$ and $P_q(s)$ change when the network is reconfigured. This routine is depicted in Fig. 4.3 (a). First, the set of modifications that will be considered during the design procedure should be defined. In this work, these modifications include the original network topology with each of the electrical lines disconnected, one by one. This set of modifications can be extended to include cases such as loss of generation units or loads in the network. Furthermore, the set of modifications can include changes in the network loading conditions or system operating point. Such changes can emphasise nonlinear properties in the system. Thus, these changes can be used to study the system's dynamic properties, which might not be observed with changes in the network configuration. These cases are also of interest, but they will not be addressed here for simplicity. The next step in the plant analysis is to apply a series of network modifications and obtain the frequency response of $P_p(s)$ and $P_q(s)$, for each configuration. These transfer functions can be obtained from a detailed small-signal model. However, if small-signal models are not available, $P_p(s)$ and $P_q(s)$ can be obtained by using system identification techniques [Jankovic et al., 2023e]. Once these models are obtained, the peaks in the frequency response (i.e., resonance

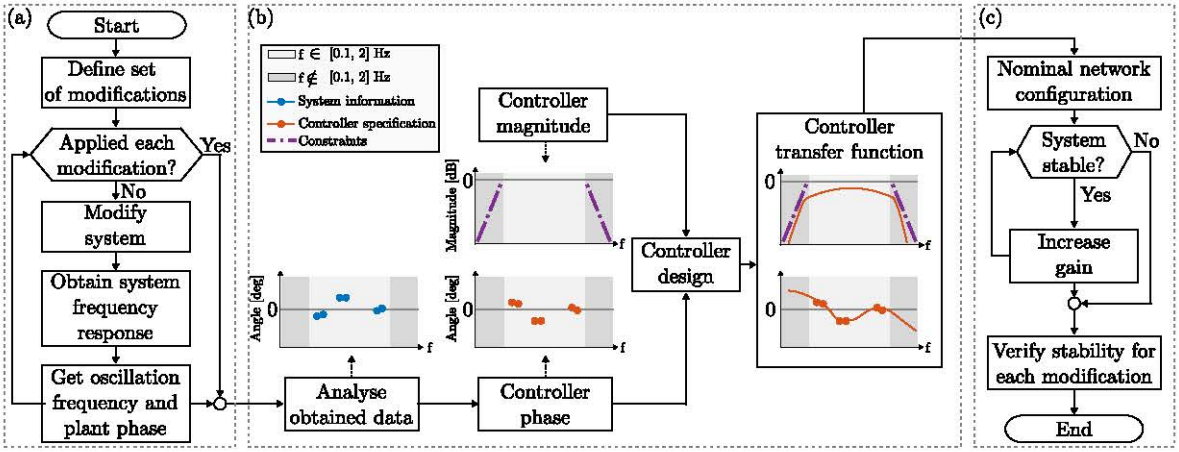

Figure 4.3: Procedure for the design of network-reconfiguration-aware POD controller. (a) Network analysis, (b) design of compensators, and (c) proportional gain design.

frequencies) are extracted. The phases at the frequencies of the conflicting modes (i.e., phase to be compensated by POD controllers) are also calculated and stored. This procedure is repeated for each modification in the given set of modifications.

Compensator Design

This routine includes the steps for designing the POD controller compensator, and it is depicted in Fig. 4.3 (b). First, the information obtained in the previous routine is sorted and analysed. In this step, the modifications that cause a significant change in the system dynamics (e.g., loss of lines connected to the power plant) are neglected. The remaining set of information is used to define the desired phase of the POD controller frequency response. In addition, two constraints are added to shape the magnitude of the frequency response. These constraints specify the reduction of controller gain for the frequencies outside the frequency range of interest. While these constraints define the shape of the magnitude of the frequency response, the final values of controller magnitude will be defined once the proportional gain is selected (this is explained in later steps). The constraints for the magnitude of the frequency response of the controller are important when the system frequency response is obtained by using system identification techniques. In that case, the information about the system is determined by the characteristics of the perturbation signal. The perturbation signal is selected to obtain information within the frequency range of interest. Therefore, there is scarce information about the system dynamics outside the frequency range of interest. Then, the controller design is defined as an optimisation problem in which the error between the specified and obtained phases is minimised. The constraints for the optimisation problem are the aforementioned requirements for the magnitude.

Design Verification

The final routine for the design is depicted in Fig. 4.3 (c). First, the system stability is examined for the nominal network configuration (i.e., all lines connected) with the POD controller included. Then, the controller gains are modified and the system response is obtained. If the system encounters instability or any other practical reason that limits the controller gain (e.g., noise amplification, etc.), the iterative procedure is stopped. At this point, the final value of the magnitude of the controller frequency response is determined. Finally, the system stability is verified for all the possible network configurations.

4.2 Plant Analysis

During the system operation, the network topology changes every time a line in the system is disconnected. Such changes have an important impact on the dynamic properties of the network. In [Klein et al., 1991], it was shown that the change in the impedance of the lines affects to the frequency of low-frequency modes. In terms of frequency response, those changes have a two-fold effect [Jankovic et al., 2023e]. First, the changes in the frequency of critical modes are seen as changes in the oscillation frequency. This means that the peak in the magnitude of the frequency response occurs at different frequencies. The second effect is the change in the phase of the frequency response.

From the system definition in Fig. 4.2, the frequency responses of $P_p(s)$ and $P_q(s)$ can be defined as:

$$P_p(j\omega_{o,i}) = A_{Pp,i}e^{j\phi_{Pp,i}}, \tag{4.1}$$

$$P_q(j\omega_{o,i}) = A_{Pq,i}e^{j\phi_{Pq,i}}, \quad \omega_{o,i} \in \Omega, \quad i \in \mathbf{I}, \tag{4.2}$$

where ω_o represents the frequency of oscillations, whereas A and ϕ represent the magnitude and phase of the frequency response at ω_o, respectively. The set $\mathbf{I}$ defines the number of oscillation frequencies. From now, i refers to an element in the set $\mathbf{I}$. The set Ω represents oscillation frequencies of interest. Then, the phases of the plants at these frequencies (expressions (4.1) and (4.2)) are organised in corresponding sets as:

$$\Phi_{Pp,n} = [\phi_{Pp,1},\ \phi_{Pp,2},\ ...,\ \phi_{Pp,i}], \tag{4.3}$$

$$\Phi_{Pq,n} = [\phi_{Pq,1},\ \phi_{Pq,2},\ ...,\ \phi_{Pq,i}]. \tag{4.4}$$

Sets $\Phi_{p,n}$, $\Phi_{q,n}$ are calculated for each network configuration $\mathcal{C} = 1,\ 2,\ ...,\ C$, where C is the number of cases considered. From now on, n refers to an element in a given set of network configurations $\mathcal{C}$. Therefore, the set Ω_n should also bear the subscript n.

Next, the information from all modifications is organised and grouped as:

$$\mathbf{\Omega} = [\Omega_1,\ \Omega_2,\ ...,\ \Omega_n], \tag{4.5}$$

$$\mathbf{\Phi_{Pp}} = [\Phi_{Pp,1},\ \Phi_{Pp,2},\ ...,\ \Phi_{Pp,n}], \tag{4.6}$$

$$\mathbf{\Phi_{Pq}} = [\Phi_{Pq,1},\ \Phi_{Pq,2},\ ...,\ \Phi_{Pq,n}],\quad \forall n \in \mathcal{C}, \tag{4.7}$$

where $\mathbf{\Omega}$, $\mathbf{\Phi_{Pp}}$, and $\mathbf{\Phi_{Pq}}$ are sets that contain oscillation frequencies and phases for all the possible network configurations. To design the POD controllers, the values in the sets $\mathbf{\Phi_{Pp}}$ and $\mathbf{\Phi_{Pq}}$ will also include the phase shift introduced by additional filters added in the loop (for more details, see Section 4.3.1).

4.3 POD Controller Design

4.3.1 Controller Structure

A band-pass filter ($B(s)$) is applied to attenuate the signal content outside the range of low-frequency oscillations – $[0.1, 2]$ Hz. It consists of a high-pass and a low-pass filter connected in series, and it is defined as:

$$B(s) = \frac{s}{s + 1/T_h}\ \frac{1}{s/T_l + 1}, \tag{4.8}$$

where T_h and T_l are the time constants of the high-pass and the low-pass filters, respectively. The values of ω_h and ω_l are selected taking into account the frequency range of low-frequency oscillations. Consequently, these cut-off frequencies need to be selected so that $B(s)$ attenuates the signal frequency content outside the range of low-frequency oscillations. At the same time, $B(s)$ will introduce an additional phase shift into the system, which needs to be added to the sets $\mathbf{\Phi_{Pp}}$ and $\mathbf{\Phi_{Pq}}$ so that it is compensated by $C_p(s)$ and $C_q(s)$.

Compensators $C_p(s)$ and $C_q(s)$ consist of a set of lead-lag filters connected in series. $C_p(s)$ and $C_q(s)$ have the same structure and their parameters are defined following the same procedure. Thus, in the rest of the document, the developments are presented only for $C_p(s)$ (for simplicity). The controller $C_p(s)$ is defined as:

$$C_p(s) = \frac{1 + sT_1}{1 + sT_2} \cdot \frac{1 + sT_3}{1 + sT_4} \cdot ... \cdot \frac{1 + sT_{c-1}}{1 + sT_c}, \tag{4.9}$$

where $T_1 - T_c$ are the compensator time constants, whereas c represents the number of time constants.

The order of the compensator (4.9) should be selected, and it depends on two requirements. First, the requirements for the phase of $C_p(j\omega)$ are defined to compensate for a set of phases obtained in the plant analysis. This set of phases includes several

points with large phase differences across a narrow frequency range. Therefore, a low-order transfer function may lead to a large deviation between the required phase and the phase introduced by $C_p(j\omega)$. On the other hand, the results achieved with very high-order transfer functions would not necessarily result in significantly improved design performance. At the same time, higher-order transfer functions are typically difficult to implement in real-time [Lyons, 2004]. Thus, the order $C_p(s)$ represents a compromise between these two considerations.

4.3.2 Design Objective

The method used to design the POD controllers is based on the phase compensation of the open-loop plant at the frequency of interest [Ogata, 2010]. The open-loop transfer function ($G(s)$) is defined as a transfer function from point J to point M, in Fig. 4.2. Analytically, the compensation objective can be written as:

$$\phi_G = 0, \tag{4.10}$$

where

$$G(j\omega_o) = A_G e^{j\phi_G}. \tag{4.11}$$

It has already been shown that this design method provides a system damping that is close to the optimal value [Jankovic et al., 2021]. Also, as the design is based on open-loop characteristics, the calculation of the compensator parameters can be easily automatised.

Two open-loop transfer functions can be calculated from Fig. 4.2. These transfer functions represent the active ($G_p(s)$) and reactive ($G_q(s)$) power dynamics, and these are defined from point J to points K and L in Fig. 4.2, respectively. In [Jankovic et al., 2021], it has been shown that the criteria from (4.10) can be met by setting phases to zero for two open-loop functions separately:

$$\phi_{Gp} = \phi_{Gq} = 0, \tag{4.12}$$

where ϕ_{Gp} and ϕ_{Gq} are phases of $G_p(j\omega_o)$ and $G_q(j\omega_o)$, respectively.

To meet the objectives presented in (4.12), each controller ($C_p(s)$ and $C_q(s)$) should compensate the phase of its corresponding open-loop system at the oscillation frequency [Jankovic et al., 2021]. Taking into account multiple oscillation frequencies and changes caused by network reconfiguration, this criteria can be defined as (only the active power loop is shown):

$$\phi_{Gp}^{i,n} = \phi_{Cp}^{i,n} - \phi_{Pp}^{i,n} = 0, \qquad \forall i \in \mathbf{I},\ \forall n \in \mathcal{C}, \tag{4.13}$$

where $\phi_{Cp}^{i,n}$ is phase of $C_p(j\omega)$.

The criteria from (4.13) means that the controller $C_p(s)$ needs to compensate the phase of the corresponding plant for all oscillation frequencies and all network configurations. Such requirements are too strict, mainly for two reasons. First, the requirements for the phase of $C_p(j\omega)$ would include many points in a very narrow frequency range (0.1 to 2 Hz). Second, plants for different network configurations might have the same frequency of oscillation with different phases. Therefore, trying to fully compensate for the phase in all the cases is not a reasonable solution. Instead, an alternative function to design the compensator is proposed in the following section.

4.3.3 Optimisation Problem Definition

A cost function is defined based on the criteria presented in (4.13):

$$\min_{\mathbf{x}} \sum_{\substack{i\in\mathbf{I},\\ n\in\mathcal{C}}} \left|\phi_{Cp}^{i,n} - \phi_{Pp}^{i,n}\right|^e, \tag{4.14}$$

where

$$\mathbf{x} = [T_1, T_2, ..., T_c]. \tag{4.15}$$

The parameter e defines the error cost, and its value depends on the complexity of the optimisation problem. Namely, the change among elements $\phi_P^{i,n} \in \mathbf{\Phi_{Pp}}$ can be different depending on the results of the plant analysis. This change has a direct impact on the complexity of the problem in (4.14). Therefore, the parameter e is case-specific, and its value depends on two criteria. The first criteria is the allowed average error for the controller design. This error determines the performance of the controller in damping multiple modes for various network configurations. The second criteria is the maximum error allowed or any of the cases. Thus, the selection of the parameter e is a compromise between these two criteria.

4.3.4 Constraints

The solution of problem (4.14) defines the controller parameters based on the required phases in the frequency range of low-frequency oscillations. Nonetheless, once the controller is introduced into the system, it affects the rest of the frequencies outside this range. If not addressed, it may lead to unwanted interactions with other control layers. To address this issue, constraints are added to the optimisation problem. These constraints ensure that the controller impact outside the range of low-frequency oscillations is lower than within this range and are defined as:

$$c : \left|C_p(j\omega_{out})\right| \leq 1, \qquad \forall\ \omega_{out} \in \mathbf{\Omega_{out}}, \tag{4.16}$$

where $\mathbf{\Omega_{out}}$ is a set of frequencies defined as:

$$\omega_{out} \notin \left[0.1, 2\right] \cdot 2\pi\ rad/s, \quad \forall\ \omega_{out} \in \mathbf{\Omega_{out}}. \tag{4.17}$$

The constraints in (4.16) limit the magnitude of $C_p(j\omega)$. It is relevant to mention the POD controller gain (i.e., the gain in the range of interest) will be tuned in the last step of the design procedure (with K_p).

Another set of constraints is linked with the set of unknowns $\mathbf{x}$ in the optimisation problem (4.14). Namely, the unknowns in this problem are controller parameters. Thus, constraints for those parameters are necessary to guarantee that the transfer function $C_p(s)$ is stable. These constraints are defined as:

$$T_a > 0, \quad \forall \quad a \in \Big\{2, 4, 6, ...\Big\}. \tag{4.18}$$

4.3.5 Controller Gain

The controller gains (K_p and K_q) are determined based on the system frequency response, following the procedure from Fig. 4.3 (c). This procedure consists of two parts. In the first part, the system is analysed for the case when all the lines are connected. Gain values are changed incrementally and the system's closed-loop frequency response is observed. The information from this analysis describes the impact of the gains on the system stability margins. Such change results in improved damping of low-frequency modes. Nonetheless, after a certain point, the damping of one or more modes would decrease. Furthermore, as the gain increases, the impact of the POD controller outside the frequency range of interest is changing. The change can be seen as a decrease in stability margins below and above the frequency range, depending on the system characteristics. Therefore, the selection of the gain value takes into account different aspects of the controller's impact on the system stability.

The second part of the procedure includes the verification of system stability with the gain value selected in the first step. Here, the system stability is verified for all the network configurations using the selected gain value. For this purpose, the set of plants for different network configurations can be used. Since these plants are obtained in the plant analysis (Section 4.2), no additional identification procedures are required. If the system is unstable for any network configuration, the first step of the procedure for the gain value selection needs to be repeated and a different gain value should be selected.

4.3.6 Controller Limits

During transients, the converter delivers active and reactive powers for to damp oscillations. Depending on the amplitude of the frequency deviation, the power references from the POD controller can exceed the converter capacity. It is, therefore, necessary to define the active and reactive power limits (p_l and q_l). These limits are changing over time based on the network operating point and the available energy from the primary energy source. For simplicity, these limits are kept constant in this work (see Section 3.2.4 for more details).

4.4 Results

The CIG-based power-plant includes two CIG units, with a nominal power $S_n = 50$ MVA each, and a nominal voltage of $V_n = 20$ kVA. The remaining parameters of CIG units are given in Appendix C.1, whereas the transformer parameters are presented in Appendix C.3.

4.4.1 Plant Analysis

The model of the IEEE 39 Bus system is represented using an electro-mechanical model. The system information is obtained using the linearisation method with the *Simulink Control Design Linearization Toolbox* from Matlab [MATLAB, 2019]. The power system model obtained has 295 states (for more details, see Section 2.5.1. Fig. 4.4 (a) and Fig. 4.4 (b) show the changes of elements in $\mathbf{\Phi_{Pp}}$ and $\mathbf{\Phi_{Pq}}$ with respect to the elements

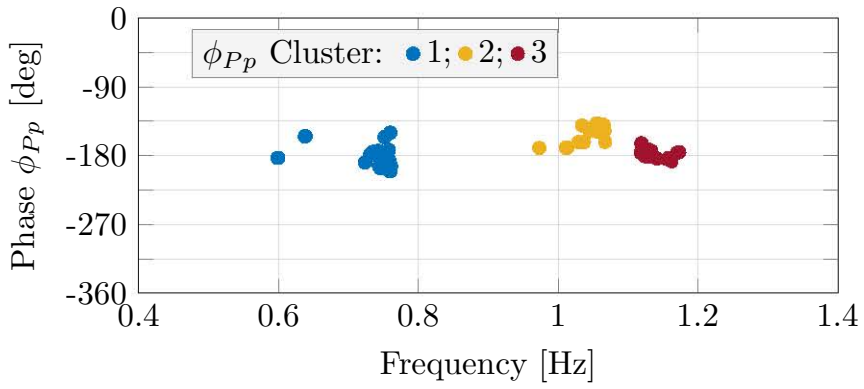

(a)

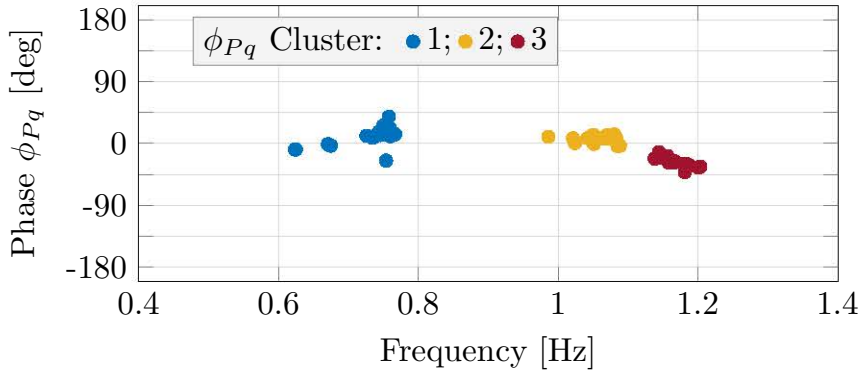

(b)

Figure 4.4: Phase of (a) $P_p(j\omega)$ and (b) $P_q(j\omega)$ for different network configurations. (blue, yellow, red) Clusters of points from three oscillation frequencies.

in $\mathbf{\Omega}$, for different network configurations. In both cases, three clusters of points are formed, which correspond to three different ranges of oscillation frequencies. These clusters are marked in blue, yellow and red in Fig. 4.4 (a) and Fig. 4.4 (b). Changes in each cluster describe how network reconfiguration affects to the interactions between different generators in the system. It can be seen that the angle and frequency variations differ between the clusters. Angles ϕ_P and ϕ_Q vary around 90 degrees while the frequency of oscillations varies in the range of 0.1 Hz.

4.4.2 Compensator Design

The compensators are designed by using the proposed method. The plant information obtained during the initial analysis was used. The optimisation problem (4.14) with constraints (4.16) is solved by using the *fmincon* function from Matlab [MATLAB, 2019]. The computational time required to design compensators $C_p(s)$ and $C_q(s)$ was 4.5 and 3.4 minutes, respectively. The optimisation problem was solved on desktop PC with *i5-8500* CPU with 8 GB RAM.

The optimisation problem (4.14) is solved using the parameter setting $m = 3$. The compensator design accuracy is verified using the error between the specified and the obtained phase of $C_p(j\omega)$ for all the elements in $\mathbf{\Omega}$. This error is defined as:

$$E_p^{i,n} = \left|\phi_{Cp}^{i,n} - \phi_{Pp}^{i,n}\right|, \qquad \forall i \in \mathbf{I},\ \forall n \in \mathcal{C}. \tag{4.19}$$

This error corresponds to the individual elements of the sum that is used to define the cost function (4.14). Thus, by minimising the cost function, the error $E_p^{i,n}$ is reduced.

Table 4.1 shows the mean and maximum errors for both compensators $C_p(s)$ and $C_q(s)$ when different compensator orders are used. For $C_p(s)$, it can be seen that the error is significantly reduced if a series of two lead-lag filters is used compared to the case with only one filter. Further increase in the number of lead-lag filters leads to a reduced design error, although the difference is not significant. Then, for $C_p(s)$ of

Table 4.1: Design errors E_p and E_q for different number of lead-lag filters.

Order	E_p		E_q	
	mean	max	mean	max
1	164	179	17	41
2	15	27	17	41
3	14	27	17	41
4	14	27	16	38
5	15	39	16	38
6	14	27	16	38

order five, the maximum error increases significantly, while the compensator of order six gives the same results as those of orders three and four. On the other hand, the error in $C_q(s)$ does not change significantly when the order increases. By increasing the order from one to three, the design error is not modified. Then, for orders four to six, the error changes, although the improvement is not significant. These results show that the relation between the compensator order and the design error is nonlinear. Therefore, the order of the compensator transfer function should be selected carefully upon determining the relation between the error and the compensator order. Based on the analysis, the orders for $C_p(s)$ and $C_q(s)$ are set to 3 and 4, respectively.

Table 4.2 shows the time constants of lead-lag filters used in $C_p(s)$ and $C_q(s)$, for the selected configuration. For $C_q(s)$, there are three lead-lag filters with similar parameters, although the optimisation problem did not have such specifications. However, this result can be expected and it is similar to the common practice in designing PSS for SGs.

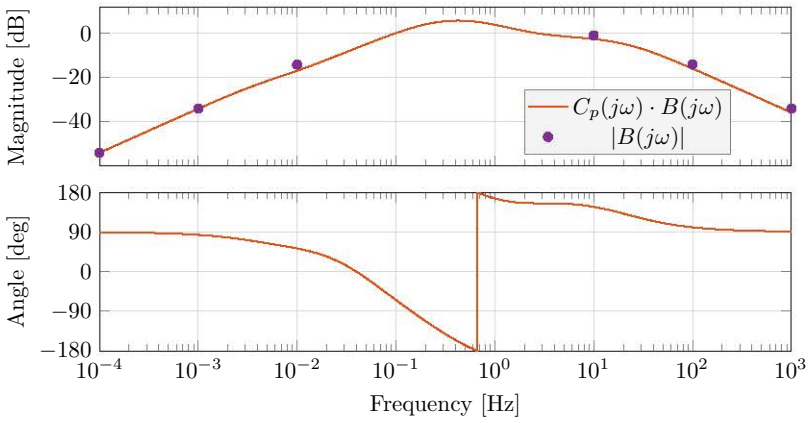

(a)

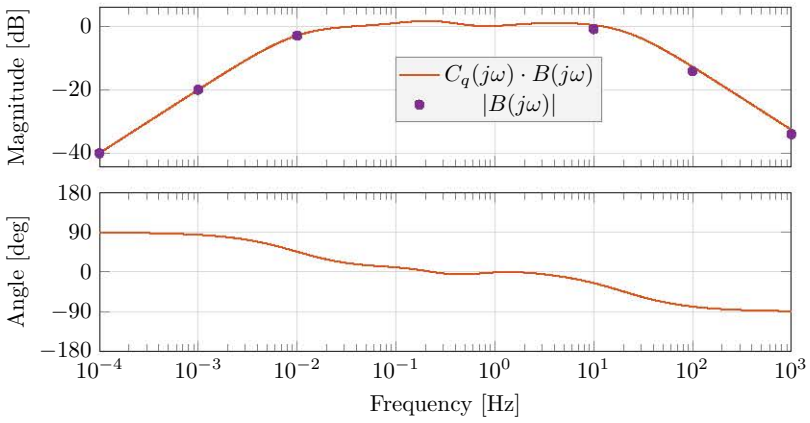

(b)

Figure 4.5: (orange) Frequency response of (a) $(C_p(s) \cdot B(s))$ and (b) $(C_q(s) \cdot B(s))$. (purple) Magnitude of $B(j\omega)$ for all elements in $\mathbf{\Omega_{out}}$.

Fig. 4.5 (a) and Fig. 4.5 (b) show the frequency response of the POD controllers designed using the proposed method. These figures show the combined frequency response of the band-pass filter and the compensators in each loop, allowing to assess the total impact of the POD controller on the system. It can be seen that the band-pass filter mainly determines the shape of the magnitude of the POD controller, due to the magnitude constraints of $C_p(j\omega)$ and $C_q(j\omega)$. Within the frequency range of interest, the POD controller magnitude deviates from the band-pass filter. This is expected because in this frequency range the requirements for the phase of $C_p(j\omega)$ and $C_q(j\omega)$ are specified and set.

Fig. 4.6 (a) and Fig. 4.6 (b) show the design errors for both $C_p(s)$ and $C_q(s)$, respectively. Overall, it can be seen that the errors in both power loops are lower than 40 degrees, while in the majority of cases, it is even lower. The mean error in active and reactive power loops is shown as an orange line in Fig. 4.6 (a) and Fig. 4.6 (b), respectively. It can be seen that the mean errors are around 15 degrees in both cases. This ensures the system is well-damped in most of the cases considered.

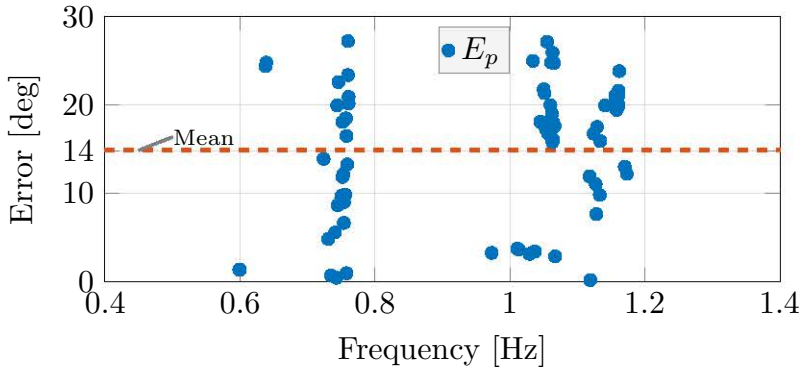

(a)

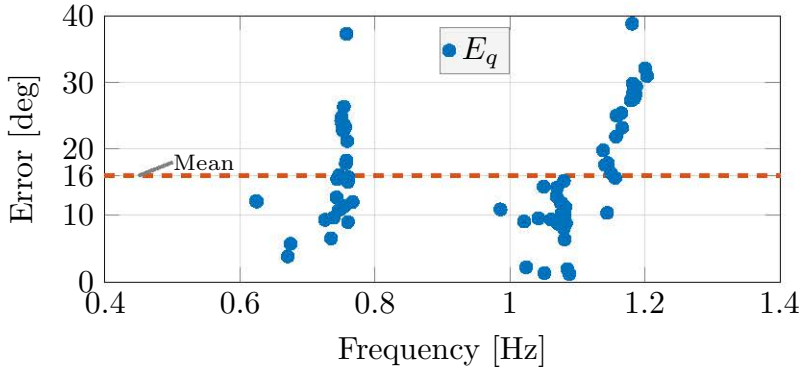

(b)

Figure 4.6: (blue) Error between the specified and achieved phase of (a) $C_p(j\omega)$ and (a) $C_q(j\omega)$. (orange) Mean absolute error.

Table 4.2: Parameters for compensators $C_p(s)$ and $C_q(s)$.

	Time constant [s]							
	T_1	T_2	T_3	T_4	T_5	T_6	T_7	T_8
$C_p(s)$	18.26	0.23	-2.79	0.67	0.07	30		
$C_q(s)$	0.27	0.57	0.27	0.57	0.27	0.57	1.28	0.13

4.4.3 Controller Gain

Fig. 4.7 shows the system frequency response when the gains K_p and K_q are modified. Here, the system is in its nominal configuration and all the lines are connected. It can be seen that an increase in the proportional gain has a twofold effect on the dynamic properties of the system. First, for three low-frequency peaks, the system magnitude decreases as the gain value increases. At the same time, a change in the opposite direction is seen for peaks outside the frequency range of interest (depicted as gray areas in Fig. 4.7). Thus, the system stability margins for frequencies outside the range of low-frequency oscillations are reduced when the controller gains increase. These results highlight the importance of analysing stability margins for frequencies within and outside the frequency range of interest. Based on this analysis, the proportional gains are set to $K_p = K_q = 1.3$ pu on the CIG unit base. These values, together with the rest of the relevant system parameters, are summarised in Table 4.3. Fig. 4.8 shows the system transient response when a disturbance is applied (gray) without and (orange) with the POD controller. A significant improvement in the damping can be seen as the system reaches a steady state within a few seconds after disturbance, compared to tens of seconds for the system without a POD controller.

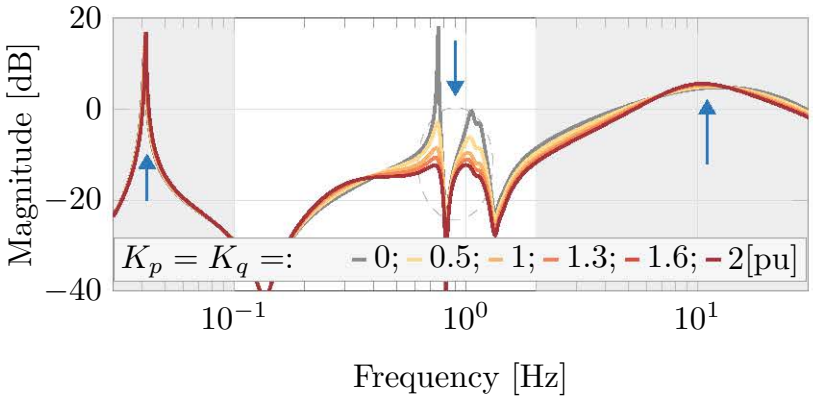

Figure 4.7: System closed-loop frequency response for variations of the proportional gain values.

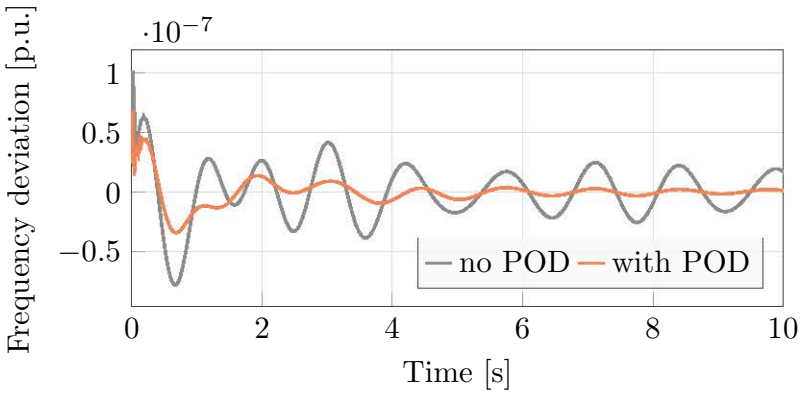

Figure 4.8: Transient response when a disturbance is applied. (gray) Without and (orange) with POD controller.

Table 4.3: POD controller parameters on the base of the CIG unit.

Parameter	T_h [s]	T_l [s]	K_p [pu]	K_q [pu]	p_l, q_l [pu]
Value	2	0.05	1.3	1.3	0.1

4.4.4 System Performance

Fig. 4.9 shows the relevant system eigenvalues for different network configurations (blue) without and (orange) with the POD controller. Here, the system is observed for all possible disconnections of lines in the network, including those that are excluded during the design procedure. It can be seen that, when the system is reconfigured and there is no POD controller, there are very significant changes in the stability margins. Moreover, for certain network topologies, the system even becomes unstable. Once the POD controller is introduced, the variations of the system eigenvalues are smaller and the damping factors are improved, for all the possible network configurations. Furthermore, the system remains stable once the network configuration changes.

4.5 Chapter Summary

In this chapter, a method to design a network-configuration-aware POD controller for CIG-based power plants is presented. The proposed design procedure takes into account the changes in the system caused by network reconfiguration. Also, it has been explained how all the necessary information for the proposed method is obtained from the system frequency response. An optimisation procedure to calculate the parameters of the POD controller has been introduced. The formulation of the optimisation problem, which includes all the system constraints, has been proposed and it's objective

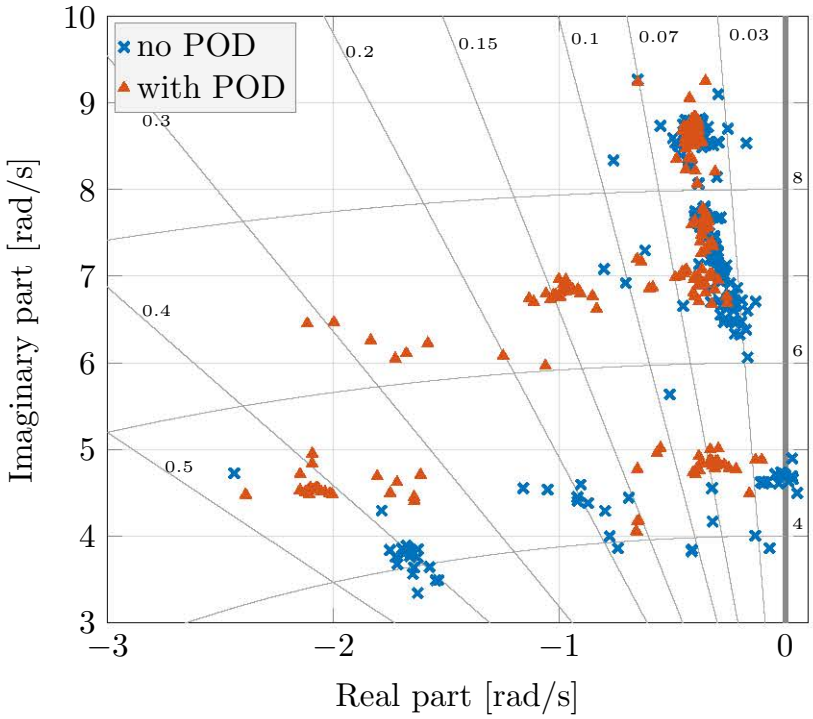

Figure 4.9: System eigenvalues for network configurations with different lines disconnected (cross) without POD controller and (triangle) with POD controller.

defined. The proposed design method was tested by using simulations in the IEEE 39 Bus benchmark system. Future work could focus on extending the set of considered cases with modifications caused by the loss of generation units and variations in the network loading conditions. Also, it is of interest to study the performance of the proposed method applied to different networks because the relation between the oscillation frequency and the compensation angles depends on the network topology.

Chapter 5

Centralised Multi-Mode POD Controllers with Stochastic Delay Compensation

This chapter describes a centralised multi-mode POD controller that compensates for the effects of stochastic communication delay. Section 5.1 gives an overview of the system and the POD controller structure, as well as the design methodology of the POD controller. Section 5.2 describes the modelling of the plant and the calculation of POD controller parameters. The procedures for modelling the stochastic communication channel delay and sampling rate are described in Section 5.3 Section 5.4 describes the results of the POD controller validation in the PHIL environment, in which a real communication network is deployed. A discussion regarding the impact of network reconfiguration and variation in delay length is given in Section 5.5. Finally, Section 5.6 summarises the main results of this chapter.

5.1 System Overview and Methodology

5.1.1 System Description

Fig. 5.1 shows the electrical and control system diagrams of the network used in this work. Fig. 5.1 (a) shows the transmission network under study, although the proposed procedure is general and can be applied to other networks. The transmission network used in this work is based on a benchmark model for inter-area oscillation studies [IEEE, 2015b]. The network is modelled following the acausal modelling principles.

It consists of three generation units and the main network. Each unit includes an SG, a governor and an exciter. There are several low-frequency oscillations: G_1 against G_2,

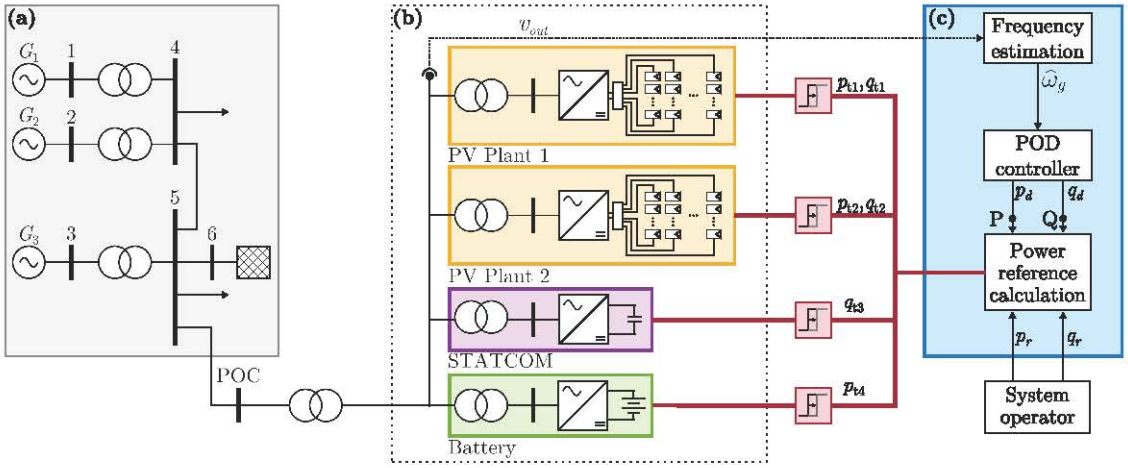

Figure 5.1: (a) Single-line diagram of the network studied in this work. (b) Hardware and (c) centralised controller of the PV power plant.

G_1 and G_2 against G_3, and the three generators against the main network. Thus, this model is suitable for studies of multi-mode oscillations. In this work, two modifications are made to the original model [IEEE, 2015b]. The first one is an additional POC at bus 5 (see Fig. 5.1 (a)) that is used to connect a PV plant. The second one is an additional delay and gain in the PSS of the SGs, which is used to deteriorate the damping of the original oscillation modes and emphasise the inter-area oscillations. The PV plant consists of four CIG units, with different primary energy sources on the dc side. These include (yellow) two PV-arrays with centralised PV inverters, (purple) a STATCOM and (green) a battery storage system. Only two PV inverters are used so that theoretical results can be fully reproduced in the experimental platform. The STATCOM delivers the reactive power required by the TSO while the battery is used to adjust the total active power delivered to the grid. This setup is used when a PV plant is required to offer grid-support services, although PV plants with alternative topologies can also be found [Bullich-Massagué et al., 2020]. All the CIG units operate in grid-following mode [Blaabjerg, 2021].

The active and reactive power references for each CIG unit are defined by a centralised PV-plant controller, which is depicted in Fig. 5.1 (c). Each power reference consists of two terms. The first one are active and reactive power set points (p_r and q_r) sent by the system operator. Their rate of change is slow so they are commonly considered constant for studying electro-mechanical oscillations. The second part of the power reference is defined by a POD controller and includes active and reactive power terms (p_d and q_d, respectively). The PV inverters receive active and reactive power references, the STATCOM only receives reactive power references and the battery only receives active power references. These references are sent via a communication channel

that is shared between all the devices. This channel introduces an additional delay and quantization that is depicted as a red element in Fig. 5.1.

5.1.2 POD Controller Overview

Fig. 5.2 shows the block diagram of (blue) the POD controller, together with (red) a model of the communication channel and (green) transfer functions that link active and reactive powers with the estimated network frequency ($P_p(s)$ and $P_q(s)$, respectively). The POD controller acts upon changes in the estimated network frequency ($\hat{\omega}_g$) and adjusts the active and reactive power references accordingly (p_d and q_d). To do so, several steps are defined. First, a high-pass filter eliminates the steady-state value from the estimated frequency that is used. Then, the compensators ($C_p(s)$ and $C_q(s)$) generate the power references (p_s and q_s) to maximise the damping effect of the PV plant. Finally, proportional gains (K_p and K_q) and power limits (p_l and q_l) modify the amplitudes defining the damping component power references. Since the power system has two main oscillation modes, both should be taken into consideration when designing the POD controller.

Power references are then sent to the CIG units via a communication channel that introduces an additional delay in the system. The stochastic nature of this delay means that the message will be received by each CIG at a different time instant. To model such behaviour, a delay model is added for each of the n CIG units, depicted as $D_1, \cdots, D_n$ in Fig. 5.2. As shown later, this delay will greatly affect the performance of the POD controller.

5.1.3 POD Controller Design Methodology

Fig. 5.3 (left) shows an overview of the methodology proposed in this work for designing the POD controller. First, the plant transfer functions are obtained. These can be obtained from a network model. However, if a model is not available, these can be identified by using system identification techniques. To do so, the system is perturbed

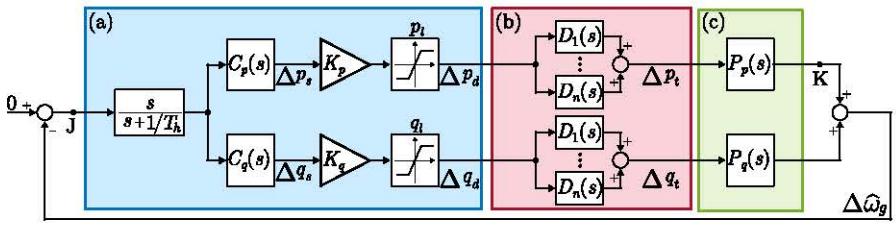

Figure 5.2: Control system block diagram of (a) POD controller, (b) delay and (c) plants (relations between active and reactive power, and measured frequency).

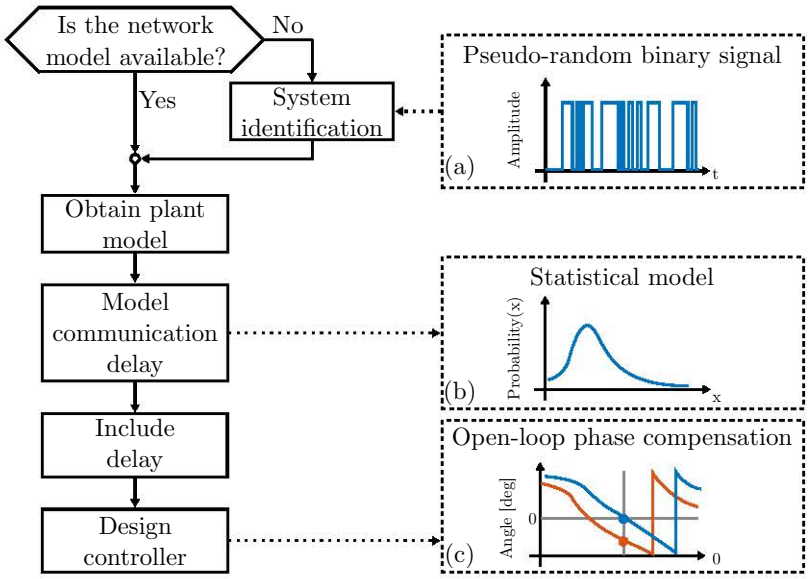

Figure 5.3: (left) POD controller design procedure. (right) Illustration of: (a) Pseudo-random binary signal (PRBS) used in the system identification, (b) statistical model of communication channel delay, and (c) phase bode plot for (orange) the plant with the delay and (blue) including the compensator.

using a pseudo-random binary signal (PRBS) (Fig. 5.3 (a)) and the system response is observed. Then, the communication channel is modelled. This step includes measuring and gathering information of the communication infrastructure. This information is used to create a statistical model of the communication channel delay, as depicted in Fig. 5.3 (b). Then, the linearised model of the communication channel is implemented and its impact on the plant is assessed. Finally, the POD controller is designed to maximise the POD controller effectiveness taking into consideration the communication channel. Fig. 5.3 (c) shows an example of a Bode phase plot where the controller (in blue) compensates for the plant phase (in orange) at the oscillation frequency.

Fig. 5.4 shows an example of the system eigenvalues for two cases. In 5.4 (a), the eigenvalues of a system with a POD controller and different values of the delay are shown (in circles). It should be noted that, as the delay is stochastic and changes fast in time, the delay cannot be treated as constant and, therefore, these circles are not valid for the representation of the system dynamics. However, under some considerations that will be fully explained later, the mean value of the delay might be used. This case is marked as a cross in the diagram. Then, in 5.4 (b), the proposed POD controller is applied that is designed taking into account the communication delay. Again, the circles represent cases for certain values of the delay, but they cannot be used for studying the system dynamics. Meanwhile, the case with the cross represents the system dynamics using the average value of the delay.

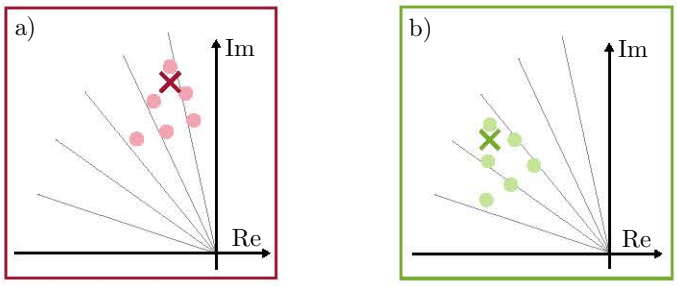

Figure 5.4: System eigenvalues when (a) the delay is neglected and (b) the delay is considered. Dots represent cases with constant delays of different lengths, which cannot be used to study systems with stochastic delays. Crosses represent cases with average delay lengths.

5.2 POD Controller Design

The POD controller will be designed by using the open-loop phase compensation method [Ogata, 2010]. A simplified version of this method was previously presented in [Jankovic et al., 2021]. It was shown that the controller of each power loop should be designed separately and compensate for the open-loop phase at the oscillation frequency of the corresponding plant. The following sections describe the procedure used for designing the active power controller (the reactive power one follows the same procedure).

5.2.1 Plant Modelling

Fig. 5.1 shows that the POD controller acts over an equivalent plant that links the active power reference with the estimated network frequency. This plant can be divided into two parts. The first part is shown in Fig. 5.1 (c) and is related to the power system and the PV-plant. The second part is shown in Fig. 5.1 (b) and is related to the communication channel.

Power System and PV Plant Model

This part of the model includes well-studied electrical and control systems elements [Kundur et al., 1994]. Thus, standard modelling methods (i.e., small-signal models) can be used. However, this approach assumes prior knowledge of the power system topology and its control systems, and such information may not always be available. In that case, the relevant information about the system can be estimated by identifying the low-frequency modes [Jin et al., 2017]. The approach used in this work relies on system identification tools to estimate plant dynamics (more details are

provided later). The following result was obtained:

$$\hat{P}_p(s) = \frac{\omega_g(s)}{p_t(s)}, \tag{5.1}$$

where $\hat{P}_p(s)$ is the estimated plant, $p_t(s)$ is the active power reference of a CIG and $\omega_g(s)$ is the frequency of the grid. The symbol " ˆ " refers to "estimated". Such a model represents the system dynamics in the frequency range of interest, and can be easily converted into a state-space model [Ogata, 2010]:

$$\dot{\hat{\mathbf{X}}}(t) = \hat{\mathbf{A}}\hat{\mathbf{X}}(t) + \hat{\mathbf{B}}\mathbf{U}(t), \tag{5.2}$$

where $\hat{\mathbf{A}}$ is the state matrix, $\hat{\mathbf{B}}$ is the input matrix, $\hat{\mathbf{X}}(t)$ is the state vector and $\mathbf{U}(t) = [\, p_t(t) \,]$ is the input vector.

Communication Channel Model

From the control system point of view, the communication channel imposes an additional time-variable delay in the system and a quantization of the information. In [Michiels et al., 2005] a theorem to transform time-varying periodical delays into distributed delays is defined. Recently, this theorem was further extended to analyse the stability of the system with time-varying delays [Milano et al., 2020]. It was shown that for analysing the system stability, a time-varying delay with a certain probability distribution function (PDF) can be modelled as a constant delay of the average length. These works analyse the stability of a closed-loop system with time-varying delays, and in both the delay has an impact on the system states. In that case, stability cannot be checked by using standard tools. However, in this work, the delay model is used for obtaining the open-loop response of the plant. This will simplify the stability analysis as it is assumed the delay does not affect the state variables, just the inputs.

As shown in Fig. 5.2, the delay is placed in series with $P_p(s)$. Therefore, the open-loop model of the PV-plant together with the communication channel can be written as:

$$\dot{\hat{\mathbf{X}}}(t) = \hat{\mathbf{A}}\hat{\mathbf{X}}(t) + \hat{\mathbf{B}}\mathbf{U}(t - \vartheta(t)), \tag{5.3}$$

where $\vartheta(t)$ represents the delay whose duration is a function of time.

Transforming (5.3) to Laplace domain yields to:

$$s\hat{\mathbf{X}}(s) = \hat{\mathbf{A}}\hat{\mathbf{X}}(s) + \hat{\mathbf{B}}\mathcal{L}\left\{ \int_{\tau_{min}}^{\tau_{max}} f(\vartheta)u(t - \vartheta)d\vartheta \right\}, \tag{5.4}$$

where $f(\vartheta)$ represents the PDF of the delay, while τ_{min} and τ_{max} are minimum and maximum durations of the delay, respectively [Milano et al., 2020].

Equation (5.4) can be further simplified to:

$$s\hat{\mathbf{X}}(s) = \hat{\mathbf{A}}\hat{\mathbf{X}}(s) + \hat{\mathbf{B}}\underbrace{\mathcal{L}\left\{\int_{\tau_{min}}^{\tau_{max}} f(\vartheta)d\vartheta\right\}}_{D(s)}\mathbf{U}(s). \tag{5.5}$$

The PDF can be transformed to the Laplace domain as follows:

$$D(s) = E[e^{-s\vartheta}] = e^{-s\theta}, \tag{5.6}$$

where $E[\cdot]$ is the expected value function and θ is the average value of the PDF.

By combining the previous results, the transfer function that relates the active power command sent from the central controller with the grid frequency can be written as follows:

$$\omega_g(s) = \hat{P}_p(s)e^{-s\theta}. \tag{5.7}$$

In this result, it is easy to see that the system dynamics can be modelled as two separate entities ($\hat{P}_p(s)$ and $e^{-s\theta}$) and then merged. In this work, $\hat{P}_p(s)$ is obtained by using system identification techniques, while $e^{-s\theta}$ will be obtained from the communication channel measurements.

5.2.2 Design Objective

The design objective is to maximise the damping of the system eigenvalues corresponding to the oscillation frequencies $\omega_{o,1}$ and $\omega_{o,2}$. To meet this objective, the open-loop shaping method is used [Ogata, 2010]. The open-loop is defined as a transfer function from point J to point K in Fig. 5.2:

$$G_p(s) = C_p(s) \cdot D(s) \cdot P_p(s). \tag{5.8}$$

The open-loop shaping method has been discussed in Chapters 3 and 4 for designing a POD controller in systems with one or multiple low-frequency modes. The transmission network from Fig. 5.1 (a) has two low-frequency modes. Thus, the POD controller design criteria can be defined as:

$$\phi_{Gp,i} = 0 \ , \ i \in (1, 2), \tag{5.9}$$

where $\phi_{Gp,i}$ is the phase response of $G_p(s)$ at $\omega_{o,i}$. The subscript i represents system variables at oscillation frequencies $\omega_{o,1}$ and $\omega_{o,2}$,

Condition (5.9) can be written in terms of the phases introduced by the compensator, the delay and the plant, yielding:

$$\phi_{Gp,i} = \phi_{Cp,i} + \phi_{D,i} + \phi_{Pp,i} = 0 \ , \ i \in (1, 2), \tag{5.10}$$

where $\phi_{Cp,i}$, $\phi_{D,i}$ and $\phi_{Pp,i}$ are the phase responses of $C_p(s)$, $D(s)$, and $P_p(s)$ at $\omega_{o,i}$, respectively. Phase $\phi_{Cp,i}$ introduced by the controller is the unknown variable in (5.10), whose value is determined by controller parameters (explained in the following section). This criteria means that two points in the frequency response should be adjusted by tuning the controller parameters. However, such criteria greatly increases the complexity of the system of equations that may even become unfeasible. This difficulty derives from the fact that the design is focused on achieving certain phases of the transfer function $C_p(s)$ in a very narrow frequency range (0.1 to 2 Hz). To address this issue, an alternative function to meet the design objective was defined:

$$\mathbf{F}(\mathbf{x}) = \begin{bmatrix} \dfrac{\phi_{Cp,1} + \phi_{Pp,1} + \phi_{D,1}}{-\phi_{Pp,2} - \phi_{D,2}} \\ \\ \dfrac{\phi_{Cp,2} + \phi_{Pp,2} + \phi_{D,2}}{-\phi_{Pp,1} - \phi_{D,1}} \end{bmatrix} = \begin{bmatrix} 0 \\ \\ 0 \end{bmatrix}, \tag{5.11}$$

where $\mathbf{x}$ is the set of variables to be solved that will be explained in the next section. It can be seen that the original equations in (5.10) have been divided by the open-loop phase of the other mode. For example, the first equation is divided by the sum of the phases of $D(s)$ and $P(s)$ at $\omega_{o,2}$. This modification allows for a comparable "improvement" in the solution for both modes. Otherwise, the solver might find a solution in which one mode is very well-damped while the other one is not or it is even deteriorated.

5.2.3 Parametrisation of the Compensator

Standard lead-lag filters in series were used to implement the compensator:

$$C_p(s) = \frac{1 + sT_1}{1 + sT_2} \frac{1 + sT_3}{1 + sT_4}, \tag{5.12}$$

where T_{1-4} represent the compensator time constants.

Then, the compensator phase response at the oscillation frequencies is calculated as:

$$\phi_{Cp,i} = \text{angle}\left(\frac{1 + j\omega_i T_1}{1 + j\omega_i T_2} \frac{1 + j\omega_i T_3}{1 + j\omega_i T_4} \right) \ , \ i \in (1, 2). \tag{5.13}$$

Therefore, the set of equations in (5.11) should fulfil the relation (5.13) for both modes and the variables to be solved can be defined as $\mathbf{x} = [T_1 \ T_2 \ T_3 \ T_4]$.

5.2.4 Resolution of the Problem

There are several algorithms available in the literature to solve the set of non-linear equations presented in (5.11) [Conn et al., 2000]. A common goal of these algorithms is to find a value of $\mathbf{x}$ for which $F(x)$ is as close to zero as possible. In this work,

this problem was solved by using the function *fsolve* of Matlab, which uses the *Trust Region Dogleg* algorithm [Conn et al., 2000]. This algorithm minimises the norm-2 of the errors. Also, this algorithm has robust convergence properties regardless of the starting point, which is an adequate property given the non-linearity of the problem. This allows simpler configuration of the initial values for unknown variables T_{1-4}.

5.2.5 Controller Limits

The controller limits p_l and q_l define the maximum power reference set by the POD controller. These limits depend on both PV plant operating point and TSO requirements. The PV-plant operating point defines the amount of active power delivered to the network. From this, a certain margin is reserved for the POD services. It can be defined as:

$$p_l = k \cdot p_r, \tag{5.14}$$

where k is the predefined margin.

Also, this defines the reactive power availability for POD services, as the total required power is limited by the ratings of the local units. This can be defined as:

$$q_l = \sqrt{S_{cn}^2 - (p_l + p_r)^2} - q_r, \tag{5.15}$$

where S_{cn} is the rated power of the local unit. Limits p_l and q_l represent the theoretical power maximum available for damping services. Nonetheless, depending on the location of the PV plant within the power system, TSO can impose certain conditions on the provision of POD services. Furthermore, the limits in active and reactive powers for POD may vary during the PV plant operation. In this work, these limits are considered as fixed predetermined values. The impact of the variation in the available active and reactive powers for POD is of interest for further study and research.

5.2.6 Controller Gain

The POD controller proportional gain is designed to increase the damping action. While an increase in the gain value improves the damping action, two points need to be considered. The first point is that an increase in the gain value also increases the controller action across the whole frequency range. This means that any noise or high-frequency oscillations would be amplified. The second point is that with an increase in gain value possible interactions among parallel connected converters may occur [Zhao et al., 2021]. Considering these limitations, the proportional gain value was selected based on the system's transient response under various disturbances.

5.3 Modelling of the Communication Channel

The communication channel model is based on the observations of the communication channel in the laboratory environment, described in Appendix A. It is assumed that all devices in the setup are connected and operating properly. Thus, loss of connection and other types of errors in communication are not considered. Nonetheless, the internal processes of sending and receiving messages are inherently included in the results.

5.3.1 Communication Channel Delay

The process of data exchange between devices involves several steps [Comer, 2013]. The data need to be processed, then wait in the queue until the message is executed and, finally, the data are pushed to the network. The first and the last steps are significantly faster and easier to predict than the middle one. Thus, the queuing delay is the step which determines the stochastic nature of the communications. The factors affecting this delay are related to the traffic and congestion in the communication network, as well as in the routing procedure [Comer, 2013]. These factors affect both delay length and its variation over time.

In order to obtain data for modelling the communication channel, a new message was sent from RTPC 1 to RTPC 3 every second for a total duration of 20 minutes. Then, the results were gathered and processed. The time difference between the sent command and its execution was measured. This was defined as the delay length. Fig. 5.5 shows that the delay length varies significantly. The medium value was 0.3 s.

5.3.2 Communication Channel Sampling Rate

An ever-changing signal was sent from RTPC 1 to RTPC 3 to quantify the communication channel sampling rate. From the obtained results, the number of unique values per second was measured. Fig. 5.6 shows the probability of receiving a certain number of messages per second. The results show that three or four messages per second were received most of the time. In a discrete time control system, this result can be interpreted as the sampling frequency of the communication channel, and it is useful to define the theoretical frequency maximum (i.e., Nyquist frequency) of the signal that can be sent through it without aliasing [Ogata, 2010]. This yields to:

$$f_{max} = f_s/2, \tag{5.16}$$

where f_{max} is the Nyquist frequency and f_s is the sampling frequency. For the experiment carried out here, the maximum frequency of the signal exchanged through the communication channel is $f_s \approx 1.6$ Hz. Therefore, it is clear that the communication channel will affect the performance of the POD controller in the frequency range of interest (0.1 to 2 Hz). Moreover, this result means that some of the frequencies of interest

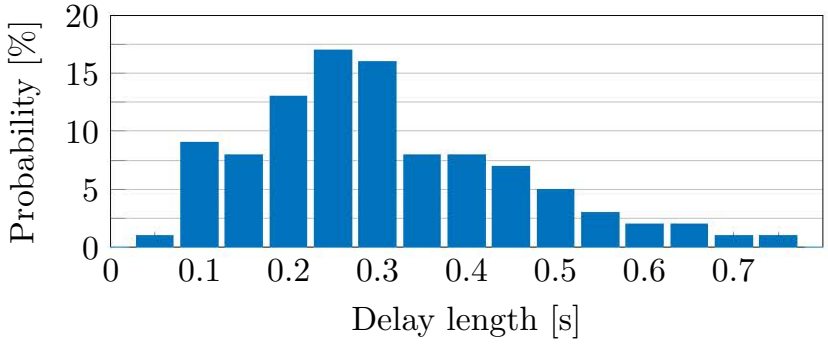

Figure 5.5: Communication channel delay length measured in the laboratory.

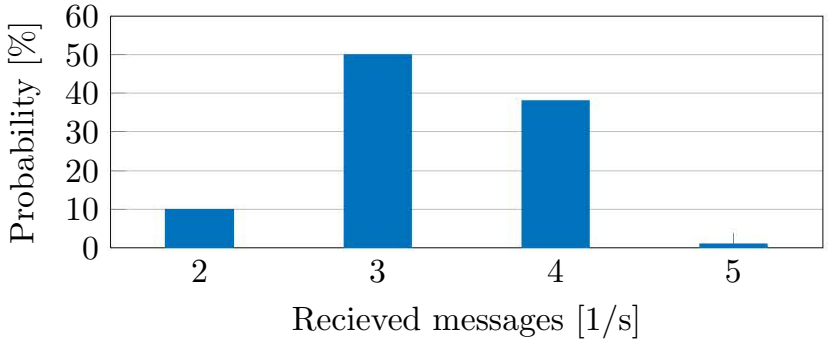

Figure 5.6: Communication channel throughput measured in the laboratory.

(close to 2 Hz) cannot be addressed by the centralised controller. For solving this issue, a faster centralised controller can be used. Another option would be to implement the POD in each of the PV inverters, as already discussed in the introduction.

5.3.3 Delay Model

In order to include the delay model $D(s)$ in the design procedure, a Padé approximation was used [Ogata, 2010]. It can be defined as:

$$D'(s) = \frac{\sum_{j=1}^{h} w_j s^j}{1 + \sum_{k=1}^{n} w_k s^k}, \tag{5.17}$$

where D' represents a Padé approximation, h and n represent its order, while j and k are iterators in numerator and denominator, respectively, and w are approximation coefficients. The delay model design criteria was to adequately represent the average delay of the communication channel in the frequency range of interest. More specifically, the goal is to achieve less than 10° error in phase between the delay and the

approximation for frequencies in the range from 0.1 to 2 Hz. This required the use of a fourth-order Padé approximation of the average delay function $D(s)$.

5.4 Experimental Results

The proposed method for POD controller design was verified using PHIL setup, described in Appendix A.1.1. The CIG based power-plant is modeled with installed power of 300 MVA in the emulated power system model, with a nominal voltage of 20 kV. The power-plant consists of four real-hardware CIG units, with nominal power $S_n = 15$ kVA and nominal voltage of $V_n = 400$ V. Therefore, the scaling factors between the PHIL environment and emulated power system model are $K_v = 0.02$ and $K_i = 99.99$ (see Appendix A.3 for more details).

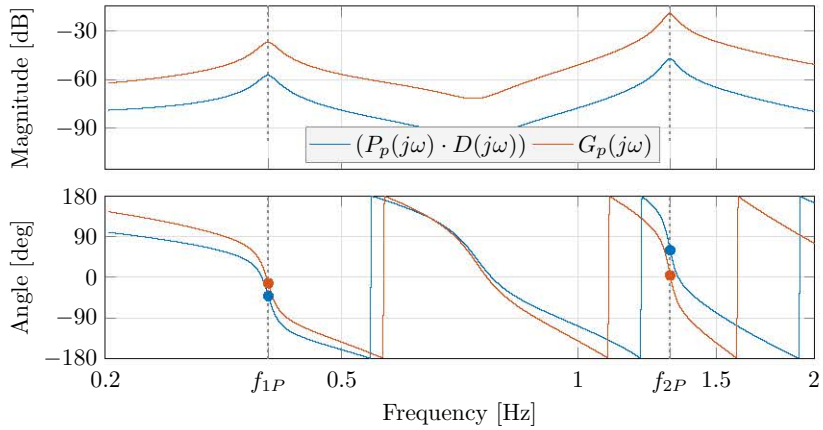

(a)

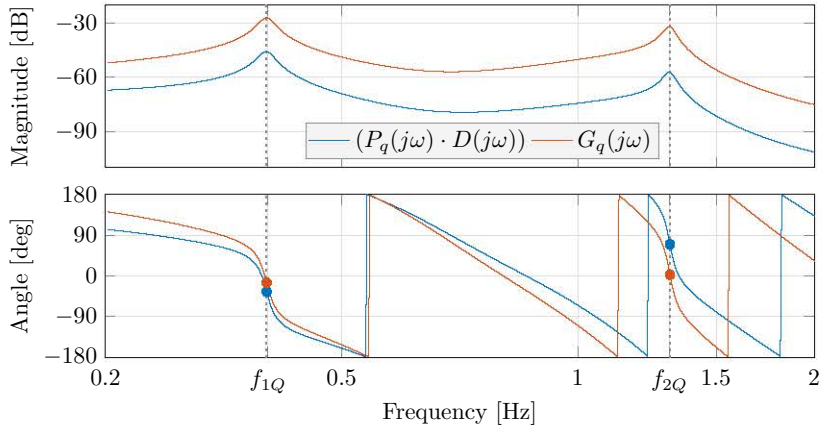

(b)

Figure 5.7: Frequency response of (blue) plant and (orange) open-loop transfer functions in (a) active and (b) reactive power loops. (marks) Phases of transfer functions at oscillation frequencies.

5.4.1 Plant Estimation and Controller Design

The POD controller was designed following the procedure presented in Section 5.2 and then verified in the laboratory. The procedure was done for both active and reactive power loops, and their combined damping action was examined. To do so, several steps were taken. First, the system was perturbed by using a pseudo-random binary signal (PRBS) in the active and reactive power references, separately. From the obtained results, the active and reactive power plants were identified based on the system frequency response. This was done by using the system identification toolbox from *Matlab* [MATLAB, 2019]. Then, the communication channel delay model obtained in Section 5.3.3 was added to the model. The frequency responses of the plants $\hat{P}_p(s)$ and $\hat{P}_q(s)$ combined with the delay $D(s)$ are shown in Fig. 5.7 (a) and Fig. 5.7 (b), respectively (in blue). Then, the POD controllers in both loops were designed. Fig. 5.7 (a) and Fig. 5.7 (b) show (in orange) the open-loop frequency response of $G_p(s)$ and $G_q(s)$,

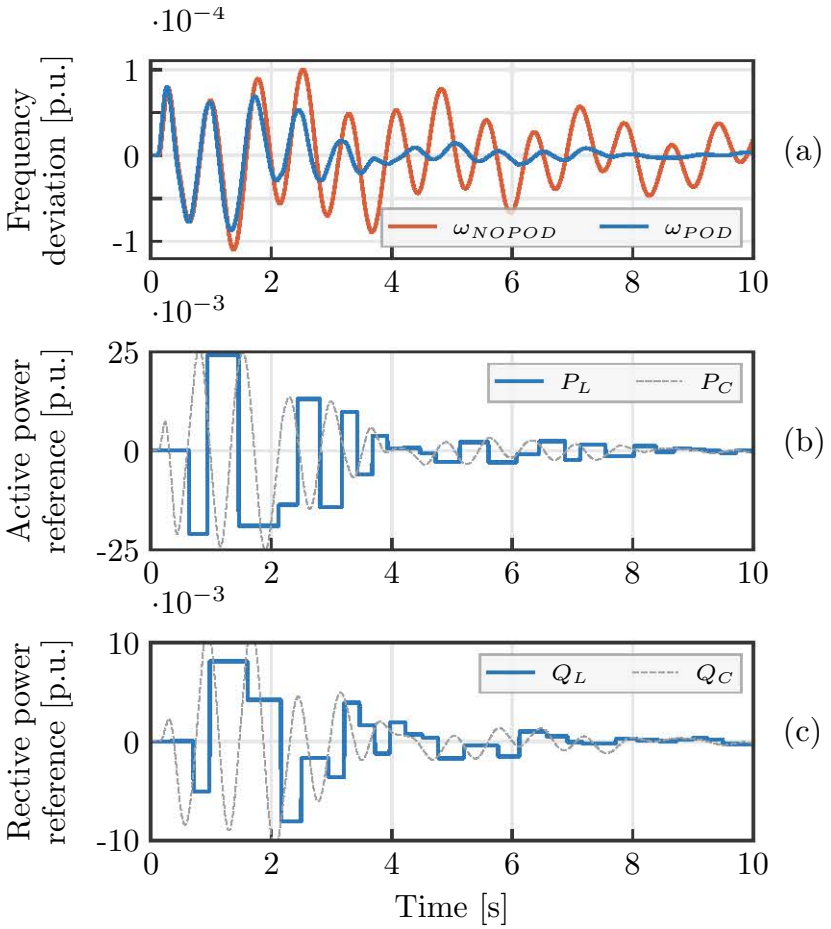

Figure 5.8: Laboratory results. (a) Frequency deviation, (b) active and (c) reactive power references sent from central controller (subscript "C") and received by the local controllers (subscript "L").

respectively. It can be seen that the open-loop phases at both oscillation frequencies are almost zero (orange marks), compared to the original phases of the plant (blue marks). Nonetheless, none of them were exactly zero, due to constraints described in Section 5.2.2.

Fig. 5.8 shows the initial seconds of the system transient response. Although steady-state has not been reached, several observations can be made. First, Fig. 5.8 (a) shows the network frequency transient for the case (orange) without and (blue) with POD controller action using both active and reactive powers. Then, Fig. 5.8 (b) and (c) show the references for the active and the reactive power generated by the POD controller, respectively.

These figures show the power references (gray) sent from centralised controller and (blue) the references received in the local units. By comparing those two, the impact of the communication channel on the power references can be observed. Although the local controllers received only 3-4 messages per second and the received signal hardly resembles a sinusoidal, the damping of both modes was greatly improved.

5.4.2 Impact of the Stochastic Communication Channel Delay

The same transient from Fig. 5.8 was repeated several times to analyse the behaviour of the system with stochastic delay. Fig. 5.9 shows (gray) fifty transients for the same disturbance. Overall, the system transient response showed an improvement compared with (orange) the case without POD controller. The impact of the stochastic communication delay was apparent in the period $t = 3 - 10$ s. It can be seen that for most of the cases, the transient followed the same trajectory and significantly improved the oscillation damping. However, for some cases, during this period the transient was sim-

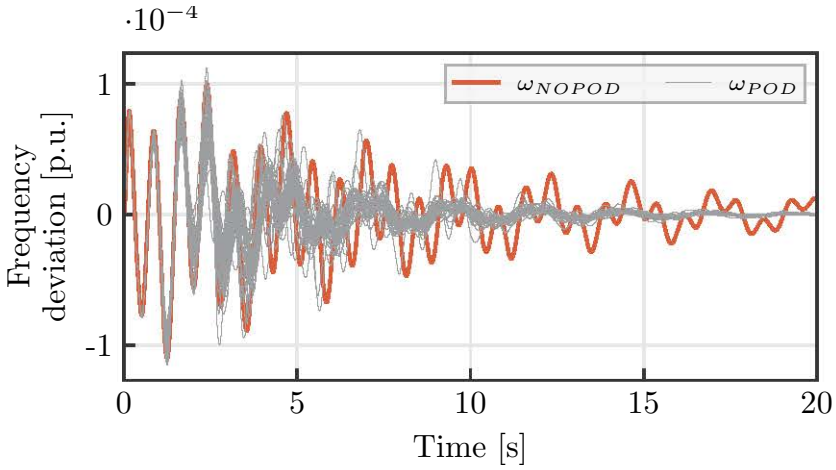

Figure 5.9: Laboratory results. (gray) Frequency transients with POD controller activated for 50 transients and (orange) without POD controller action.

ilar to the case without POD controller. This was due to increased delay length during the transient. Then, once the communication network fault was cleared, the system damping was improved. These results show that the wide range of the delay duration had an impact on the centralised POD controller performance during the initial part of the transient. However, the impact of a possible increase of delay length after the oscillation was damped (i.e., after $t = 15$ s) could not be observed. Despite the fact that the POD controller was designed by taking into account the communication channel delay, its action on the system was limited during the communication fault. However, as such faults were not frequently occurring, an overall improvement in the oscillation damping was achieved.

5.4.3 Performance Under Different Loading Conditions

Fig. 5.10 shows the frequency transient for several loading levels with the POD controller included. In this case, the constant current loads have been modified because of their larger impact on the system stability [IEEE, 2015b]. The results show that the change in loading affects the damping of both slower and faster modes. The change in damping is different for the two modes with increase and decrease of loading.

Even though the POD controller was designed by taking into consideration the communication channel delay, its action on the system was limited during the communication fault. However, as such faults were not always present, an overall improvement in the oscillation damping was achieved.

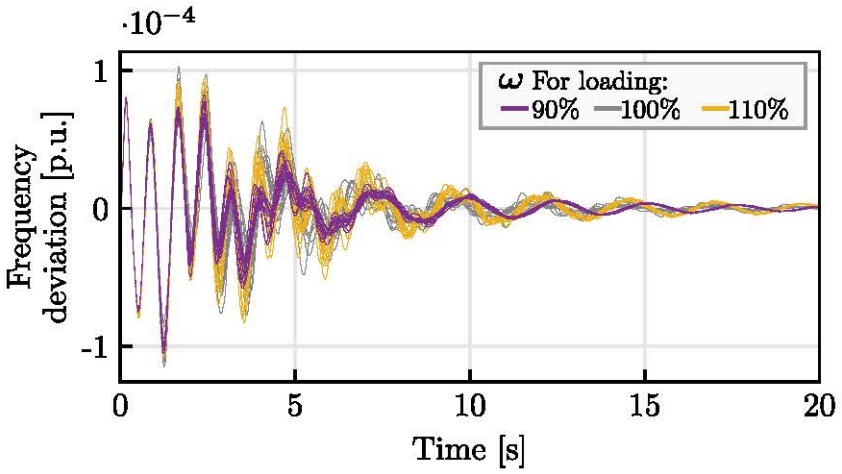

Figure 5.10: Transient response of the frequency of the system with the POD controller, under different loading conditions.

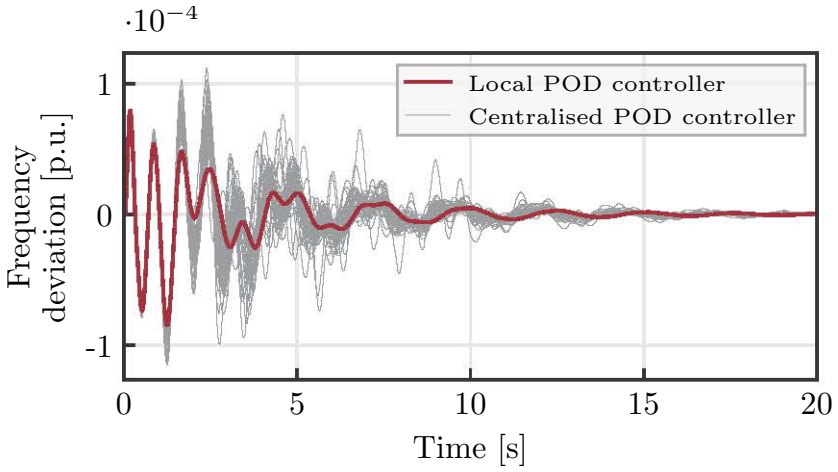

Figure 5.11: Frequency transient response after demand step-up with POD controller implemented in (red) local units and (gray) centralised platform.

5.4.4 Comparison with Local POD Controller Implementation

Fig. 5.11 shows the frequency transient responses for the POD controller implemented on (gray) a centralised platform and (red) local units. The local POD controllers were designed following the same procedure, except for the steps related to delay modelling and compensation. It can be seen that the transient, in the case of the local POD controller, is always the same because there are no modifications in the system. Also, the damping of both critical low-frequency modes is improved by using a local POD controller. This is a consequence of an additional long delay in the communication network, affecting the performance of the centralised POD controller. Furthermore, the variation of the delay has a negative effect on the performance of the centralised POD controller. This comparison shows that the local POD controller improves the damping of both low-frequency oscillation modes. However, for the implementation of a local POD controller, it is necessary to have access to the local unit control algorithm. Also, the implementation of POD controllers in local units requires additional computational power, which may not be available.

5.5 Discussion

5.5.1 Network Reconfiguration

During the system operation, the power system is changing and both the operating point and the network configuration vary. These modifications lead to a discrepancy between the real and the estimated plant since the frequencies of oscillations and the plant phases at those frequencies change. To address this problem, the POD controller

design needs to consider the power system model under different operating conditions. Another approach to addressing network reconfiguration is to perturb the system periodically. Then, the identification procedure needs to be repeated and a new solution of (5.11) obtained. In this work, the nominal network configuration is considered, with modifications applied to the system operating point. However, the change in network configuration and its impact on the centralised POD controller is relevant and of increased interest for future work.

5.5.2 Delay Variation

The length of communication channel delay varies over time, following a certain probability distribution. During certain periods of the PV plant operation, the delay length might be larger than the average. This period might have a negative effect on the PV plant performance, mainly in tracking power references sent from the centralised controller. If the reference change is fast it could create interactions between local units that operate in the grid-following mode. The synchronisation relies on the measurements of voltage at the point of connection. With rapid changes of power injection, this voltage would be continuously varying. Then, a difference in the estimated angle inside the local units may occur, leading to possible instabilities [Zhao et al., 2021].

5.6 Chapter Summary

In this chapter, a centralised POD controller for a PV plant that utilises both active and reactive powers has been presented. The controller is capable of damping multiple modes in the range of low-frequency oscillations. To achieve this, it relies on the communication network, which introduces additional control system constraints. The procedure for modelling and addressing the communication channel constraints is presented. The obtained model is then used to design the POD controller using open-loop design techniques. The POD controller is experimentally validated using a laboratory setup, in which four 15 kVA converters were connected to a 75 kVA grid emulator, which emulated the dynamics of a transmission network. The communication between the converters and the PV plant controller was established by using the TCP/IP protocol.

Chapter 6

Multi-Mode POD Controller Synthesis using Vector Fitting

This chapter describes the synthesis of a multi-mode POD controller using a VF algorithm. Section 6.1 gives an overview of the system and POD controller structure. Section 6.2 describes the POD controller design methodology, as well as a description of the VF algorithm. Section 6.4 describes the POD controller design methodology, whereas simulation results are presented in Section 6.5. Finally, the main results of this chapter are summarised in Section 6.6.

6.1 System and Controller Overview

6.1.1 System Description

Fig. 6.1 (a) shows the single-line diagram of the transmission network under study. The network is based on a benchmark model for low-frequency oscillation studies [IEEE, 2015a]. Each of the three generator units ($G_{1,2,3}$) includes an SG with an excitation controller and a PSS. Compared to the original model, two modifications are made. First, the PSS parameters of the three SGs are modified so that the damping of the critical modes decreases. The second modification is an additional connection point to the Bus 5, where the CIG unit is connected to.

Fig. 6.1 (b) shows the CIG unit connected to Bus 5. The CIG is modelled as a voltage source converter (VSC), and it operates in a grid-following mode. For simplicity, the VSC dc-side is assumed to be connected to an ideal voltage source and any application-specific dc-side dynamics are neglected. Nonetheless, this is of interest for further research. The VSC output current (i_{out}) and voltage (v_{out}) are used as feedback signals for the internal controllers. These controllers ensure that the active and reactive powers delivered to the grid are following their corresponding references (p_t and q_t). Each of

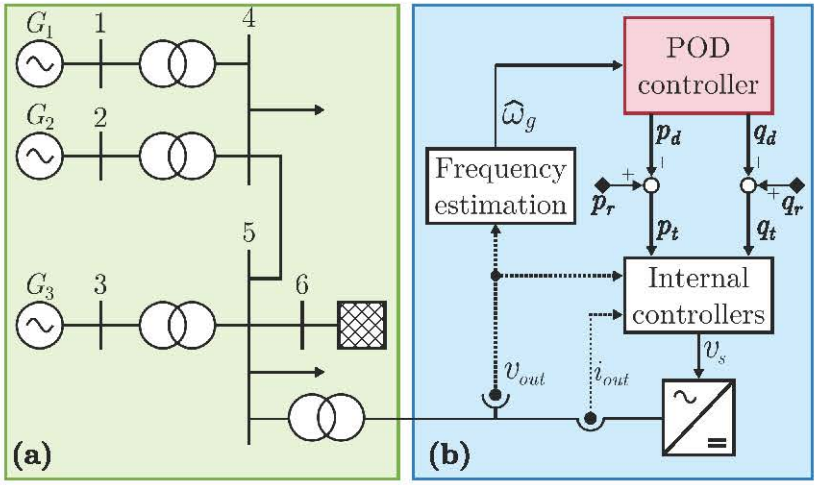

Figure 6.1: Diagram of (a) studied network and (b) CIG and the control system.

the power references consists of two terms. The first term is the power set point for active and reactive power (subscript c) while the second term is the output of the POD controller (subscript d). The POD controller modifies the power references based on the estimated network frequency (ω_g) in order to damp oscillations.

6.1.2 POD Controller Overview

Fig. 6.2 shows the block diagram representation of the plant model as seen from the CIG and the POD controller. There are two POD controllers. One for active power ($C_p(s)$ and another one for reactive power $C_q(s)$). Both include saturation blocks to limit their reference values (p_l and q_l). The POD controllers define the power references (p_s and q_s) based on the network frequency deviation. Then, the saturators limit the references and define the final control commands (p_d and q_d). The second section includes the transfer functions that represent the system dynamics from the CIG active and reactive power references to the estimated network frequency. These plants are named $P_p(s)$ and $P_q(s)$, respectively.

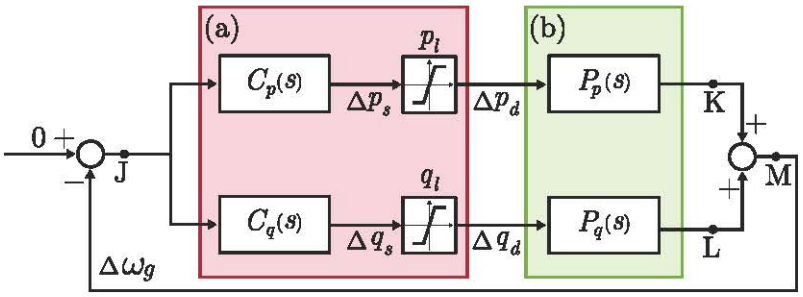

Figure 6.2: Block diagram of (a) POD controller and (b) plant models.

6.2 Proposed Methodology

6.2.1 Overview

Fig. 6.3 shows the proposed procedure for synthesising POD controllers. First, the phase of the system frequency response is obtained, either from a theoretical network model or from an identified model. Then, a band-pass filter should be designed. This filter has to attenuate frequencies outside the range of low-frequency oscillations (i.e., from 0.1 to 2 Hz) [Hatziargyriou et al., 2021]. The phase and magnitude information of this filter should be extracted, as depicted in blue in Fig. 6.3. Then, the controller specifications for both the gain and phase responses are calculated as the contributions of the band-pass filter and the plant phase to be compensated. These are depicted in orange in Fig. 6.3 and are used as inputs for the VF algorithm. Finally, the VF algorithm is used to synthesize a transfer function that represents a rational approximation. This means that the problem of finding the structure and parameters of a multi-mode POD controller is solved automatically. Moreover, due to the VF properties, the best possible fit to the specified points in the frequency domain is obtained. Next, the system stability margins are verified. If the system is stable, the controller gain is increased, and the fitting procedure is repeated. Once the system reaches instability, the iterative procedure is stopped. Finally, the POD controller with the best damping performance is selected, from the set of designs.

6.2.2 Vector Fitting

VF is a numerical method for rational approximation in the frequency domain [Gustavsen and Semlyen, 1999], [Gustavsen, 2006]. The first step in the VF algorithm is to obtain a rational function approximation based on the given set of points in the frequency domain. This rational function approximation can be written

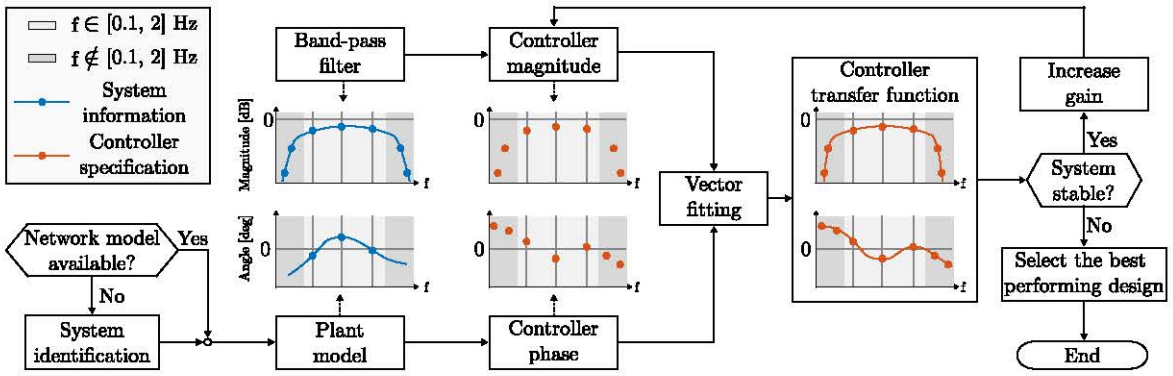

Figure 6.3: Procedure for POD controller synthesis using vector fitting method.

as follows:

$$C(s) = \sum_{i=1}^{n} \frac{\mathbf{R}_i}{s - \lambda_i} + \mathbf{D} + s\mathbf{E}, \tag{6.1}$$

where λ_i are the eigenvalues, i is the eigenvalue number, $\mathbf{R}_i$ are the residues, and $\mathbf{D}$ and $\mathbf{E}$ are matrices that represent the inputs and their derivatives, respectively. For this specific problem, as the controller has to be implemented in real-time, $\mathbf{E}$ must be zero.

By using VF, λ_i, $\mathbf{R}_i$ and $\mathbf{D}$ are estimated in two steps. First, the parameters of a simplified system (without zeros) are identified. Then, a second step is used to calculate the zeros and improve the accuracy. This procedure is executed iteratively until the best solution is found. The full description of the method can be found in [Gustavsen, 2006].

6.2.3 Comparison with *Robust* POD Controller Design

This procedure brings several benefits compared with the one presented in Chapter 4. First, the algorithm tends to pass through all specified points, achieving higher design accuracy. Furthermore, the design is repeated for each increase in the gain, unlike in Chapter 4 where the shape of the magnitude of controller frequency response is defined prior to final gain value selection. This results in a wider set of design choices and allows for a more precise selection of the controller with the desired shape of the magnitude of frequency response. However, there are certain disadvantages to using VF for POD controller synthesis. For example, undesired peaks in the magnitude of frequency response might occur. Also, the VF algorithm lacks an option to define constraints in the given optimisation problem. Those disadvantages and the way to address them are discussed in the following sections.

6.3 POD Controller Design Objectives

The POD controller design procedure is based on the open-loop phase compensation method [Ogata, 2010]. There are two design objectives, divided by the frequency range. The first design objective is defined for the frequencies in the range of interest, while the second one covers frequencies outside this range.

6.3.1 In the Frequency Range of Interest

In this range, the design objective is to maximise the CIG damping effect. This objective can be defined by using the error ($E(s)$) and open-loop ($G(s)$) transfer functions [Ogata, 2010]. First, $G(s)$ is the transfer function between points M and J in

Fig. 6.2. Based on this one, $E(s)$ is defined as:

$$E(s) = \frac{1}{1 + G(s)}. \tag{6.2}$$

The design objective is chosen to maximise the controller effect in (6.2) at the oscillating frequencies (ω_o^i). Even though this condition does not guarantee the best damping of the closed-loop poles, the solutions achieved are very close to the optimum. Moreover, the controller parameters can be calculated knowing just the frequency response of the plant at the frequencies of interest (i.e., a parametric model of the plant is not strictly needed). This condition can be written as follows:

$$\min |E(j\omega_o^i)| = \min \left| \frac{1}{1 + G(j\omega_o^i)} \right|, \tag{6.3}$$

where $G(j\omega_o^i) = A_G^i e^{j\phi_G^i}$. For a given of controller amplification (A_G^i) in (6.3), $|1 + G(j\omega_o^i)|$ will be maximum (and then $E(j\omega_o^i)$ minimum) if:

$$\phi_G^i = 0. \tag{6.4}$$

Therefore, this condition will be used in the following sections to design the POD controller.

6.3.2 Outside the Frequency Range of Interest

In this range, the design objective is to limit the controller impact. The reason behind this objective is twofold. First, for the case in which the plant model is estimated, it might not include the dynamics outside a specific range. This range depends on the type of perturbations used during the system identification procedure. Commonly, this frequency range coincides with the range for which the controller is designed. Thus, the information about the system outside this range is unreliable, and the interaction between the POD controller and the system is unknown. Therefore, the POD controller gain should be lower outside the range considered in the system identification procedure.

The second reason behind this objective is the VF algorithm used to synthesize the POD controller. This method solves an optimisation problem in which the objective is to fit the transfer function for a given set of points in the frequency domain. The obtained transfer function would have a frequency response as close as possible to the given points. However, for the rest of the frequencies, the frequency response is not controllable. This means that although the resulting transfer function achieves the desired frequency response for a given set of points, its overall impact on the system is unknown.

To address these constraints, the controller is designed to act as a band-pass filter in the frequency range of interest. This filter is defined as follows:

$$B(s) = \frac{s}{s + 1/T_h} \frac{1}{s/T_l + 1}, \tag{6.5}$$

where T_h and T_l are used to sed the band-pass of the filter.

6.4 POD Controller Design

The POD controller is designed using the open-loop phase compensation method [Ogata, 2010]. A simplified version of this method was previously used in [Jankovic et al., 2021]. It was shown that the POD controller in active and reactive power loops should be designed separately, relying on the superposition principle in linear control system theory. Thus, in this section, the POD controller design for the active power loop is presented, since the one in the reactive power loop follows the same procedure.

6.4.1 Design Specifications

From Fig. 6.2 the open-loop transfer function in the active power loop is defined from point J to point K as:

$$G_p(s) = C_p(s)P_p(s), \tag{6.6}$$

and its frequency response at ω_o^i is defined as:

$$\underbrace{A_{Gp}^i e^{j\phi_{Gp}^i}}_{G_p(j\omega_o^i)} = \underbrace{A_{Cp}^i e^{j\phi_{Cp}^i}}_{C_p(j\omega_o^i)} \cdot \underbrace{A_{Pp}^i e^{j\phi_{Pp}^i}}_{P_p(j\omega_o^i)}. \tag{6.7}$$

Recalling the design criteria presented in (6.4) and applying this result to (6.7), the following result is obtained:

$$\phi_{Gp}^i = \phi_{Cp}^i + \phi_{Pp}^i = 0. \tag{6.8}$$

This means that the controller phase should compensate the plant phase at ω_o^i. For the rest of the design specifications, the frequency response of the band-pass filter is used. It is defined as:

$$B(j\omega) = A_B e^{j\phi_B}. \tag{6.9}$$

Therefore, the specified magnitude of the frequency response for the controller is defined as:

$$A_C^* = A_B, \tag{6.10}$$

and the phase of the frequency response is specified as:

$$\phi_C^* = \left\{ \begin{array}{c} -\phi_P, \quad \omega \in \Omega_o \\ \phi_B, \quad \omega \notin [0.1,\ 2] \cdot 2\pi \ \ \text{rad/s} \end{array} \right\}, \tag{6.11}$$

where Ω_o is the set of frequencies of oscillations in the low-frequency range. The superscript "$*$" stands for specified points for the VF algorithm.

6.4.2 Fitting Controller Transfer Function

In this step, the goal is to obtain the transfer function with a frequency response as close as possible to the given set of points. To do so, the VF algorithm is used. Its output is a transfer function with a determined number of poles and zeros (specified by the user). Several parameters can be modified in order to improve the fitting in the frequency range of interest. These parameters are described here:

Transfer Function Order

It is determined by the number of specified points. The maximum transfer function order is defined as:

$$N_s = N_t - 1, \tag{6.12}$$

where N_t is the number of specified points, while N_s is the transfer function order. Nonetheless, the transfer function order can be reduced, possibly achieving better fitting or reducing undesired peaks in the frequency response. Also, from (6.12) one should note that the maximum order of transfer function can be increased by increasing the number of specified points. This can be applied when the given set of specifications leads to a difficult optimisation problem. If that is the case, specifying additional points (e.g., outside the frequency range of interest), introduces additional degrees of freedom for solving the optimisation problem. However, increasing the transfer function order can impose challenges for real-time implementation, since the frequency response of a discretised high-order transfer function might differ from the one in continuous time [Lyons, 2004].

Weights

The weights should be specified for the given set of points. Depending on the given set of points, the fitted transfer function might not meet the design criteria in the frequency range of interests. In that case, the weight of the specific points can be increased, to achieve better fitting in the range of low-frequency oscillations.

Selection of Points Outside the Frequency Range of Interest

plays an important role in the fitting procedure. By neglecting this fact, the given set of points may result in requesting an unfeasible solution. In that case, the obtained transfer function would not correspond to the given set of specifications. In this paper, the points in this frequency range are inherited from the band-pass filter. However, different criteria for defining the points outside the range of low-frequency oscillations might be used. This is of interest for further research.

6.5 Simulation Results

The CIG based power-plant has nominal power $S_n = 300$ MVA each, and nominal voltage $V_n = 20$ kVA. The parameters of CIG unit, and the structure of inner control loops are given in Appendix C.1, while transformer parameters are described in Appendix C.3.

6.5.1 Fitted POD Controllers

Fig. 6.4 (a) and Fig. 6.4 (b) show (marks) a given set of points in the frequency domain and the frequency responses of fitted $C_p(j\omega)$ and $C_q(j\omega)$, respectively. In both cases, the achieved phase in the frequency range of interest (light area) corresponds well with the design specifications. At the same time, the magnitude of the frequency response

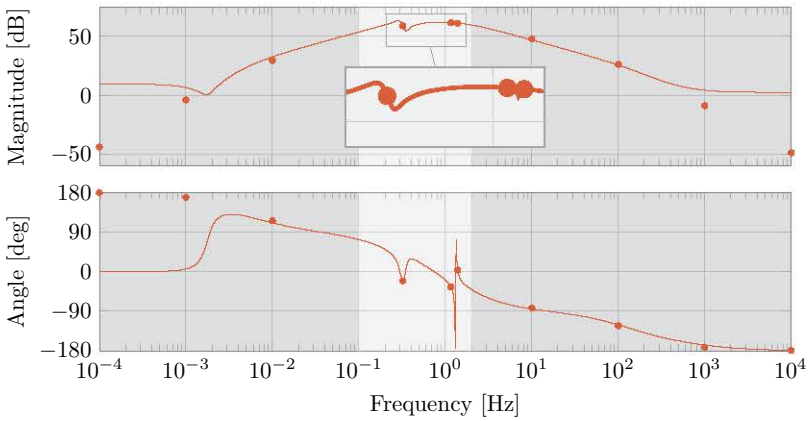

(a)

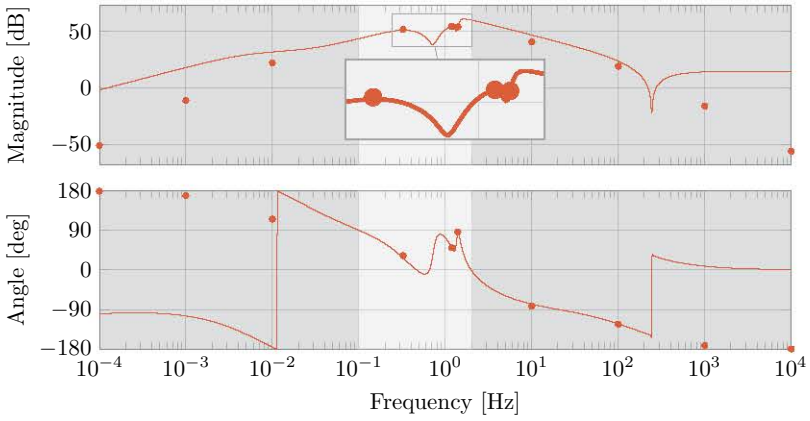

(b)

Figure 6.4: Frequency response of (a) $C_p(j\omega)$ and (b) $C_q(j\omega)$. (marks) Design specification.

has an undesired peak in both cases. For $C_p(s)$ there is an undesired amplification of frequencies between 0.1 and 0.2 Hz, while the same result can be seen for $C_q(s)$ for frequencies between 1 and 1.1 Hz. For frequencies outside the range of interest (dark area), the fitted transfer functions comply with the given specification in the majority of cases. Overall, the magnitude and phase of the obtained transfer functions follow the shape of a band-pass filter.

6.5.2 System Performance

The frequency responses of estimated plant models $P_p(j\omega)$ and $P_q(j\omega)$ are depicted in blue in Fig. 6.5 (a) and Fig. 6.5 (b), respectively. In both cases, the magnitudes

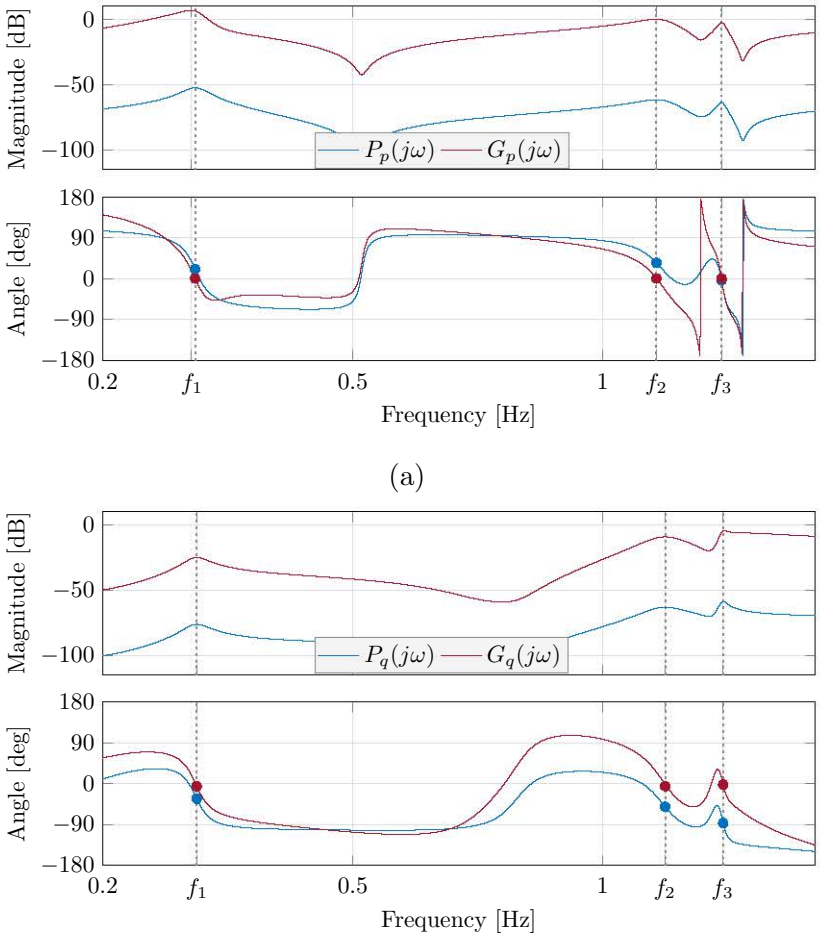

Figure 6.5: Frequency response of (blue) (a) $P_p(j\omega)$ (b) $P_q(j\omega)$. The frequency response of open-loop transfer functions (a) (red) $G_p(j\omega)$ and (b) $G_q(j\omega)$. (marks) Phases of each transfer function at oscillation frequencies.

of frequency responses show three local maxima at $f_{1,2,3}$ corresponding to three low-frequency oscillations in the system. The phases of frequency responses at those frequencies are used for the design of the POD controllers. Then, the frequency responses of open-loop transfer functions $G_p(j\omega)$ and $G_q(j\omega)$ are depicted in red in Fig. 6.5 (a) and Fig. 6.5 (b), respectively. It can be seen that the achieved phase responses for both $G_p(j\omega)$ and $G_q(j\omega)$ are close to zero. This means that the introduced POD controllers $C_p(s)$ and $C_q(s)$ compensated the plant phases at the frequencies of oscillations. Furthermore, the magnitudes of both $G_p(j\omega)$ and $G_q(j\omega)$ are higher than the magnitudes of corresponding plants. Thus, the POD controllers met both design requirements in the frequency range of interest.

6.5.3 EMT Simulations

An electro-magnetic transient (EMT) simulation was performed in Matlab/SimPowerSystems software [MATLAB, 2019], to validate the performance of the proposed POD controllers. Fig. 6.6 shows the transient of the estimated grid frequency deviation for two cases, without (blue) and with (red) POD controllers in both active and reactive power loops. For the case without POD controller action, the transient response shows several poorly damped oscillations. By introducing the POD controllers in CIG active and reactive power loops, the damping of those oscillations is improved. However, it can be seen that it takes almost 15 seconds to dampen the faster oscillations, and 30 seconds to dampen the slow one. Further increase in the POD controller gain results in oscillations at higher frequencies. The reason behind this is likely the lack of information about the system at higher frequencies since the plant models are based on system identification. Further analysis in this respect is required and it is of interest for future work.

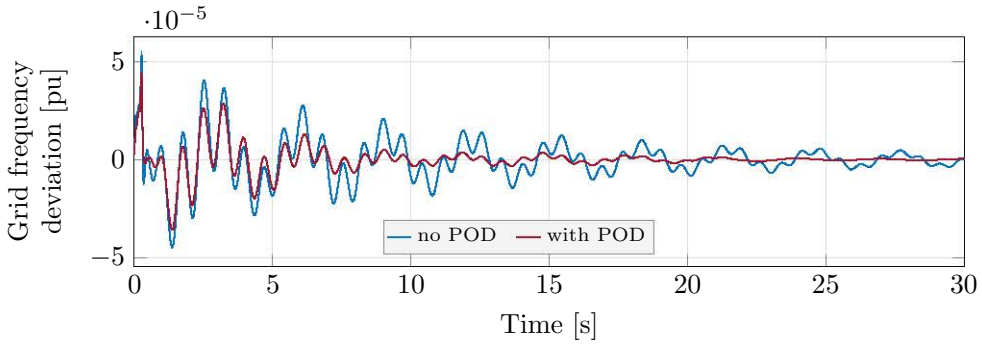

Figure 6.6: Grid frequency deviation during transient for the cases (blue) without and (red) with POD controller.

6.6 Chapter Summary

In this chapter, a method to design POD controllers for damping multiple low-frequency oscillations has been presented. The proposed method is based on the VF algorithm that is used to synthesise the controllers. First, the information required for the design of the transfer function to be compensated has been explained. Then, the procedure and options used in the VF algorithm have been described. It has been shown the fitted transfer function could result in an undesired amplification of certain frequencies because the given set of specifications is used to solve an optimisation problem. To address this issue, several steps have been proposed, including the verification of the stability margins and adjustments in the design procedure. Future work will focus on improving the controller synthesis by adding more design requirements. Such requirements can address undesired peaks in the magnitude of frequency response and further limit the controller impact outside the range of low-frequency oscillations. The application of the VF algorithm to the design of robust POD controllers will also be studied, as well as the implementation in larger networks.

Chapter 7

Single-Mode POD Controllers for CIG in Grid-Forming Mode

In this chapter, a POD controller with decoupled active and reactive powers for VSM is presented. Section 7.1 gives an overview of the system and POD controller structure. The mechanism for decoupling active and reactive powers for oscillation damping is described in Section 7.2. Section 7.3 describes the POD controller design methodology. Simulation results are presented in Section 7.4, while the main results of this chapter are summarised in Section 5.6.

7.1 System Overview

7.1.1 Application Description

Fig. 7.1 (a) shows the single-line diagram of the system studied in this work. It is based on the two-area benchmark network for low-frequency oscillation studies [IEEE, 2015a]. It consists of four generation units (G_{1-4}) that form two areas. Each generation unit includes an SG, a governor, an exciter and a power system stabiliser (PSS). There are two modifications compared to the model described in [IEEE, 2015a]. First, the proportional gain in each PSS has been reduced so that the inter-area mode is poorly damped. The second modification is an additional connection point in Bus 6 that is used to connect a CIG unit.

Fig. 7.1 (b) shows the CIG power stage. The primary energy source is connected to the dc side and it is modelled as an ideal dc voltage source that provides the required power. The primary source model is not considered here, but it is considered of interest for further research. The ac side of the power converter is connected to the rest of the system via an LC filter and a step-up transformer.

Fig. 7.1 (c) shows the block diagram of the internal loops and the VSM control

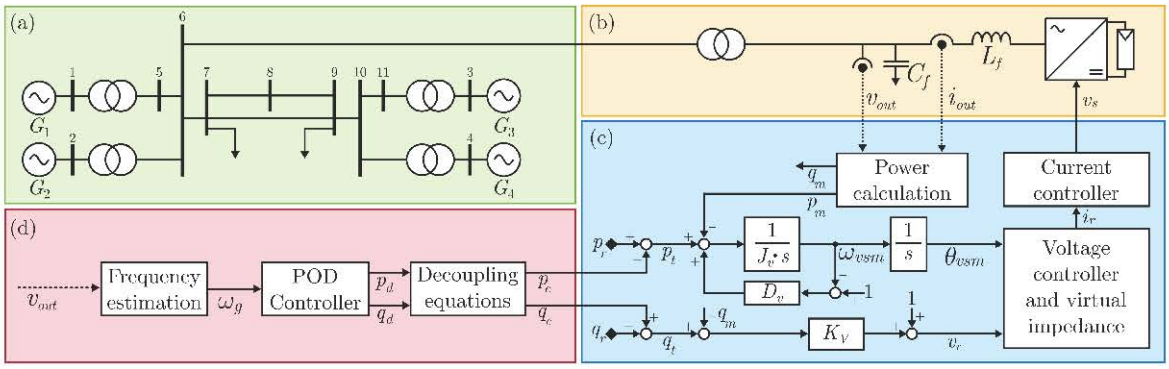

Figure 7.1: (a) Single-line diagram of two-area power system, (b) CIG power-stage, (c) internal loops and VSM, and (d) proposed POD controller.

algorithm. The inner current and voltage loops regulate the output current and voltage while the virtual impedance is used to simplify the integration with the rest of the network elements [Wang et al., 2015]. The voltage (V) and angle (θ) are references for the internal controllers by the VSM, and s is the Laplace variable. The definition of the VSM control algorithm and its parameters can be found in [Roldán-Pérez et al., 2019]. The values of the virtual impedance and VSM parameters (K_V, J_v and D_v) are calculated according to the grid requirements [D'Arco et al., 2015].

Fig. 7.1 (d) shows the proposed POD controller. This controller acts on the estimated frequency of the grid (ω_g) and calculates the additional active and reactive power references that are used to damp oscillations (p_c and q_c, where c stands for "coupled"). The requirements for these two power components might vary depending on the available active power from the primary energy source and the converter ratings. Nonetheless, if applied directly, the power references would result in CIG delivering both power components as active and reactive powers are coupled. This poses an important problem because, if the power demanded from the primary source is larger than the available power, the CIG may collapse. For that reason, the implementation of a decoupling mechanism is of interest.

7.1.2 POD Controller Description

Fig. 7.2 (a) shows the block diagram of the POD controller. The frequency deviation ($\Delta\omega_g$) is used as the input signal for the POD controller (Δ stands for "incremental"). A high-pass filter ($H(s)$) is applied to eliminate the steady-state value of the frequency so that the controller only acts on frequency variations. Then, lead-lag compensators ($C_p(s)$ and $C_q(s)$) are applied to compensate the open-loop phase of the plants while proportional gains (K_p and K_q) are used to amplify the command signals [Jankovic et al., 2023e].

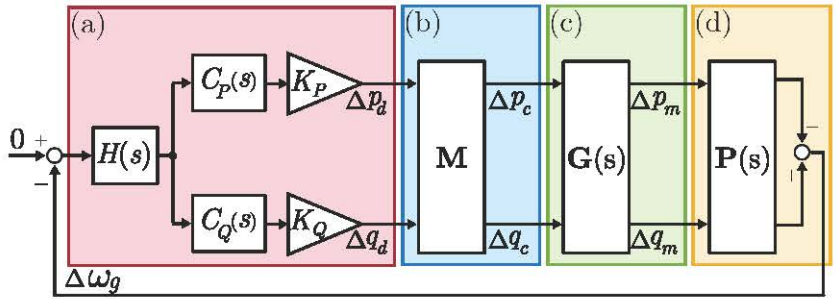

Figure 7.2: (a) POD controller block diagram with (b) power decoupling mechanism and (c) dynamic model of the plant.

Fig. 7.2 (b) shows the decoupling system. This control block allows the operation with decoupled power references calculated by the POD controllers (p_d and q_d) applied to the original power references (p_c and q_c), that are coupled. This is done by multiplying p_d and q_d by a decoupling matrix ($\mathbf{M}$). The details and alternatives for the calculation of this decoupling matrix are explained in the following section. Fig. 7.2 (c) shows the inherent coupling $\boldsymbol{G(s)}$ between references and measured active and reactive powers. The injected active and reactive powers from CIG to the system affect the system frequency. The dynamic relationships between these variables are summarised in $\boldsymbol{P(s)}$, shown in Fig. 7.2 (d).

7.2 Decoupling of Active and Reactive Powers

7.2.1 System Modelling

For a VSM connected to a power network, if any power reference is modified, the injection of both active and reactive power will change. This is not considered to be a problem, but rather a characteristic of the grid (e.g., by injecting active power both the voltage and the frequency change). If the system is operating in a steady state and only small disturbances are considered, the coupling between active and reactive power can be described as follows:

$$\begin{bmatrix}\Delta P_m(s)\\ \Delta Q_m(s)\end{bmatrix} = \underbrace{\begin{bmatrix}G_{pp}(s) & G_{pq}(s)\\ G_{qp}(s) & G_{qq}(s)\end{bmatrix}}_{\boldsymbol{G}(s)} \begin{bmatrix}\Delta P_c(s)\\ \Delta Q_c(s)\end{bmatrix}, \tag{7.1}$$

where $\boldsymbol{G}(s)$ represents the system dynamics and subindex m stands for "measured". This system has a structure of a multiple-input multiple-output (MIMO) linear dynamic system [Skogestad and Postlethwaite, 1996]. The decoupling mechanism is designed to

counteract the coupling effect of the power components. It is defined as follows:

$$\begin{bmatrix}\Delta P_c(s)\\ \Delta Q_c(s)\end{bmatrix} = \mathbf{M}\begin{bmatrix}\Delta P_d(s)\\ \Delta Q_d(s)\end{bmatrix}, \tag{7.2}$$

where $\mathbf{M}$ is a 2×2 matrix.

7.2.2 Decoupling Options

The three most common methods to decouple MIMO systems are described in the following list [Skogestad and Postlethwaite, 1996]:

1. The first method is called *dynamic decoupling* and it allows decoupling of each input-to-output response during both transients and in steady-state. To achieve such a requirement, the decoupling matrix is selected as follows:

$$\mathbf{M} = \hat{\mathbf{G}}^{-1}(s), \tag{7.3}$$

   where $\hat{\mathbf{G}}(s)$ is a model of $\mathbf{G}(s)$. Even though this method is accurate, it has some important shortcomings. First, $\hat{\mathbf{G}}^1(s)$ will have unstable poles if the original plant has right-hand place zeros. Also, $\hat{\mathbf{G}}^1(s)$ usually has more zeros than poles, and therefore it cannot be easily implemented. The most common practical approach for addressing this is to multiply $\hat{\mathbf{G}}^1(s)$ by additional high-frequency poles, but this increases the complexity and order of the system.

2. The second method is commonly called *decoupling at frequency* (e.g., ω_o). In this case, $\mathbf{M}$ is chosen to be exactly equal to $\hat{\mathbf{G}}^1(s)$ at some specific frequency (ω_o). This can be written as follows:

$$\mathbf{M} = \hat{\mathbf{G}}^{-1}(j\omega_o). \tag{7.4}$$

   Such a decoupling mechanism would be of interest in poorly damped systems, where the frequency response is greatly affected by the frequency. This method is suitable for the application considered in this work. However, the main drawback is that $\mathbf{M}$ now consists of four complex numbers. Then, in order to implement this decoupling system, the complex multiplication would need to be implemented with additional filters (e.g., lead-lag filters).

3. The third method is called *steady-state decoupling*. This method is a particular case of the one described in the previous point, but for $\omega_o = 0$:

$$\mathbf{M} = \hat{\mathbf{G}}^{-1}(0). \tag{7.5}$$

   This selection decouples the response of the MIMO inputs and outputs, in a steady state. The main benefit of this alternative is its simplicity since $\mathbf{M}$

contains only real numbers. The coefficients of $\mathbf{M}$ can be readily calculated in real applications by applying step changes to the system inputs. Although the steady-state decoupling mechanism does not guarantee full decoupling during the transients, it contributes to the dynamic decoupling between the inputs as well [Skogestad and Postlethwaite, 1996]. This way of decoupling will be used in this work.

7.3 Design of the POD Controller

7.3.1 Preliminaries

The design objective of the POD controller is to maximise the CIG damping action. To carry out the design, it is assumed the power system is operating in a steady state and that the linearised model is calculated. Then, the POD controllers for the active and the reactive powers are designed separately, as discussed in [Ogata, 2010]. Only the design of the active power controller is described here since the procedure to design the one for the reactive power is the same.

7.3.2 POD Controller Blocks

First, a high-pass filter is applied to the frequency so that the POD controller acts only over variations of $\Delta\omega_g$. It is defined as follows:

$$H(s) = s/(s + 1/T_h), \tag{7.6}$$

where T_h is the time constant of the high-pass filter.

The compensator $C_p(s)$ is designed following the open-loop phase compensation method [Ogata, 2010]. First, the plant phase (ϕ_P) at the oscillation frequency (ω_o) is obtained. Then, the $C_p(s)$ is designed to compensate for that phase at that frequency (see [Jankovic et al., 2023e] for more details). The compensator $C_p(s)$ used for that purpose has the following structure:

$$C_p(s) = \frac{1 + sT_1}{1 + sT_2}, \tag{7.7}$$

where T_1 and T_2 are parameters of the lead-lag compensator.

The proportional gain (K_p) is designed in an iterative procedure where a compromise between the damping coefficient of the mode addressed and the negative impact on other modes should be considered. See [Jankovic et al., 2023e] for more details.

In addition, the power references are limited by using saturators so that the CIG ratings are not exceeded [Jankovic et al., 2023e].

7.4 Numerical Results

The CIG-based power-plant has nominal power $S_n = 100$ MVA each, and nominal voltage $V_n = 20$ kVA. The parameters of the CIG unit and the structure of inner control loops are given in Appendix C.1, while transformer parameters are described in Appendix C.3.

7.4.1 Decoupling Power Components

Fig. 7.3 shows the transient response after changes applied to the active power reference (at $t = 10$ s) and to the reactive power reference (at $t = 30$ s). In blue, without decoupling, and in red, with the decoupling mechanism. For the case without decoupling equations, the steps are applied on p_r and q_r (i.e., the original power references). For the case with decoupling equations, the step changes are applied on p_d and q_d. These results show that the change of the active power reference causes a change of the reactive power, and vice versa. It can be seen that without the decoupling mechanism, the coupling between power components is more pronounced. Moreover, it is removed in a steady state. This result shows that this simple mechanism greatly helps to decouple power components.

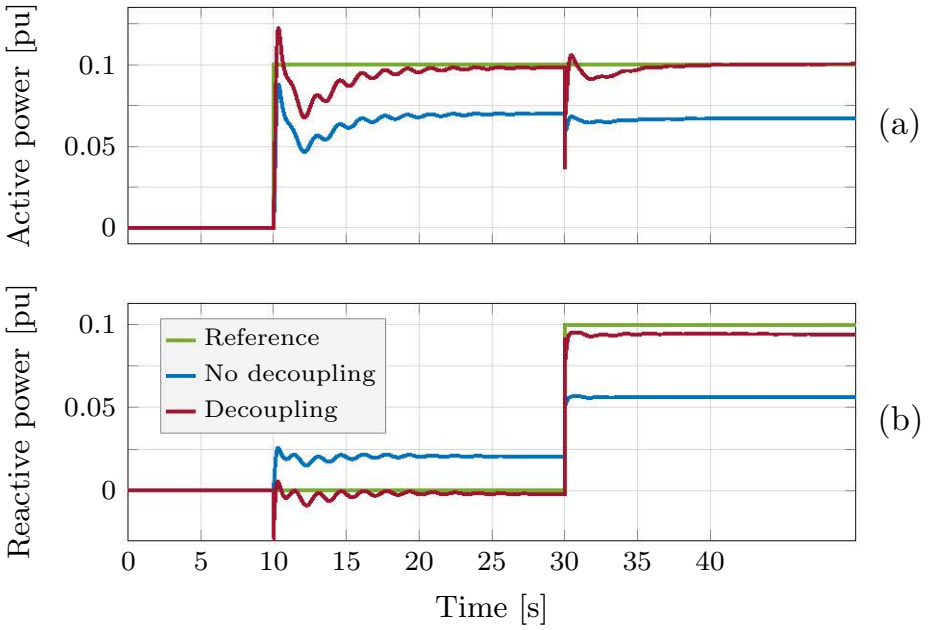

Figure 7.3: Transient response of (a) active and (b) reactive powers after a step in the power references. (blue) Without and (red) with the decoupling mechanism.

7.4.2 Damping of Oscillatory Modes

Fig. 7.4 shows the critical system eigenvalues for the original system, and for the POD controller applied to active power, reactive power, and on both components. This eigenvalue has been obtained by using system identification techniques [MATLAB, 2019]. It can be seen that POD action by either (blue) active or (green) reactive power improves the damping of critical eigenvalue, compared to the original network (in gray). Then, the combined action of both power components (red) results in a further improvement of the damping of the critical eigenvalue. This result shows that each of the POD controllers has a positive effect on the critical eigenvalue. Furthermore, thanks to the decoupling system, undesired interactions between control loops are avoided.

Fig. 7.5 shows the deviation of the estimated frequency (ω_g) after a disturbance,

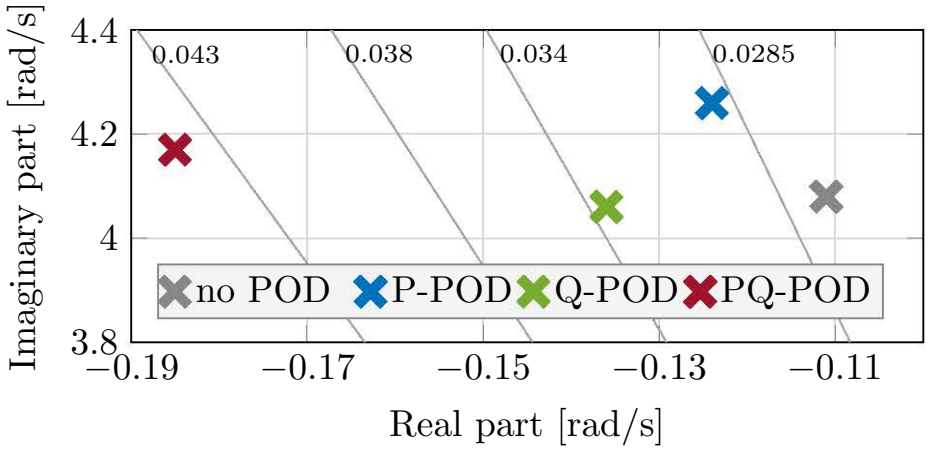

Figure 7.4: Critical eigenvalue of the identified system for (gray) no POD, and POD with (blue) active, (green) reactive and (red) active and reactive power.

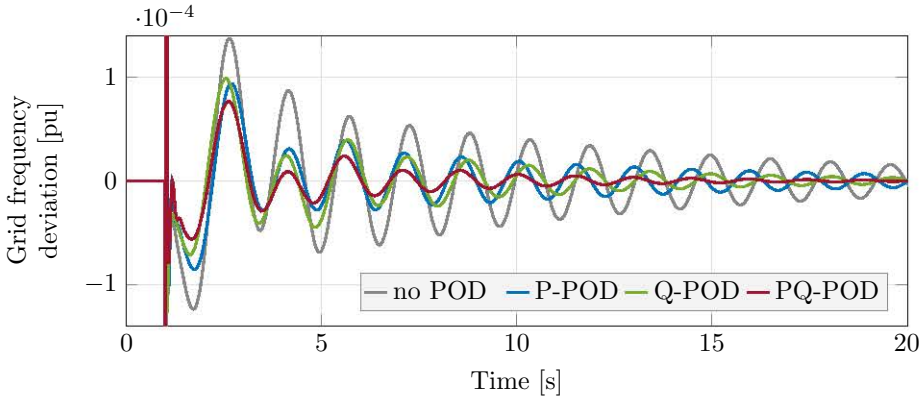

Figure 7.5: Frequency deviation during the transient response (gray) without POD controller, and with POD controller based on (yellow) active power, (red) reactive power, and (green) both power components.

for four cases. The large frequency deviation in the first milliseconds is the result of electromagnetic transients and the response of the phase-locked loop (PLL) that is used to estimate the frequency. Then, the undamped low-frequency oscillation is the result of the interaction between the electrical areas. The action of either (blue) active or (green) reactive power improves the system damping and then the oscillations vanish earlier. Then, the combined action of both power components (in red) further improves the transient response. These numerical results confirm the theoretical ones presented in Fig. 7.4.

Fig. 7.6 shows the active and reactive powers injected during the frequency transients when only one component is used to damp oscillations. In Fig. 7.6 (a) (blue), it can be seen that the delivered active power is higher when active power is used to damp oscillations. However, there is also some reactive power injection in Fig. 7.6 (b) (blue). A similar issue happens when only the reactive power controller is applied (green curves). It should be noted that the injection of active and reactive powers during these transients is a result of the natural response of the VSM to variations in the grid frequency. This means that these oscillations are natural and cannot be avoided using the decoupling system implemented in the POD controller. These oscillations are of interest for further research.

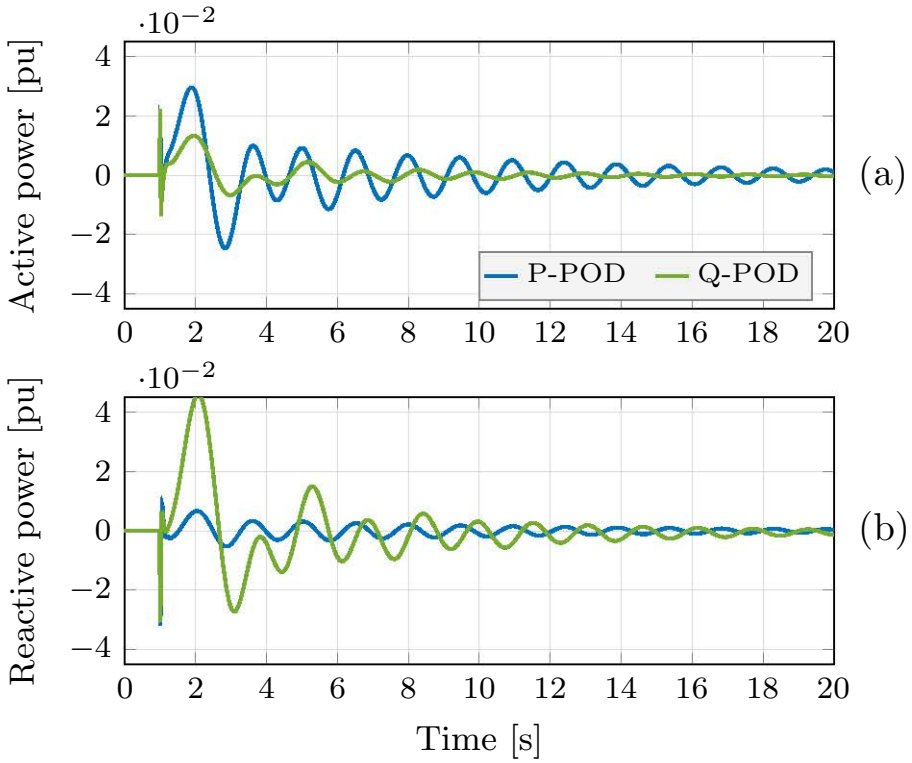

Figure 7.6: Delivered powers during the transient response (blue) with P-POD controller, and (green) with Q-POD controller.

7.5 Chapter Summary

In this chapter, a decoupled POD controller for low-frequency oscillation damping using CIG units has been proposed. The controller features an outer loop for CIG units operating as VSMs and can be deployed even if access to the CIG inner control loops is not available. The proposed POD controller is based on a steady-state decoupling mechanism and the traditional open-loop phase compensation technique. Only the open-loop phase of the plant at the frequency of the oscillation is required to design the controller. This makes the controller suitable for application in cases when the full power system model is unavailable. Future work could focus on developing a decoupling mechanism capable of acting not only in a steady state but also during transients. Also, the impact of the dc-side dynamics and the constraints on the primary source of energy might be considered.

Chapter 8

Conclusions, Contributions and Suggestions for Further Research

In this thesis, different aspects of the provision of POD services with CIG units have been addressed. Multiple factors affecting the CIG capability to contribute to the damping of low-frequency modes have been identified and analysed. Moreover, modifications in the POD controller structure to address those factors have been proposed. In this regard, there are five contributions, addressing different aspects of POD service provision from CIG. Two contributions are focused on guaranteeing the power system stability under variations in the network topology. The impact of stochastic communication channel delay on the performance of centralised POD controllers is also examined, and a method to compensate for the effects of such a delay is proposed. One contribution is focused on the synthesis of POD controllers by utilising a VF algorithm. Converters operating in grid-forming mode are also capable of providing POD services and one contribution discussed the decoupled use of active and reactive powers for this purpose. Several contributions of this thesis were tested in a PHIL environment. A real communication network deployed was used for testing the centralised POD controller. In this chapter, the summary, conclusions and the list of publications in which the author of this thesis contributed is presented. Finally, a list of suggestions for further research is given.

8.1 Summary and Conclusion

In this section, the work presented in this document is summarised, together with the conclusions drawn from it.

- The work presented in this thesis shows that the information obtained from the system frequency response is sufficient to design POD controllers, even for addressing different system conditions (e.g. different network topologies). Such an

approach opposes the established way of addressing the system stability. Namely, over the last decades, the problem of low-frequency oscillations was addressed by designing POD and PSS controllers in closed loop. This approach relies on the availability of a detailed linearised model of the power system, which should represent the system in high detail. However, with the recent change in the power generation paradigm, the share of renewable energy sources is ever-increasing. To address this change, the power system models need to be revised often. However, such procedure is facing limitations, as control systems of newly connected devices are often not accessible, due to the intellectual property of the manufacturers. On the other hand, the system frequency response from the point of connection of CIG can be obtained by using system identification methods. For example, the system can be perturbed at certain frequencies and the equivalent transfer function can be obtained using system identification tools. This allows to design POD controller with an estimated model of the system and avoids the need for a detailed linearised model of the power system. In this regard, the approach presented in this document could be useful.

- During the power system operation, changes are constantly occurring. The majority of these changes (e.g., minor modifications in load consumption) do not have an important effect on the system stability in the domain of low-frequency oscillations. However, from time to time, changes such are planned or unplanned disconnection of network elements (e.g. transmission lines) might occur. If not addressed properly, these changes can lead the system to instability as POD controllers are acting on a system different from the one used in the design stage. In this regard, there are two ideas presented in this work that address such cases. The first one is to modify the POD controller parameters once a system change is detected. To do so, an adjustment mechanism is defined based on a system study. Another approach is to design a POD controller robust against changes in the network topology. In this case, the POD controller design procedure needs to take into account all the possible system operating modes. In both cases, the system information needs to be obtained prior to enabling the POD controller action. Here, the information from the system frequency response could be used.

- The integration of CIG-based power generation on a large scale often includes several local CIG units and a centralised power plant controller. The CIG units deliver the power available from the primary energy source (e.g., PV panels). The centralised power plant controller coordinates the action of the local CIG units to meet the system requirements. A communication network is used to exchange information between the centralised controller and local units. In the case of systems with undamped low-frequency modes, the POD controller might be implemented in a centralised controller if the control systems of local units

are not accessible. However, in this case, the communication network has an important impact on the POD controller performance, mainly for two reasons. The first reason is the stochastic communication delay, whereas the second reason is the stochastic sample rate of the communication channel. The information about both factors is critical and needs to be taken into consideration when the POD controller is designed. Therefore, in this document, a method to quantify both the stochastic delay and the sampling rate of the communication channel is presented. This method does not require any information about the way the communication network operates (e.g., topology, protocol used, etc.). Once this information is obtained, a POD controller can be designed to compensate for such a delay. In the work presented in this document, it was shown that the open-loop phase compensation method is a viable solution. This method allows compensating for both the average phase delay of the communication channel and the phase of the system. Such an approach presents a simplified, yet effective, method for the design of a centralised POD controller addressing the stochastic nature of communication channel delay.

- Once the system information is available, either from a detailed linearised model of the system or from the system frequency response, the parameters of the POD controller should be determined. This presents a major challenge in addressing low-frequency modes, due to the high non-linearity of the problem. The majority of methods used in this regard introduce some sort of optimisation problem, in which the POD controller parameters are calculated. In this document, two methods that follow the same approach are presented. Both methods are suitable for systems with multiple low-frequency modes. However, during the implementation of these methods, the potential drawbacks have been noticed. These are mostly related to the selection of the optimisation algorithm and the starting points for solving the optimisation problem. Therefore, a method to synthesise POD controllers by using a VF technique has been proposed. The performance of this method was tested on a power system with three undamped low-frequency modes. The presented method relies on the VF algorithm, which is commonly used for estimating transfer functions based on frequency response measurements. Here, this method was used to meet the design requirements of the POD controller. These requirements had to be defined in the frequency domain. In particular, the magnitude and phase of frequency response of the POD controller should be selected. The POD controller synthesis using VF shows good initial results, although additional work is required in addressing undesired peaks in the controller frequency response.

- The majority of CIG-based units in the system operate in grid-following mode, delivering available power to the system. However, CIG-based units can also

operate in grid-forming mode. In this case, the unit defines its output voltage magnitude and the angle, mimicking the behaviour of SGs. As the share of CIG-based units increases, different POD requirements are being imposed for units operating in either of the two modes. For units operating in grid-forming mode, this presents a major challenge, since the active and reactive powers delivered to the grid are not strictly controlled. Also, depending on the system properties, the coupling between the two power components can be significant. This presents a challenge for the reliable operation of CIG units in grid-following mode offering POD services. Namely, during the transients produced by the low-frequency oscillations, the active power requirements can exceed the power available in the primary source of energy (e.g., the PV panels). In this case, the requirement would result in a drop of dc voltage, which would lead to the disconnection of the CIG unit. Therefore, the decoupled use of the two power components for participating in damping low-frequency oscillations is a requirement. The active and reactive power decoupling mechanism presented in this work could be used in this regard.

8.2 Contributions

The main contributions of the work presented in this document are:

- An adaptive mechanism for a POD controller that is suitable for network reconfiguration has been proposed. This mechanism was focused on the relation between the changes in the phase of the system frequency response and the frequency of the undamped mode. Then, the POD controller parameters were updated according to that mechanism and the estimated frequency of the low-frequency oscillation. This proposal was tested on the PHIL platform. The experimental results verified the applicability of this method for a CIG unit operating in real time.

- A POD controller with a fixed structure and parameter values that is resilient against network reconfiguration has been proposed. This design was the outcome of an optimisation procedure in which POD controller parameters were designed taking into account multiple network configurations. The procedure was based on the system frequency response, omitting the use of detailed linearised power system models.

- The centralised POD controller that compensates for stochastic communication delay has been proposed. To properly design the centralised POD controller, the statistical model representing the stochastic delay length and sampling rate is required, In this work, the method for quantifying both communication delay

length and throughput rate has been developed and implemented on a system with real communication network.

- The method for synthesis of a multi-mode POD controller using VF has been presented. Such an approach was inspired by a standard use of a VF algorithm in which the transfer function is obtained based on a measured system frequency response. Here, the same algorithm was used to obtain POD controller parameters based on the desired controller frequency response. This desired POD controller frequency response was defined to compensate for the plant open-loop phase, as well as to reduce the controller impact outside the range of low-frequency oscillations. Once those requirements were defined, the VF algorithm was used to determine the POD controller parameters.

- A mechanism for decoupled active and reactive power control for CIG operating as a VSM has been proposed. Such a mechanism improves the tracking of a given power reference while reducing the undesired coupling between two power components. This has an important role in the reliable operation of CIG taking into account the energy available in the primary energy source. The proposed method resulted in better tracking of power references and was later used to provide a POD service with CIG operating as a VSM.

8.3 Publications

Results presented in Chapters 3 and 5 were published in [Jankovic et al., 2021], [Jankovic et al., 2023e], and [Jankovic et al., 2023b]:

- N. Jankovic, J. Roldan-Perez, M. Prodanovic (2021). Power Oscillation Damping Using Converter-Interfaced Generators under Constrained Active and Reactive Powers, *IEEE PES ISGT Europe*.

- N. Jankovic, J. Roldan-Perez, M. Prodanovic, J. Suul, S. D'Arco, L. Rouco-Rodriguez, (2023). Power oscillation damping method suitable for network reconfigurations based on converter interfaced generation and combined use of active and reactive powers, *International Journal of Electrical Power & Energy Systems*, vol. 149, pp. 109010.

- N. Jankovic, J. Roldan-Perez, M. Prodanovic, L. Rouco-Rodriguez, (2023). Centralised Multimode Power Oscillation Damping Controller for Photovoltaic Plants with Communication Delay Compensation, *IEEE Transactions on Energy Conversion*, in press.

Results presented in Chapter 4 were compiled and submitted for possible publication [Jankovic et al., 2023d]:

- N. Jankovic, J. Roldan-Perez, M. Prodanovic, J. Suul, S. D'Arco, L. Rouco-Rodriguez, (2023). Network-Reconfiguration-Aware Power Oscillation Damping Controller for Newly Commissioned Converter-Interfaced Power Plants, *arXiv*, eprint 2304.06555.

Results presented in Chapters 6 were presented in a conference [Jankovic et al., 2023c]:

- N. Jankovic, J. Roldan-Perez, M. Prodanovic, J. Suul, S. D'Arco, L. Rouco-Rodriguez, (2023). Multimode Power Oscillation Damping Controller Synthesis using Vector Fitting, *IEEE PowerTech Europe*.

In addition, the author of this thesis worked in the field of ancillary services, in particular in the field of frequency and voltage support. The results from this work were presented in two conferences [Jankovic et al., 2022], [Jankovic et al., 2023a]:

- N. Jankovic, M. Prodanovic, J. Roldan-Perez, (2023). Ancillary Frequency and Voltage Support Provision by Renewable Energy Sources in a Medium Voltage Distribution Network, *IEEE PES ISGT Europe*.

- N. Jankovic, M. Nogales Balderrama, J. Roldan-Perez, M. Prodanovic, (2023). Battery Sizing and Location for Provision of Network Support Services, *IEEE GT&D Europe*.

Furthermore, the author of this thesis collaborated actively in [Moutevelis et al., 2023]:

- D. Moutevelis, J. Roldan-Perez, N. Jankovic, M. Prodanovic, (2023). Recursive Secondary Controller for Voltage Profile Improvement Based on Primary Virtual Admittance Control, *IEEE Transactions on Smart Grid*, vol. 14, no. 6, pp. 4296–4311.

8.4 Suggestions for Further Research

The following suggestions for further research are made based on the results obtained throughout this thesis:

1. The method to design POD controllers presented in Chapter 3 is based on an adaptation mechanism that addresses changes in the network topology. However, the proposed mechanism requires a reliable detection of the frequency of the low-frequency oscillations and precision in the offline power system analysis. This might lead to inaccuracies in calculating the POD controller parameters, leading the power system to instability. Therefore, it is of interest to study methods for detecting changes in the network topology. These methods could be used to detect wrong setting in POD controllers and update the parameters according to the changes detected in the power system.

2. Another method for addressing changes in the network topology is presented in Chapter 4. The proposed method is used to determine the parameters of a POD controller with a fixed structure. As a result, the POD controller contributes to improve the system stability margins over the range of network configurations considered. However, the amount of possible changes that might have an impact on the low-frequency oscillations is much higher. Thus, further research is needed to develop a method to design POD controllers covering a large set of variations in the network topology, the system operating point, as well as the loss of certain network elements.

3. The impact of stochastic communication delay and a method to account for it in the design stage of the POD controller are addressed in Chapter 5. The POD controller designed with the proposed method provided sufficient damping of multiple low-frequency modes. However, the design method relies on the assumption of a reliable communication channel, and only variations in the delay length and sampling rate are considered. Nonetheless, the presence of a communication network in the control system can affect the system in other ways. For example, the overall distribution of the delay length might change. Moreover, the data packets received and sent might be corrupted or even lost. Therefore, it is of interest to develop a method to address these aspects of the communication network operation, making the centralised POD controller reliable in a wider range of operating conditions.

4. Chapter 6 describes a method to synthesise POD controllers using a VF algorithm. The results have shown that the VF algorithm can be used to design POD controllers, and adequate results in terms of damping of multiple low-frequency modes were achieved. However, during the development, multiple challenges arose for the selection of the POD controller transfer function with a given set of design requirements. For example, certain frequencies had undesired amplifications, and the phase of the transfer functions obtained was changing significantly in a very narrow frequency range. Further research could improve the results of POD controller synthesis using VF by addressing those challenges and imposing additional design requirements.

5. Decoupled use of active and reactive powers to damp oscillations with VSMs is addressed in Chapter 7. The proposed method allows to use of either active or reactive power, or a combination of both, for damping low-frequency oscillations. However, the proposed decoupling mechanism is designed taking into account the system steady-state response. Although such a mechanism contributes to the decoupling of two power components, the change in one power reference causes a change in both power components during transients. Therefore, it is of in-

terest to design a more advanced decoupling mechanism for active and reactive power in VSMs. Also, the inclusion of the dc-side dynamics, which addresses the constraints imposed by the primary energy source, would be of interest.

Bibliography

[Abumeteir and Vural, 2022] Abumeteir, H. A. and Vural, A. M. (2022). Design and optimization of fractional order PID controller to enhance energy storage system contribution for damping low-frequency oscillation in power systems integrated with high penetration of renewable sources. *Sustainability*, 14(9).

[Adib et al., 2018] Adib, A., Mirafzal, B., Wang, X., and Blaabjerg, F. (2018). On stability of voltage source inverters in weak grids. *IEEE Access*, 6:4427–4439.

[AEMO, 2016] AEMO (2016). Future power system security program progress report. Technical report, Australian Energy Market Operator.

[Aien et al., 2016] Aien, M., Hajebrahimi, A., and Fotuhi-Firuzabad, M. (2016). A comprehensive review on uncertainty modeling techniques in power system studies. *Renewable and Sustainable Energy Reviews*, 57:1077–1089.

[Ali, 2014] Ali, E. (2014). Optimization of power system stabilizers using bat search algorithm. *International Journal of Electrical Power & Energy Systems*, 61:683–690.

[Basu et al., 2021] Basu, M., Mahindara, V. R., Kim, J., Nelms, R. M., and Muljadi, E. (2021). Comparison of active and reactive power oscillation damping with PV plants. *IEEE Transactions on Industry Applications*, 57(3):2178–2186.

[Beza and Bongiorno, 2015] Beza, M. and Bongiorno, M. (2015). An adaptive power oscillation damping controller by STATCOM with energy storage. *IEEE Transactions on Power Systems*, 30(1):484–493.

[Blaabjerg, 2021] Blaabjerg, F. (2021). *Control of Power Electronic Converters and Systems*. Academic Press.

[Boukarim et al., 2000] Boukarim, G., Wang, S., Chow, J., Taranto, G., and Martins, N. (2000). A comparison of classical, robust, and decentralized control designs for multiple power system stabilizers. *IEEE Transactions on Power Systems*, 15(4):1287–1292.

[Boukhenfouf et al., 2023] Boukhenfouf, J., Guillaud, X., and Bruyere, A. (2023). Impact of grid-forming converter on electromechanical oscillations. In *2023 IEEE Belgrade PowerTech*, pages 1–6.

[Bullich-Massagué et al., 2020] Bullich-Massagué, E., Cifuentes-García, F.-J., Glenny-Crende, I., Cheah-Mañé, M., Aragüés-Peñalba, M., Díaz-González, F., and Gomis-Bellmunt, O. (2020). A review of energy storage technologies for large scale photovoltaic power plants. *Applied Energy*, 274:115213.

[Chaiyatham and Ngamroo, 2017] Chaiyatham, T. and Ngamroo, I. (2017). Improvement of power system transient stability by PV farm with fuzzy gain scheduling of PID controller. *IEEE Syst. Journal*, 11(3):1684–1691.

[Chau et al., 2018] Chau, T. K., Yu, S. S., Fernando, T., Iu, H. H.-C., and Small, M. (2018). A load-forecasting-based adaptive parameter optimization strategy of STATCOM using ANNs for enhancement of LFOD in power systems. *IEEE Transactions on Industrial Informatics*, 14(6):2463–2472.

[Chaudhuri et al., 2004] Chaudhuri, B., Majumder, R., and Pal, B. (2004). Application of multiple-model adaptive control strategy for robust damping of interarea oscillations in power system. *IEEE Transactions on Control Systems Technology*, 12(5):727–736.

[Chung et al., 2003] Chung, C., Wang, K., Tse, C., Bian, X., and David, A. (2003). Probabilistic eigenvalue sensitivity analysis and PSS design in multimachine systems. *IEEE Transactions on Power Systems*, 18(4):1439–1445.

[Comer, 2013] Comer, D. E. (2013). *Internetworking with TCP/IP*. Addison – Wesley Professional.

[Conn et al., 2000] Conn, A., Gould, N., and Toint, P. (2000). *Trust-region methods*. MPS/SIAM Series on Optimization. SIAM.

[Demello and Concordia, 1969] Demello, F. P. and Concordia, C. (1969). Concepts of synchronous machine stability as affected by excitation control. *IEEE Transactions on Power Apparatus and Systems*, PAS-88(4):316–329.

[Deng et al., 2019] Deng, J., Suo, J., Yang, J., Peng, S., Chi, F., and Wang, T. (2019). Adaptive damping control strategy of wind integrated power system. *Energies*, 12(1).

[D'Arco et al., 2015] D'Arco, S., Suul, J. A., and Fosso, O. B. (2015). Small-signal modeling and parametric sensitivity of a virtual synchronous machine in islanded operation. *International Journal of Electrical Power & Energy Systems*, 72:3–15.

[Edrah et al., 2016] Edrah, M., Lo, K. L., and Anaya-Lara, O. (2016). Reactive power control of DFIG wind turbines for power oscillation damping under a wide range of operating conditions. *IET Generation, Transmission & Distribution*, 10(15):3777–3785.

[EirGrid, 2009] EirGrid (2009). All island TSO facilitation of renewables studies. Technical report, EirGrid.

[Elliott et al., 2014] Elliott, R., Byrne, R., Ellis, A., and Grant, L. (2014). Impact of increased photovoltaic generation on inter-area oscillations in the western north american power system. In *IEEE PES General Meeting*, pages 1–5.

[ENTSOE, 2015] ENTSOE (2015). Future system inertia. Technical report, ENTSOE.

[ENTSOE, 2017] ENTSOE (2017). Analysis of CE inter-area oscillations of 1st december 2016. Technical report, ENTSOE.

[ENTSOE, 2018] ENTSOE (2018). Oscillation event 3.12.2017. Technical report, ENTSOE.

[Eslami et al., 2014] Eslami, M., Shareef, H., Taha, M. R., and Khajehzadeh, M. (2014). Adaptive particle swarm optimization for simultaneous design of UPFC damping controllers. *International Journal of Electrical Power & Energy Systems*, 57:116–128.

[EU, 2010] EU (2010). Communication from the commission to the european parliament, the council, the european economic and social committee and the committee of the regions energy 2020 a strategy for competitive, sustainable and secure energy. Technical report, European Union.

[Ge et al., 2016] Ge, J., Zhao, D.-w., Ma, J., Wang, Y.-s., Du, H.-j., and Qian, M.-h. (2016). Wide-area damping controller design of large-scale PV power plants in interconnected power systems. In *2016 China International Conference on Electricity Distribution (CICED)*, pages 1–5.

[Ghali et al., 1994] Ghali, F., El-Khashab, H., and Abdel-Motaleb, M. (1994). Dynamic stability analysis of PV-injected power into a parallel AC-DC power system. In *Proceedings of 1994 IEEE 1st World Conference on Photovoltaic Energy Conversion - WCPEC (A Joint Conference of PVSC, PVSEC and PSEC)*, volume 1, pages 1056–1059.

[Gurung et al., 2019] Gurung, S., Jurado, F., Naetiladdanon, S., and Sangswang, A. (2019). Optimized tuning of power oscillation damping controllers using probabilistic approach to enhance small-signal stability considering stochastic time delay. *Electrical Engineering*, 101(3):969–982.

[Gustavsen, 2006] Gustavsen, B. (2006). Improving the pole relocating properties of vector fitting. *IEEE Transactions on Power Delivery*, 21(3):1587–1592.

[Gustavsen and Semlyen, 1999] Gustavsen, B. and Semlyen, A. (1999). Rational approximation of frequency domain responses by vector fitting. *IEEE Transactions on Power Delivery*, 14(3):1052–1061.

[Hatziargyriou et al., 2021] Hatziargyriou, N. et al. (2021). Definition and classification of power system stability – revisited amp; extended. *IEEE Transactions on Power Systems*, 36(4):3271–3281.

[Huerta et al., 2016] Huerta, F., Gruber, J. K., Prodanovic, M., and Matatagui, P. (2016). Power-hardware-in-the-loop test beds: evaluation tools for grid integration of distributed energy resources. *IEEE Industry Applications Magazine*, 22(2):18–26.

[IEA, 2021] IEA (2021). Total primary energy supply (tpes) by source, year and country. Technical report, International Energy Agency. Accessed: 2022-25-05.

[IEEE, 2005] IEEE (2005). Ieee recommended practice for excitation system models for power system stability studies. Technical report, IEEE Power Engineering Society.

[IEEE, 2015a] IEEE (2015a). Benchmark systems for small-signal stability analysis and control. Technical report, IEEE.

[IEEE, 2015b] IEEE (2015b). Benchmark systems for small-signal stability analysis and control. Technical report, IEEE.

[Impram et al., 2020] Impram, S., Varbak Nese, S., and Oral, B. (2020). Challenges of renewable energy penetration on power system flexibility: A survey. *Energy Strategy Reviews*, 31:100539.

[Jankovic et al., 2023a] Jankovic, N., Nogales Balderrama, M., Roldan-Perez, J., and Prodanovic, M. (2023a). Battery sizing and location for provision of network support services. In *2023 IEEE Generation, Transmission & Distribution*.

[Jankovic et al., 2022] Jankovic, N., Prodanovic, M., and Roldan-Perez, J. (2022). Ancillary frequency and voltage support provision by renewable energy sources in a medium voltage distribution network. In *2022 IEEE PES ISGT Europe*, pages 1–5.

[Jankovic et al., 2021] Jankovic, N., Roldan-Perez, J., and Prodanovic, M. (2021). Power oscillation damping using converter-interfaced generators under constrained active and reactive powers. In *IEEE ISGT Europe*, pages 1–8.

[Jankovic et al., 2023b] Jankovic, N., Roldan-Perez, J., Prodanovic, M., and Rouco, L. (2023b). Centralised multimode power oscillation damping controller for photovoltaic plants with communication delay compensation. *IEEE Transactions on Energy Conversion*.

[Jankovic et al., 2023c] Jankovic, N., Roldan-Perez, J., Prodanovic, M., Suul, J. A., D'Arco, S., and Rouco-Rodriguez, L. (2023c). Multimode power oscillation damping controller synthesis using vector fitting. In *2023 IEEE PowerTech*.

[Jankovic et al., 2023d] Jankovic, N., Roldan-Perez, J., Prodanovic, M., Suul, J. A., D'Arco, S., and Rouco-Rodriguez, L. (2023d). Network-reconfiguration-aware power oscillation damping controller for newly commissioned converter-interfaced power plants.

[Jankovic et al., 2023e] Jankovic, N., Roldan-Perez, J., Prodanovic, M., Suul, J. A., D'Arco, S., and Rodriguez, L. R. (2023e). Power oscillation damping method suitable for network reconfigurations based on converter interfaced generation and combined use of active and reactive powers. *International Journal of Electrical Power & Energy Systems*, 149:109010.

[Jia et al., 2017a] Jia, Q., Yan, G., Cai, Y., and Li, Y. (2017a). Small signal stability analysis of paralleled inverters for multiple photovoltaic generation units connected to weak grid. *The Journal of Engineering*, 2017(13):2015–2020.

[Jia et al., 2017b] Jia, Q., Yan, G., Cai, Y., and Li, Y. (2017b). Small-signal stability analysis of photovoltaic generation connected to weak AC grid. *Journal of Modern Power Systems and Clean Energy*, 2019(7):254—-267.

[Jin et al., 2017] Jin, T., Liu, S., Flesch, R. C., and Su, W. (2017). A method for the identification of low frequency oscillation modes in power systems subjected to noise. *Applied Energy*, 206:1379–1392.

[Kalaitzakis and Vachtsevanos, 1987] Kalaitzakis, K. C. and Vachtsevanos, G. J. (1987). On the control and stability of grid connected photovoltaic sources. *IEEE Transactions on Energy Conversion*, EC-2(4):556–562.

[Khadanga and Satapathy, 2015] Khadanga, R. K. and Satapathy, J. K. (2015). Time delay approach for PSS and SSSC based coordinated controller design using hybrid pso–gsa algorithm. *International Journal of Electrical Power & Energy Systems*, 71:262–273.

[Klein et al., 1991] Klein, M., Rogers, G., and Kundur, P. (1991). A fundamental study of inter-area oscillations in power systems. *IEEE Transactions on Power Systems*, 6(3):914–921.

[Knuppel et al., 2012] Knuppel, T., Kumar, S., Thuring, P., Stottrup, M., and Friman, J. (2012). Towards a reactive power oscillation damping controller for wind power plant based on full converter wind turbines. In *2012 IEEE PES General Meeting*, pages 1–8.

[Konara and Annakkage, 2016] Konara, A. I. and Annakkage, U. D. (2016). Robust power system stabilizer design using eigenstructure assignment. *IEEE Transactions on Power Systems*, 31(3):1845–1853.

[Kumar et al., 2020] Kumar, S., Saket, R., Dheer, D. K., Holm-Nielsen, J. B., and Sanjeevikumar, P. (2020). Reliability enhancement of electrical power system including impacts of renewable energy sources: a comprehensive review. *IET Generation, Transmission & Distribution*, 14(10):1799–1815.

[Kundur et al., 1994] Kundur, P., Balu, N., and Lauby, M. (1994). *Power system stability and control*. EPRI power system engineering series. McGraw-Hill.

[Kundur et al., 1989] Kundur, P., Klein, M., Rogers, G., and Zywno, M. (1989). Application of power system stabilizers for enhancement of overall system stability. *IEEE Transactions on Power Systems*, 4(2):614–626.

[Kurose and Ross, 2012] Kurose, J. and Ross, K. (2012). *Computer Networking: A Top-Down Approach*. Pearson Education.

[Lacerda et al., 2023] Lacerda, V. A., Araujo, E. P., Chea-Mañe, M., and Gomis-Bellmunt, O. (2023). Phasor and EMT models of grid-following and grid-forming converters for short-circuit simulations. *Electric Power Systems Research*, 223:109662.

[Larsen and Swann, 1981a] Larsen, E. V. and Swann, D. A. (1981a). Applying power system stabilizers part i: General concepts. *IEEE Transactions on Power Apparatus and Systems*, PAS-100(6):3017–3024.

[Larsen and Swann, 1981b] Larsen, E. V. and Swann, D. A. (1981b). Applying power system stabilizers part i: General concepts. *IEEE Transactions on Power Apparatus and Systems*, PAS-100(6):3017–3024.

[Li et al., 2023] Li, C., Yang, Y., Cao, Y., Aleshina, A., Xu, J., and Blaabjerg, F. (2023). Grid inertia and damping support enabled by proposed virtual inductance control for grid-forming virtual synchronous generator. *IEEE Transactions on Power Electronics*, 38(1):294–303.

[Li et al., 2016] Li, M., Wang, Y., Xu, N., Wang, W., Liu, Y., Wang, H., and Weizheng, Y. (2016). A power decoupling control strategy for droop controlled inverters and virtual synchronous generators. In *2016 IEEE IPEMC-ECCE Asia*, pages 1713–1719.

[Li et al., 2020] Li, M., Xiong, L., Chai, H., Xiu, L., and Hao, J. (2020). Mechanism of PV generation system damping electromechanical oscillations. *IEEE Access*, 8:135853–135865.

[Li et al., 2021] Li, T., Hu, W., Zhang, B., Zhang, G., Li, J., Chen, Z., and Blaabjerg, F. (2021). Mechanism analysis and real-time control of energy storage based grid power oscillation damping: A soft actor-critic approach. *IEEE Transactions on Sustainable Energy*, 12(4):1915–1926.

[Liao et al., 2019] Liao, K., Xu, Y., and Zhou, H. (2019). A robust damping controller for DFIG based on variable-gain sliding mode and kalman filter disturbance observer. *International Journal of Electrical Power & Energy Systems*, 107:569–576.

[Liu et al., 2019] Liu, M., Dassios, I., Tzounas, G., and Milano, F. (2019). Stability analysis of power systems with inclusion of realistic-modeling WAMS delays. *IEEE Transactions on Power Systems*, 34(1):627–636.

[Liu and Milano, 2018] Liu, M. and Milano, F. (2018). Small-signal stability analysis of power systems with inclusion of periodic time-varying delays. In *2018 Power Systems Computation Conference (PSCC)*, pages 1–7.

[Liu et al., 2016] Liu, Y., Zhu, L., Zhan, L., Gracia, J. R., King, T. J., and Liu, Y. (2016). Active power control of solar PV generation for large interconnection frequency regulation and oscillation damping. *International Journal of Energy Research*, 40(3):353–361.

[Ljung, 1999] Ljung, L. (1999). *System Identification: Theory for the User*. Prentice Hall information and system sciences series. Prentice Hall PTR.

[Lyons, 2004] Lyons, R. G. (2004). *Understanding digital signal processing, 3/E*. Pearson Education India.

[Martins and Lima, 1990] Martins, N. and Lima, L. (1990). Determination of suitable locations for power system stabilizers and static VAR compensators for damping electromechanical oscillations in large scale power systems. *IEEE Transactions on Power Systems*, 5(4):1455–1469.

[Mary Linda and Kesavan Nair, 2013] Mary Linda, M. and Kesavan Nair, N. (2013). A new-fangled adaptive mutation breeder genetic optimization of global multi-machine power system stabilizer. *International Journal of Electrical Power & Energy Systems*, 44(1):249–258.

[MATLAB, 2019] MATLAB (2019). *version 9.7.0 (R2019b)*. The MathWorks Inc., Natick, Massachusetts.

[Michiels et al., 2005] Michiels, W., Van Assche, V., and Niculescu, S.-I. (2005). Stabilization of time-delay systems with a controlled time-varying delay and applications. *IEEE Transactions on Automatic Control*, 50(4):493–504.

[Milano et al., 2020] Milano, F., Dassios, I., Liu, M., and Tzounas, G. (2020). *Eigenvalue Problems in Power Systems*. Taylor & Francis Limited.

[Moutevelis et al., 2023] Moutevelis, D., Roldan-Perez, J., Jankovic, N., and Prodanovic, M. (2023). Recursive secondary controller for voltage profile improvement based on primary virtual admittance control. *IEEE Transactions on Smart Grid*, pages 1–1.

[Musca et al., 2022] Musca, R., Gonzalez-Longatt, F., and Gallego Sánchez, C. A. (2022). Power system oscillations with different prevalence of grid-following and grid-forming converters. *Energies*, 15(12).

[NAERC, 2019] NAERC (2019). Interconnection oscillation analysis - reliability assessment. Technical report, North American Electric Reliability Corporation.

[Nan et al., 2021] Nan, J., Yao, W., Wen, J., Peng, Y., Fang, J., Ai, X., and Wen, J. (2021). Wide-area power oscillation damper for DFIG-based wind farm with communication delay and packet dropout compensation. *International Journal of Electrical Power & Energy Systems*, 124:106306.

[Ogata, 2010] Ogata, K. (2010). *Modern control engineering*. Prentice hall.

[Pagola et al., 1989] Pagola, F. L., Pérez-Arriaga, I. J., and Verghese, G. C. (1989). On sensitivities, residues and participations. *IEEE Transactions on Power Systems*, 4(1):278–285.

[Patrice, 2016] Patrice, B. (2016). 10-machine new-england power system ieee benchmark. `https://www.mathworks.com/matlabcentral/fileexchange/54771-10-machine-new-england-power-system-ieee-benchmark`. Accessed: 2023-10-24.

[Pawar et al., 2021] Pawar, B., Batzelis, E. I., Chakrabarti, S., and Pal, B. C. (2021). Grid-forming control for solar PV systems with power reserves. *IEEE Transactions on Sustainable Energy*, 12(4):1947–1959.

[Rahmatian and Seyedtabaii, 2019] Rahmatian, M. and Seyedtabaii, S. (2019). Multimachine optimal power system stabilizers design based on system stability and nonlinearity indices using hyper-spherical search method. *International Journal of Electrical Power & Energy Systems*, 105:729–740.

[Ramakrishna and Malik, 2010] Ramakrishna, G. and Malik, O. (2010). Adaptive PSS using a simple on-line identifier and linear pole-shift controller. *Electric Power Systems Research*, 80(4):406–416.

[Red Eléctrica, 2019] Red Eléctrica, d. E. n. (2019). *Technical norm of supervision on electrical generation modules according to EU Regulation 2016/631, (Spanish).*

[Renedo et al., 2021] Renedo, J., Garcia-Cerrada, A., Rouco, L., and Sigrist, L. (2021). Coordinated design of supplementary controllers in VSC-HVDC multi-terminal systems to damp electromechanical oscillations. *IEEE Transactions on Power Systems*, 36(1):712–721.

[Renedo et al., 2019] Renedo, J., Sigrist, L., and Rouco, L. (2019). Design of power system stabilizers to damp low frequency inter-area oscillations with limited information. In *2019 IEEE Milan PowerTech*, pages 1–6.

[Rimorov et al., 2015] Rimorov, D., Kamwa, I., and Joos, G. (2015). Coordinated design of active and reactive power modulation auxiliary loops of wind turbine generators for oscillation damping in power systems. In *2015 IEEE PES General Meeting*, pages 1–5.

[Rodríguez-Amenedo and Gómez, 2021] Rodríguez-Amenedo, J. L. and Gómez, S. A. (2021). Damping low-frequency oscillations in power systems using grid-forming converters. *IEEE Access*, 9:158984–158997.

[Rogers, 2012] Rogers, G. (2012). *Power system oscillations*. Springer Science & Business Media.

[Roldán-Pérez et al., 2021] Roldán-Pérez, J., P. Morán-Rio, D., Moutevelis, D., Rodríguez-Ortega, P., Jankovic, N., Ebrahim Zarei, M., and Prodanovic, M. (2021). Emulation of complex grid scenarios by using power hardware in the loop (PHIL) techniques. In *2021 IEEE Toronto IECON*, pages 1–6.

[Roldán-Pérez et al., 2019] Roldán-Pérez, J., Rodríguez-Cabero, A., and Prodanovic, M. (2019). Design and analysis of virtual synchronous machines in inductive and resistive weak grids. *IEEE Transactions on Energy Conv.*, 34(4):1818–1828.

[Roldán-Pérez et al., 2018] Roldán-Pérez, J., Suul, J. A., D'Arco, S., Rodríguez-Cabero, A., and Prodanovic, M. (2018). Virtual synchronous machine control of VSC HVDC for power system oscillation damping. In *IECON 2018*, pages 6026–6031.

[Rouco, 2001] Rouco, L. (2001). Coordinated design of multiple controllers for damping power system oscillations. *International Journal of Electrical Power & Energy Systems*, 23(7):517–530.

[Rouco and Pagola, 1997] Rouco, L. and Pagola, F. (1997). An eigenvalue sensitivity approach to location and controller design of controllable series capacitors for damping power system oscillations. *IEEE Transactions on Power Systems*, 12(4):1660–1666.

[Rouco and Pagola, 2001] Rouco, L. and Pagola, F. (2001). On the sign of the feedback applied by power system damping controllers. In *2001 IEEE Porto Power Tech Proceedings (Cat. No.01EX502)*, volume 2.

[Rouco et al., 1996] Rouco, L., Pagola, F., García-Cerrada, A., Rodríguez, J., and Sanz, R. (1996). Damping electromechanical oscillations in power systems with superconducting magnetic energy storage systems: Location and controller design. In *Proceedings of the 12th Power Systems Computation Conference*, pages 1097–1104.

[Saadatmand et al., 2021a] Saadatmand, M., Gharehpetian, G. B., Moghassemi, A., Guerrero, J. M., Siano, P., and Alhelou, H. H. (2021a). Damping of low-frequency oscillations in power systems by large-scale PV farms: A comprehensive review of control methods. *IEEE Access*, 9:72183–72206.

[Saadatmand et al., 2021b] Saadatmand, M., Mozafari, B., Gharehpetian, G. B., and Soleymani, S. (2021b). Optimal coordinated tuning of power system stabilizers and wide-area measurement-based fractional-order PID controller of large-scale PV farms for LFO damping in smart grids. *International Transactions on Electrical Energy Systems*, 31(2):e12612.

[Schleif and White, 1966] Schleif, F. R. and White, J. H. (1966). Damping for the northwest - southwest tieline oscillations - an analog study. *IEEE Transactions on Power Apparatus and Systems*, PAS–85(12):1239–1247.

[Seppanen, 2017] Seppanen, J. (2017). *Methods for Monitoring Electromechanical Oscillations in Power Systems*. PhD thesis, Aalto University, Finland.

[Shabani et al., 2013] Shabani, H., Vahidi, B., and Ebrahimpour, M. (2013). A robust PID controller based on imperialist competitive algorithm for load-frequency control of power systems. *ISA Transactions*, 52(1):88–95.

[Shah et al., 2012] Shah, R., Mithulananathan, N., and Lee, K. Y. (2012). Design of robust power oscillation damping controller for large-scale PV plant. In *2012 IEEE PES General Meeting*, pages 1–8.

[Shah et al., 2013a] Shah, R., Mithulananthan, N., and Bansal, R. (2013a). Oscillatory stability analysis with high penetrations of large-scale photovoltaic generation. *Energy Conversion and Management*, 65:420–429.

[Shah et al., 2013b] Shah, R., Mithulananthan, N., and Lee, K. Y. (2013b). Large-scale PV plant with a robust controller considering power oscillation damping. *IEEE Transactions on Energy Conversion*, 28(1):106–116.

[Shah et al., 2014] Shah, R., Mithulananthan, N., and Lee, K. Y. (2014). Low-order robust damping controller design for large-scale PV power plants. In *IEEE PES General Meeting*, pages 1–5.

[Shair et al., 2022] Shair, J., Xie, X., Yang, J., Li, J., and Li, H. (2022). Adaptive damping control of subsynchronous oscillation in DFIG-based wind farms connected to series-compensated network. *IEEE Transactions on Power Delivery*, 37(2):1036–1049.

[Shintai et al., 2014] Shintai, T., Miura, Y., and Ise, T. (2014). Oscillation damping of a distributed generator using a virtual synchronous generator. *IEEE Transactions on Power Delivery*, 29(2):668–676.

[Silva-Saravia et al., 2021] Silva-Saravia, H., Pulgar-Painemal, H., M. Tolbert, L., A. Schoenwald, D., and Ju, W. (2021). Enabling utility-scale solar PV plants for electromechanical oscillation damping. *IEEE Transactions on Sustainable Energy*, 12(1):138–147.

[Silva-Saravia et al., 2021] Silva-Saravia, H., Pulgar-Painemal, H., Tolbert, L. M., Schoenwald, D. A., and Ju, W. (2021). Enabling utility-scale solar PV plants for electromechanical oscillation damping. *IEEE Transactions on Sustainable Energy*, 12(1):138–147.

[Skogestad and Postlethwaite, 1996] Skogestad, S. and Postlethwaite, I. (1996). *Multivariable Feedback Control: Analysis and Design*. Wiley.

[Varma and Maleki, 2019] Varma, R. K. and Maleki, H. (2019). PV solar system control as STATCOM (PV-STATCOM) for power oscillation damping. *IEEE Transactions on Sustainable Energy*, 10(4):1793–1803.

[Wang et al., 2015] Wang, X., Li, Y. W., Blaabjerg, F., and Loh, P. C. (2015). Virtual-impedance-based control for voltage-source and current-source converters. *IEEE Transactions on Power Electronics*, 30(12):7019–7037.

[Werner et al., 2003] Werner, H., Korba, P., and Yang, T. C. (2003). Robust tuning of power system stabilizers using LMI-techniques. *IEEE Transactions on Control Systems Technology*, 11(1):147–152.

[Yazdani and Iravani, 2010] Yazdani, A. and Iravani, R. (2010). *Grid-Imposed Frequency VSC System: Control in -Frame*, pages 160–203. John Wiley and Sons, Ltd.

[You et al., 2017] You, S., Kou, G., Liu, Y., Zhang, X., Cui, Y., Till, M. J., Yao, W., and Liu, Y. (2017). Impact of high PV penetration on the inter-area oscillations in the U.S. eastern interconnection. *IEEE Access*, 5:4361–4369.

[Yuan and Yan, 2020] Yuan, C. and Yan, X. (2020). Multi-objective robust tuning of STATCOM controller parameters for stability enhancement of stochastic wind-penetrated power systems. *IET Generation, Transmission & Distribution*, 14:4805–4814.

[Zeni et al., 2016] Zeni, L., Eriksson, R., Goumalatsos, S., Altin, M., Sørensen, P., Hansen, A., Kjær, P., and Hesselbæk, B. (2016). Power oscillation damping from VSC–HVDC connected offshore wind power plants. *IEEE Transactions on Power Delivery*, 31(2):829–838.

[Zhao et al., 2021] Zhao, J., Huang, M., Yan, H., Tse, C. K., and Zha, X. (2021). Nonlinear and transient stability analysis of phase-locked loops in grid-connected converters. *IEEE Transactions on Power Electronics*, 36(1):1018–1029.

[Zhou et al., 2017] Zhou, L., Yu, X., Li, B., Zheng, C., Liu, J., Liu, Q., and Guo, K. (2017). Damping inter-area oscillations with large-scale PV plant by modified multiple-model adaptive control strategy. *IEEE Transactions on Sustainable Energy*, 8(4):1629–1636.

[Zhou and Beerten, 2023] Zhou, W. and Beerten, J. (2023). Black box-based incremental reduced-order modeling framework of inverter-based power systems. *IEEE Open Journal of the Industrial Electronics Society*, 4:506–518.

[Zhou et al., 2022] Zhou, X., Cheng, S., Wu, X., and Rao, X. (2022). Influence of photovoltaic power plants based on VSG technology on low frequency oscillation of multi-machine power systems. *IEEE Transactions on Power Delivery*, 37(6):5376–5384.

Appendix A

Laboratory Setup

This appendix describes the laboratory setup used for the verification of some of the ideas presented in this thesis. Section A.1 gives an overview of the laboratory configuration used to verify the performance of the centralised POD controller, presented in Chapter 5. The hardware configuration and the communication network topology are described in Sections A.1.1 and A.1.2, respectively. In Section A.2, the hardware setup used to verify the performance of the adaptive POD controller is described. Finally, Section A.3 describes the scaling factors used for interconnecting the PHIL environment and the emulated transmission network models.

A.1 Centralised Platform

A.1.1 Hardware Elements

Fig. A.1 (a) shows the single-line diagram of the laboratory facilities. The nominal network voltage was 400 V and the nominal frequency was 50 Hz. One 75 kVA converter is used to form the local network, as it is depicted in Fig. A.1 (c). Then, the battery and the STATCOM of the PV plant were emulated by using two 15 kVA converters (Fig. A.1 (d)). A similar set of converters was used to emulate the PV inverters (Fig. A.1 (e)). Each of the 15 kVA converters was connected to the main busbar via an LCL filter. Fig. A.2 shows a photograph of the experimental setup.

The dc side of all the converters was kept constant at 680 V by using non-controlled rectifiers (in gray). The switching and sampling frequencies for the 75 kVA and 15 kVA VSCs were 8 kHz and 10 kHz, respectively (see [Roldán-Pérez et al., 2021] for more details).

A.1.2 Communication Network

Fig. A.1 (b) shows the control and communication set-up used for the tests. Three real-time PCs (RTPCs) were used to execute the control algorithms of the power converters.

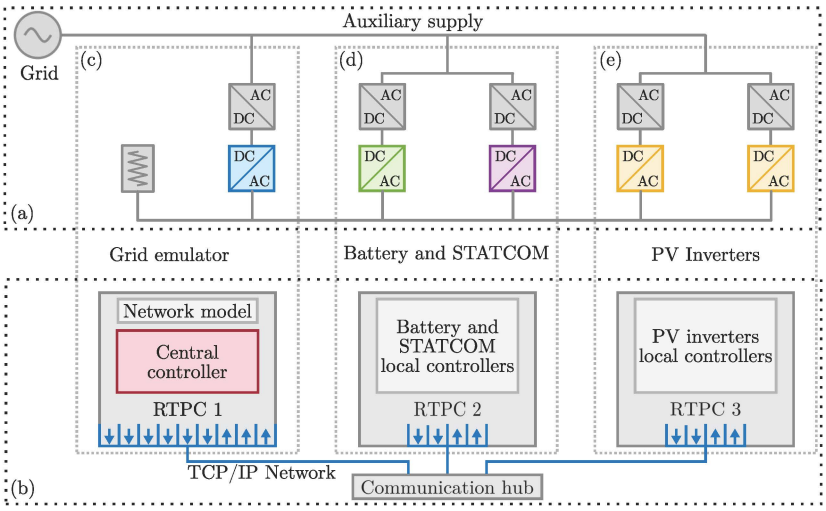

Figure A.1: (a) Electric diagram of the laboratory facilities. Converters representing the emulated (blue) grid, (yellow) PV generators, (purple) STATCOM, (green) battery. (gray) Additional resistive load. (b) RTPCs executing control algorithms. (blue) Communication network connecting three RTPCs and communication hub using TCP/IP protocol.

Figure A.2: Laboratory photograph. (a) Four 15 kVA converters, (b) 75 kVA converter, (c) ac-busbars, (d) real-time computers, and (e) communication hub.

In particular, the network model and the centralised POD controller were executed in RTPC 1. Then, RTPC 2 and RTPC 3 executed the control algorithms of the CIG units. Each RTPC was receiving and sending a certain set of variables, depicted as blue arrows in Fig. A.1 (b). A communication hub was used to manage the data flow between the three RTPCs. The communication between devices was established by using TCP/IP protocol.

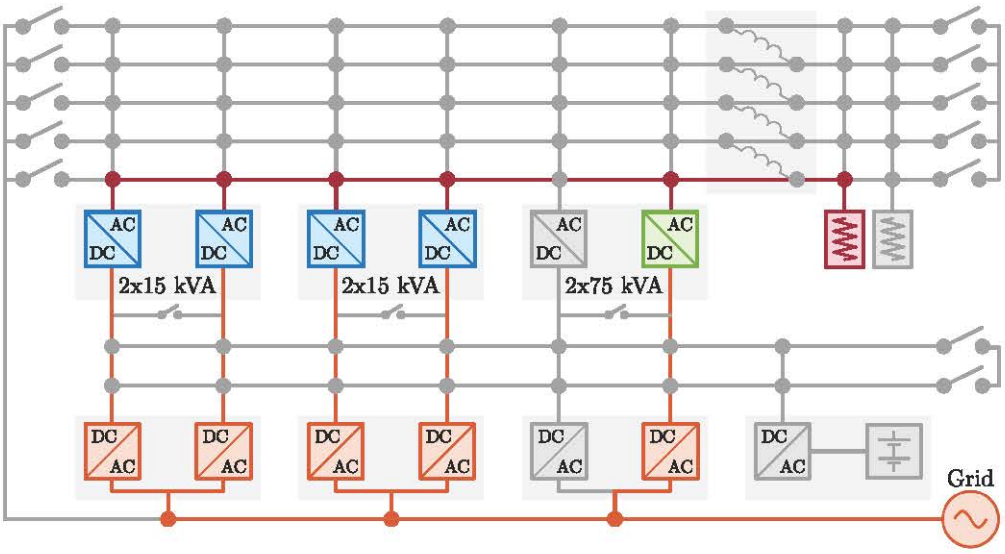

Figure A.3: Electric diagram of the laboratory facilities. (green) Grid emulator and (blue) VSCs used as CIGs.

A.2 Local POD Controller Implementation

The proposed POD controller performance was experimentally validated in a laboratory [Roldán-Pérez et al., 2021]. Fig. A.3 shows a single-line diagram of the laboratory facilities. The nominal network voltage was 400 V and the nominal frequency was 50 Hz. The two-area power system depicted in Fig. 3.1 (a) was emulated by using one 75 kVA VSC. This converter includes fast internal controllers so it can readily emulate grids [Roldán-Pérez et al., 2021]. The CIGs were emulated by using four 15 kVA VSCs connected to the grid via their LCL filters. Each of these CIGs included an adaptive POD controller. The CIGs did not have communication links between them. All the CIGs were connected to the same busbar (the POC), which is the output of the grid emulator. There was an additional resistive load connected to the POC to avoid reverse power-flows during the system start-up procedure. The dc sides of all converters were maintained constant at 680 V by using uncontrolled rectifiers. The switching and sampling frequencies for the 75 kVA and 15 kVA VSCs were 8 kHz and

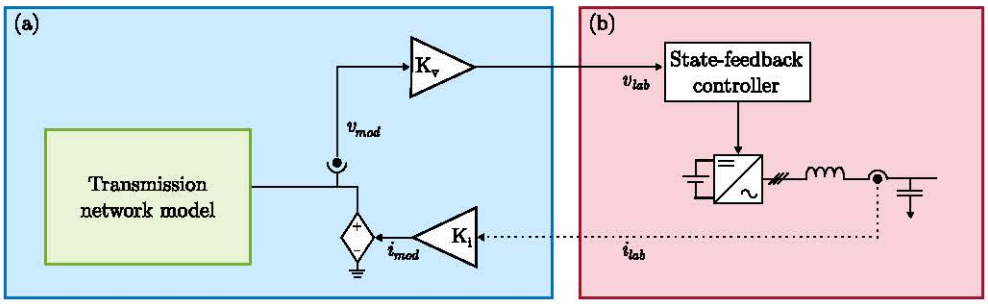

Figure A.4: Link between (a) emulated transmission network model and (b) PHIL environment.

10 kHz, respectively (see [Roldán-Pérez et al., 2021] for more details). The laboratory measurements were scaled up so that 15 kVA in the laboratory was seen as 100 MVA in the emulated power system. For the internal current controllers of the CIGs, the settling time was set to 5 ms and the overshoot to 10 %. PLLs were used in the CIG to synchronise them with the voltage at the connection point. In these PLLs, the settling time was set to 80 ms and the overshoot to 10 % by using traditional design methodologies [Yazdani and Iravani, 2010]. The zoom-FFT algorithm was adjusted to operate in a frequency range between 0.1 and 2 Hz [Lyons, 2004].

A.3 Connection between PHIL and Emulated Network Model

Fig. A.4 shows the set-up used for establishing the connection between the emulated transmission network and the PHIL environment. In the emulated network model, the voltage at the POC (v_{mod}) is measured and multiplied by the scale factor K_v. This defines the voltage reference (v_{lab}) used for controlling the voltage of the actual converter in the PHIL environment. The scaling factor for voltage (K_v) is calculated as:

$$K_v = \frac{V_{n,lab}}{V_{n,mod}}, \tag{A.1}$$

where $V_{n,lab}$ and $V_{n,mod}$ are the nominal voltage levels in the PHIL environment and the emulated network model at the connection point, respectively.

The scaling factors for currents are calculated in a two-step procedure. First, the scaling factor for power (K_s) is calculated so that a certain power measured in the laboratory is scaled up to the desired power level in the emulated model. This is defined as:

$$K_s = \frac{S_{n,mod}}{S_{n,lab}}, \tag{A.2}$$

where $S_{n,mod}$ and $S_{n,lab}$ are the powers defined in the emulated model and in the laboratory, respectively. Then, the current scaling factor (K_i) is applied to the current measured in the laboratory to achieve the desired power scale-up. This factor is calculated as:

$$K_i = \frac{I_{n,mod}}{I_{n,lab}} = K_s \cdot K_v, \tag{A.3}$$

where $I_{n,mod}$ and $I_{n,lab}$ are the current levels corresponding to the powers defined in the emulated model and in the laboratory, respectively.

For more details on the PHIL setup and the emulation of power systems, see [Roldán-Pérez et al., 2021] and [Huerta et al., 2016].

Appendix B

Communication Network Performance

This appendix describes the delay present in the communication networks. Also, it gives an overview of the factors affecting the communication network delay.

B.1 Communication Network Delay

During the system operation, the communication network delay varies significantly. The root causes of this variation can be divided into two groups. The first group is related to the procedures used in the endpoints of the communication network. For sending messages, these procedures are responsible for gathering and preparing information from other routines. For receiving messages, these procedures are used to unpack the message and forward the information to other routines. Depending on the platform used, these procedures can be implemented in hardware or software. Hardware implementation is more predictable and contributes only as a constant delay. However, procedures implemented in software might introduce variations in delay length, depending on whether the code is executed on a real-time platform or not.

The other group of factors affecting the delay variation is related to the communication network operation and performance. There are many factors in this group that could contribute to the variation of the delay. The ones that have the most influence are:

- *Network traffic:* Network traffic has an important effect on the overall network performance and delay length [Comer, 2013]. For a network without traffic, the delay would be minimal. In this case, the delay is caused only by the time required by the hardware to transfer information from one point to another. As the network

traffic increases, the variation in the delay length can be estimated as:

$$\sigma = \frac{1}{1 - L}, \qquad 0 \leq L \leq 1, \tag{B.1}$$

where L is the current network load and σ is the network traffic level. Therefore, the variation in the delay increases as the network load increases.

- *Congestion:* Congestion in communication networks occurs in two cases [Comer, 2013]. In the first case, one device connected to the communication network is sending messages at a rate higher than the communication channel throughput rate. The second case occurs when many devices are sending messages at a low rate to one router. Over time, the queue on the router end increases, causing congestion in the network traffic. In both cases, the devices in the network would face an increase in the delay length. Furthermore, if the communication protocol does not have a mechanism for addressing congestion, the increased delay would result in increased traffic, leading to a congestion collapse.

- *Routing:* Routing is a procedure used to define communication paths between devices in a network [Kurose and Ross, 2012]. This procedure is implemented in routers and its main objective is to find the best paths between devices, taking into account the network topology and the traffic flow. In case of congestion, the routing would finally decrease the delay by finding a new path between devices.

These factors affect the communication channel delay length and result in changes over time. However, in general, the difference in delay length between two consecutive messages is not significant [Comer, 2013]. Fig. B.1 shows the round trip delay length for 200 messages sent in a communication network with TCP protocol (adapted

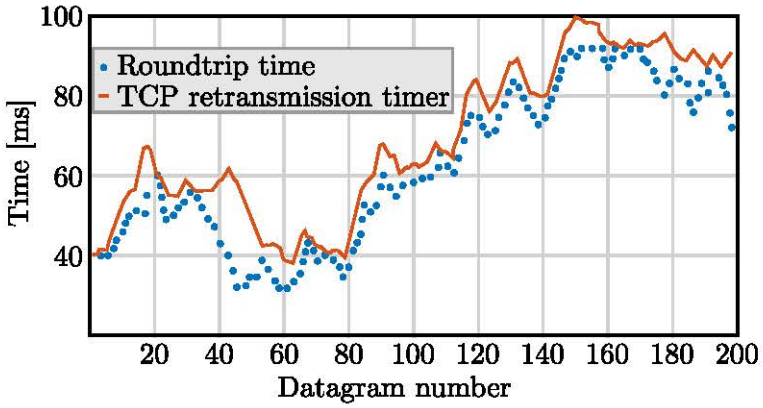

Figure B.1: (dots) Roundtrip times and (solid) retransmission timer in a communication network with TCP protocol.

from [Comer, 2013]). Although the average delay changes from 30 ms to 100 ms, the difference between two successive messages (two dots) is less than 5 ms. This is relevant for applications in which a centralised controller is sending identical command references to multiple devices. A large deviation in the delay length between two messages would cause a difference in the action of devices. However, as this variation is not significant, and it is faster than the response time of outer control loops, it does not lead to a discrepancy in following the command sent from the centralised controller.

Appendix C

CIG Parameters

This appendix describes the structure of the CIG control algorithms used throughout this thesis. Section C.1 describes the control algorithm implemented for CIG units operating in grid-following mode. The structure and parameters of the control algorithm used for CIG units operating in grid-forming mode are given in Section C.2. The parameters of the step-up transformer unit used in the test cases are presented in Section C.3.

C.1 CIG Operating in Grid-Following Mode

Fig. C.1 shows the power stage and structure of the control algorithms of the CIG units operating in grid-following mode. Fig. C.1 (a) presents the control algorithm implemented to follow active and reactive power references. The CIG output current reference is calculated according to the specified power references and the voltage at the connection point. Then, the current regulator defines the converter reference voltage. This value is transferred from the local synchronous reference frame (SRF) to a three-phase modulation signal. In the PHIL setup, this signal is used to calculate the

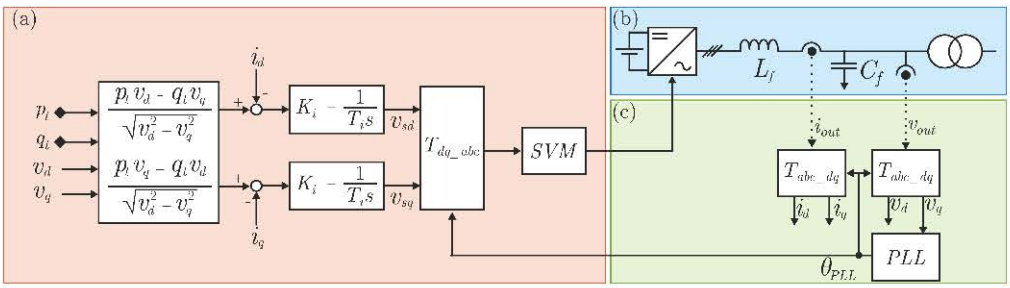

Figure C.1: Overview of the control algorithm of CIG units operating in grid-following mode, and single-line diagram of CIG power stage.

Table C.1: Parameters for CIG operating in grid-following mode. Parameters are given on CIG unit base.

Group	Parameter	Value
Output filter	L_f [pu]	0.04
	C_f [pu]	0.07
Current controller	K_i	0.2252
	T_i	0.00019
Phase-locked loop	K_{PLL}	115
	T_{PLL}	0.017

switching signals for the semiconductors by using the space-vector modulation (SVM) technique. Table C.1 shows the value of the parameters.

Fig. C.1 (b) shows the CIG power stage, which includes several elements. An ideal dc voltage source is used to represent the primary source of energy. This means that dc side dynamics are not modelled in this thesis. A six-module three-leg inverter is considered for the converter topology. In simulation models, this converter is represented as an average model. Setups in the PHIL environment include the real hardware of a 15 kVA converter used for this purpose. The converter ac output is connected to an LC filter. The output currents and voltages are measured and used as feedback signals in the control algorithm. Then, the CIG unit is connected to the rest of the system via a step-up transformer unit.

In Table C.1, the values of the LC filter of the CIG are given. Section C.3 includes the parameters of the transformer unit, which are the same in all the test cases. In every test case, the base power of the transformer is made equal to the CIG base power while the secondary voltage is defined by the transmission network voltage level.

Fig. C.1 (c) shows the measurements and transformations used for representing the measured values of voltages and currents in the CIG control algorithm. The output current (i_{out}) and output voltage (v_{out}) are measured as three-phase signals. Then, these signals are transformed to the CIG local SRF using the following transformation [Yazdani and Iravani, 2010]:

$$T_{abc-dq} = \sqrt{\frac{2}{3}} \begin{bmatrix} \sin\theta & \sin(\theta - \frac{2\pi}{3}) & \sin(\theta + \frac{2\pi}{3}) \\ \cos\theta & \cos(\theta - \frac{2\pi}{3}) & \cos(\theta + \frac{2\pi}{3}) \end{bmatrix}, \tag{C.1}$$

where θ is the angle of the local SRF. This angle is calculated by using a phase-locked loop (PLL), which is defined as [Yazdani and Iravani, 2010]:

$$PLL(s) = K_{PLL}\left(1 + \frac{1}{T_{PLL}s}\right), \tag{C.2}$$

where K_{PLL} and T_{PLL} are PLL proportional gain and time constant, respectively, while s is the Laplace operator. The value of those two parameters is given in C.1.

It is necessary to transform the signals from the local SRF to three-phase signals since the CIG control algorithm is implemented in the local SRF. This is done by using the inverse transformation of T_{abc-dq}, which is defined as [Yazdani and Iravani, 2010]:

$$T_{dq-abc} = \sqrt{\frac{2}{3}} \begin{bmatrix} \sin\theta & \cos\theta \\ \sin(\theta - \frac{2\pi}{3}) & \cos(\theta - \frac{2\pi}{3}) \\ \sin(\theta + \frac{2\pi}{3}) & \cos(\theta + \frac{2\pi}{3}) \end{bmatrix}, \tag{C.3}$$

C.2 CIG Operating in Grid-Forming Mode

Fig. C.2 shows an overview of the control algorithm used for a CIG operating in grid-forming mode, as well as the CIG power stage. Specifically, Fig. C.2 (a) shows the diagram of the control algorithm. The main idea of this control algorithm is to mimic the behaviour of a SG, hence the name - virtual synchronous machine (VSM). The output voltage magnitude and angle are calculated based on the power references and the measured powers. The angle value is used to define the local SRF. Also, the voltage magnitude and angle calculated by the controller are used to define the voltage references in the local SRF (v_{rd} and v_{rq}). These references are compared with the actual values of the output voltage ($v_m d$ and $v_r q$). Furthermore, an additional term representing a virtual impedance (L_v) is introduced to simplify the connection of the CIG to the network. Then, a PI controller is applied to regulate the current based on the given voltage references. The current controller is implemented as a PI that defines the converter output voltage. Finally, this voltage is transformed from the local SRF to a three-phase signal by using (C.3), and then the modulation signals are calculated.

Fig. C.2 (b) shows the single-line diagram of the power stage of a CIG operating

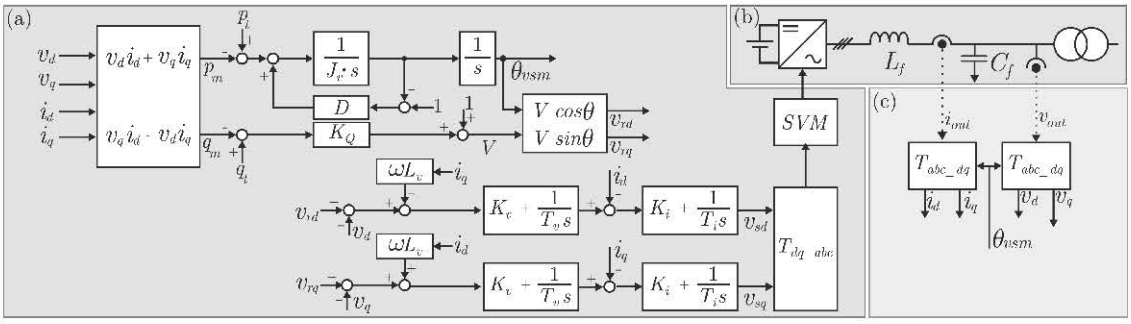

Figure C.2: Overview of the control algorithm used in CIG operating in grid-forming mode, and single-line diagram of the CIG power stage.

in grid-forming mode. The primary energy source is modelled as an ideal dc voltage source, thus neglecting the dc side dynamics. The converter is modelled as an average three-phase inverter since the fast switching transients would not have a major impact on the accuracy of the results. The converter is connected to the rest of the system via an LC output filter and a step-up transformer.

Table C.2 shows the parameters of the LC filter of the CIG units and Section C.3 shows the parameters of the transformer unit.

Fig. C.2 (b) shows the transformation of the three-phase output current i_{out} and output voltage v_{out} measurements. These signals are transformed to local SRF by using (C.1), with the angle value calculated by VSM (θ_{VSM}).

C.3 Step-Up Transformer Unit

The step-up transformer connects the CIG with the rest of the network. It is used for both CIG units operating in grid-following and grid-forming modes (see Fig. C.1). The primary side of the transformers is connected to the CIG while the secondary side is connected to a high-voltage transmission network. Table C.3 gives the values of the transformer parameters, in per unit (on the transformer unit base). The transformer base power and secondary side voltage are test-case dependent, and they are specified in Section C.4. Transformer magnetization is not modelled.

Table C.2: Parameters for CIG unit operating in grid-forming mode. Parameters are given on CIG unit base.

Group	Parameter	Value
Nominal voltage	V_n [kV]	20
Output filter	L_f [pu]	0.04
	C_f [pu]	0.07
Current controller	K_i	0.2252
	T_i	0.00019
Voltage controller	K_v	0.8021
	T_v	0.0016
Virtual impedance	L_v	0.2
Reactive power droop	K_Q	0.2
Virtual synchronous machine	J_v	4
	D_v	60

Table C.3: Step-up transformer unit parameters. Values are given in [pu] on the transformer base.

Group	Parameter	Value
Primary widing	Voltage [kV]	20
	Resistance [pu]	$1 \cdot 10^{-5}$
	Inductance [pu]	0
	Connection	Δ (D1)
Secondary widing	Voltage [kV]	Case dependant
	Resistance [pu]	$1 \cdot 10^{-4}$
	Inductance [pu]	0.25
	Connection	Y_g

C.4 Test-Case Information

Table C.4 gives information about the CIG unit base power and transmission network voltage levels, for each test case presented in this thesis.

Table C.4: Test-case information.

Chapter	Parameter	Value
Chapter 3	CIG Base power [MVA]	100
	Network voltage [kV]	230
Chapter 4	CIG Base power [MVA]	50
	Network voltage [kV]	345
Chapter 5	CIG Base power [MVA]	300
	Network voltage [kV]	500
Chapter 6	CIG Base power [MVA]	300
	Network voltage [kV]	500
Chapter 7	CIG Base power [MVA]	100
	Network voltage [kV]	230